EVALUATION OF SELECTED RADAR CROSS SECTION MEASUREMENT RANGES

Volume IIa: Cylinder Tests and Range Evaluation Procedures

Thomas M. Smith
Eugene F. Knott
Ralph E. Hiatt
University of Michigan

This document is subject to special export controls and each transmittai to foreign governments, foreign nationals or representatives thereto may be made only with prior approval of RADC (EMASP), GAFB, NY 13440.

7462-1-F = RL-2156

FOREWORD

This final technical report was prepared by the University of Michigan Radiation Laboratory, Dept of Electrical Engineering, Ann Arbor, Michigan 48108 under contract AF 30(602)-3872, Project 6512, Task 651207. The work was performed during the period July 1965 through April 1968 under the direction of Professor Ralph E. Hiatt. The number used by the contractor to identify the report is 7462-1-F. The project engineer was D. M. Montana, Rome Air Development Center, EMASP, Griffiss Air Force Base, NY 13440.

The authors are pleased to acknowledge the contributions of Dr. T.B.A. Senior on several phases of the program. Thanks are due to Mr. Tony Hsu for his considerable help in reading patterns and organizing the data.

Distribution of this report is limited because it discloses the current U.S. state of the art in radar reflectivity measurements.

This technical report has been reviewed and is approved.

ABSTRACT

This is the second part of a three part final report on the evaluation of radar cross section measuring facilities. In Volume IIa, the results from measurements on five right circular cylinders, which are scale models of one another, are discussed in detail. Evaluation procedures are set forth in order to determine how well each of the ranges performed their tasks. These procedures involve the comparison of measurements on cylinders which should give the same results, or results which should differ by known scale factors, and secondly the comparison of theoretical and experimental results for end-on and broadside aspect angles. Five outdoor radar ranges took part in this evaluation program. Limited tests were made on two of the smaller cylinder models at a sixth facility, an indoor range.

TABLE OF CONTENTS

LIST OF ILLUSTRATIONS

LIST OF TABLES

I

INTRODUCTION

This is Volume IIa of the final report on the evaluation of radar cross section measurement facilities. A history and summary of the program are found in Volume I. Volume IIa contains a detailed analysis and evaluation of backscattering tests performed on five closed cylinder models which constituted the main portion of the evaluation program. Volume IIb is classified and is a summary of test results on two satellite models which represent a more typical target.

In a brief statement, the purpose of this volume is to describe the cylinder models, the range environment in which they were tested, the theoretical scattering characteristics of these targets, and most important, the analysis of the cylinder backscattering patterns submitted by the ranges taking part in this test program.

To begin our story we start with a restatement of the program and the required tests set forth by the contract, parts of which have already been stated in Volume I, then we briefly describe the procedure we used to reduce and evaluate the data. At the end of this introduction, we give a short outline for the remaining chapters in this volume.

The evaluation procedure is specified in detail in Exhibit A of the Contract. Summaries and excerpts are given below for those parts which apply to the cylinder models and tests.

1.1 Objectives

a) To evaluate existing radar cross section measurement facilities.

b) To provide a guide to optimize utilization of existing radar cross section measurement facilities.

c) To identify critical problem areas in radar cross section measurements.

d) To develop plans for attacking the critical problem areas identified. Special emphasis is to be placed on the measurement of large objects (30 feet or longer).

1.2 Work Requirements

1.2.1 Experiments to be Performed

A series of radar backscatter measurements shall be performed at the following ranges.

a) Conductron Corporation, Ann Arbor, Michigan

b) Radiation Incorporated, Melbourne, Florida

c) General Dynamics, Fort Worth, Texas

d) RAT SCAT, Holloman AFB, New Mexico

e) Micronetics, San Diego, California

f) Air Force Avionics Laboratory, Wright-Patterson AFB, Ohio.

Measurements shall be performed on five cylinders at the frequencies shown in Table I-1. The frequency tolerance is $\pm$ 0.1 percent. Four polarization combinations, HH, VV, HV, and VH shall be required at all frequencies and both phase and amplitude data shall be recorded for all facilities which have the needed polarization and phase capabilities. Amplitude and phase information is to be provided as a function of target aspect angle through 360^{o} about a plane containing the longitudinal axis of the model. In addition to the analog data, digital data is to be recorded in the finest increments of aspect and amplitude normally available from each of the several ranges. In all cases, measurements are to be made for a single, specified roll angle for the cylinders. Measurements at the Air Force Avionics Laboratory shall be limited to the 1/8 and 1/16 scale cylinders at 1360 and 2720 MHz.

1.2.2 Models

The Contractor (The University of Michigan) shall provide five cylinders, the largest of which is to be 32 feet long and 5 feet in diameter. The other four cylinders are to be 1/2, 1/4, 1/8 and 1/16 scale models of the largest cylinder.

1.2.3 Theoretical Computations

The Contractor shall compute expected radar cross section for each of the cylinders under the experimental frequencies and polarization conditions specified. To avoid duplication, the results of a parallel contract, AF 33(615)-3166, with the Norair Division of Northrop Corporation shall be used to the maximum extent possible.

1.2.4 Data Analysis

The Contractor shall perform an analysis of all data using the technique most appropriate for the attainment of the stated objective. Comparisons shall be made between measured data and theoretical calculations, between similar measurements at different ranges, and between full size and scaled measurements.

Comparisons shall be made of the total performance of the several ranges and any special measurement capabilities that are demonstrated should be noted.

TABLE I-1

FREQUENCY-SCALE MATRIX FOR CYLINDER TESTS
SHOWING RESULTING ka VALUES

Frequency (MHz) \ Scale	(32') Full	(1/2)	(1/4)	(1/8)	(1/16)
170	2.72	1.36	—	—	—
340	5.44	2.72	1.36	—	—
680	10.9	5.44	2.72	1.36	—
1360	21.7	10.9	5.44	2.72	1.36
2720	—	21.7	10.9	5.44	2.72

Explanations are needed for the meaning of the polarization terminology and the significance of Table I-1. The polarization terms HH and VV are the co-polarized and VH and HV are the cross polarized symbols. Here V and H refer to the orientation of the electric field vector relative to the ground; V indicates that the E field is vertical and H that it is horizontal. The first letter represents the polarization of the transmitting antenna and the second letter that of the receiving antenna.

Table I-1 is a summary of the frequency and size relationships and the ka values for each frequency - scale combination for which tests are performed; k is the wave number $2\pi/\lambda$, a is the cylinder radius and λ is the incident wavelength. The five cylinders vary in length from 2 feet (1/16 scale) to 32 feet (1/1 scale) and the five frequencies vary from 170 MHz to 2720 MHz. These model sizes and frequencies are combined to produce five electric circumferences (ka): 1.36, 2.72, 5.44, 10.9 and 21.7. This range in ka extends from the resonant region (1.36 and 2.72) into the physical optics region (10.9 and 21.7) with ka=5.44 being in the transition region between the two. Patterns with the same ka and polarization should have identical forms but be shifted in absolute power levels by some multiple of 6 dB, depending on the ratio of the frequencies being compared. For example if the frequency ratio is 2 to 1 there is a 6 dB difference in power levels, if the ratio is 4 to 1 the difference is 12 dB, and so on.

1.3 Some Difficulties in Evaluating Radar Ranges

There are no formal standards set forth by recognized authorities by which radar cross section ranges can be evaluated because of the large variety of shapes that range customers need measured as well as the number of conditions under which the measurements can be made. An obvious standard might be the comparison of theory and experiment for a body whose scattering behavior is known exactly enough to be considered a standard, but, aside from the sphere, such a body is hard to come by. In subsequent portions of this report, we assume that the cylinder is understood well enough to be a standard in this context, but the reader will soon see deficiencies even in this simple model. Furthermore, even if the "standard" target is agreed upon, there arises the question what constitutes standard performance. Obviously, it is not logical to demand that a given range measure a given target with an accuracy of $\pm$ 1 dB without specifying if this figure applies to a 20 dBsm scatterer or a -10 dBsm scatterer, or if it applies to a flat plate or to a cone-sphere, or if it is to hold at 3000 MHz or at 300 MHz, or if it refers to the peak values of the static pattern or those on the slope of the fourth sidelobe. Range standards clearly involve many more parameters than we were able to investigate in this project.

Evaluation of the range data was colored by our concept of a typical range user. Being users of our own experimental facility, we had pre-conceived ideas how to judge the patterns the facility produces. Firstly, one looks for a calibration level and decides if the scatterer that produced it is an acceptable one, Secondly, one examines how well the pattern itself was centered on the grid of the paper. Then, because the target usually has features of symmetry, one folds the chart paper in half and holds it up to the light to verify symmetry in the recording itself. Further evaluation proceeds to finer and finer examination; sidelobe levels are checked against theoretical predictions if the body is simple enough, null depths are examined, and null locations compared about the points of symmetry. Near field effects are potential sources of degradation and missing sidelobes signal this possibility. As "typical" range users, we thought these were some of the possible ways data could be evaluated if time and resources permitted.

But the evaluation of data in truth depends upon the use to which it will be put. If one is designing a radar to be used to detect a class of objects, it is the level of expected cross sections one seeks to know and the measurement of specular echoes with an accuracy of 3 dB could well be sufficient. One might wish to develop a discrimination scheme that depends upon the number of nulls in a pattern, so that amplitudes are even less important. On the other hand, if range data are to be used for scattering matrix investigations, better accuracy is desired and the data should be recorded in digital form. Since we cannot foresee all the uses of the data from a typical radar cross section range, we will develop a generalized, as opposed to a specific, approach.

Throughout the report we present details of performance in such a way that the reader can assign his own rating if he disagrees with our ratings. We give tables listing, for example, the number of errors less than one dB that a given range produced for a given target at a given frequency; we assign a rating to that performance, but the reader is free to assign his <u>own</u> rating, depending upon <u>his</u> concept of the accuracy of the data <u>he</u> would need.

1.4 Evaluation Procedures

An enormous amount of data were collected during the course of the range evaluation program. Seventy-two cross and co-polarized measurements were made on the five cylinder targets at each range to produce a total of 360 separate backscattering patterns for evaluation. One of the larger and more important tasks in this program was to determine efficient, informative, and accurate methods for reducing and presenting the raw scattering data. Unfortunately it is difficult for more than a few people at a given time and place to agree on universal and identical definitions for the three underlined adjectives in the previous sentence. As in many practical problems the underlined adjectives contradict one another in their extremes and a trade-off is necessary to achieve an optimum satisfaction of all three at the same time. What is optimum for one situation is not necessarily so for another and herein lies the problem of obtaining a universal evaluation process. Even if the reader disagrees with the methods used here we hope some of the techniques will be helpful to him in achieving a more acceptable form of evaluation.

Shortly after samples of the test patterns started to arrive in Ann Arbor, overlay comparisons were made on a light table between similar test data and between theory and measurements. Although the observer obtains much information by making the comparisons, he finds it difficult to represent the results of such a comparison unless facts and figures are recorded. In addition, we knew that patterns to be submitted by two of the ranges would have different scaling factors, thus restricting the effectiveness of direct comparisons on a light table. It appeared that whatever reduction method was used, some form of point by point recording technique would have to be developed to take the place of direct overlay comparisons. After considerable deliberation we decided to record the amplitude of pattern peaks and the angular location of pattern nulls. Heavy emphasis was placed on the lobe structure in the neighborhood of end-on and broadside angles of incidence where the only specular returns are located. Limited peak and null information was recorded in the aspect region near and about 45^{o} also.

After 60 percent of the data were reduced and recorded in tables, some cursory examinations of these tabulations were made. We observed that there was sufficient disagreement in the end-on and broadside data alone to point out the difficulties each range had performing their tasks. Furthermore with 40 percent of the data expected to be available to us only in the closing days of the contract, we had to reduce the amount of data to be evaluated to a level which we could handle in the time allotted. After considering the surrounding circumstances we concluded that a detailed analysis of the two spectular points ($\theta = 0^{o}$ and 90^{o}) would allow us enough time to evaluate the data and at the same time sufficiently indicate the achievement of the ranges' measuring abilities for most radar applications. In our final critique of the measured data we pass judgement based largely on the amplitude of the end-on and broadside returns.

Comparison and evaluation tests are divided into two groups a) Intra-range tests and b) Inter-range tests. Intra-range tests are a comparison of scaled data from within a given range. No theoretical values are used in these comparisons. Data which should be scaled in 6 dB steps are examined and all deviations are noted. Also in the intra-range tests comparisons are made between the VV and HH returns at end-on incidence. These two values should be the same and any differences are considered errors.

In the inter-range tests measurements from all the ranges are compared with one another and theory on bar graphs. This is done for the amplitude at end-on (VV and HH together), VV broadside, HH broadside and the sidelobes immediately adjacent to broadside (VV and HH spearately). Grades are assigned only to the performance at the end-on and broadside aspect positions.

For the cross polarized patterns (VH and HV) isolation comparisons are made. For pattern cuts taken in a plane of symmetry, such as in the case of these cylinder tests, theoretically there should be no cross polarized return. Thus the cylinder patterns recorded during this program should have no VH or HV return and any return that does exist is due to unwanted coupling, background or related effects. In the isolation test the maximum cross (VH or HV) returns (in dB)

are subtracted from the maximum direct (HH or VV) returns. As a rule, the maximum cross and direct returns are located near or at broadside. The larger the difference between the cross and direct returns the better the isolation. Final results showed that the isolation levels for the ranges are between 20 and 30 dB.

The measurements show that the patterns obtained by all the ranges for tests of the same model are similar in form. There are cases where differences larger than 2 dB were found between measurements of different ranges and between measurements and theory. The largest single cause of errors was near-field distortion, which occurs when the distance between the radar and the target is not sufficiently large. Near-field problems are easy to recognize and predict. For some applications, the size and rate of occurrence of the errors found in this evaluation may not be tolerable and for other applications they may be acceptable; the reader must be the final judge of this.

1.5 Outline of Volume IIa Contents

The next chapter is a description of the cylinder models and the range environment in which they were tested Chapters III through VI cover all the material related to the directly polarized VV and HH tests. Chapter VII covers all the cross polarized VH and HV tests and is similar in form to the previous four chapters. The final chapter (VIII) is the conclusion, but many additional remarks and suggestions are found in Volume I regarding the results presented here.

A further breakdown on the four chapters dealing with the directly polarized topics is as follows. Chapter III contains all the theoretical material for the VV and HH backscattering. Particular emphasis is placed on the physical optics model for calculating continuous theoretical patterns. More accurate calculations than the physical optics results are given for both polarizations at end-on and broadside aspect angles.

Experimental measurements for all the different pattern shapes encountered in the tests are shown in Chapter IV. Also shown here are samples of patterns from each of the outdoor ranges. Some of the difficulties that arose in the measurements are pointed out and analyzed.

In Chapters V and VI the procedures used to reduce and evaluate the data are discussed. Grades are assigned to each of the ranges for their performances in the various tests. These two chapters contain the main critique for the measurements.

II

CYLINDER MODELS AND RANGE ENVIRONMENT

The five scaled cylinders and the range environment in which they were measured are discussed in this chapter. Since part of the test program is based on a comparison of scaled frequency-model tests outlined in Table I-1, it was important that these models be carefully designed and constructed to insure that the accuracy of their dimensions would not be questioned. A short description of the ranges is given along with references to information which contain more details on each of the measuring facilities.

2.1 Cylinder Models

Five right circular, aluminum cylinders were the primary models used in the evaluation program. The full scale cylinder is 32 feet long and 5 feet in diameter and the others are 1/2, 1/4, 1/8, and 1/16 scale models of the largest cylinder. A cylinder is well suited to this program since its scattering pattern can be described rather accurately for most aspect angles by readily available theoretical formulations. On the other hand, its scattering patterns are complicated enough, providing many peaks and nulls, to furnish healthy exercises for testing the ranges.

The scaled models are measured at five frequencies in such a manner as to produce a series of test results which are related to one another by multiples of 6 dB. When these measurements are compared, it is possible to check range accuracies independently of any theoretical calculations. Such tests are called intra-range tests in this report and are comparisons of scaled patterns having the same ka and polarization.

To avoid errors in the scaled measurements and in the theoretical experimental checks, high tolerances were set on the cylinder dimensions. The models were made with sufficient skin thickness and internal bracing to withstand normal handling without deformation or damage. The cylinder dimensions and specified

tolerances are given in Table II-1a. These are essentially as specified in the special instructions associated with the present contract.

The two smaller cylinders were made in The University of Michigan machine shops. The 2 foot cylinder was turned on a lathe from a solid bar of aluminum and the 4 foot cylinder was turned from a piece of standard, thick-walled aluminum tubing. No difficulties were experienced in the fabrication or in meeting the specified tolerances.

Due to the close tolerances and large size of the three larger cylinders, we found it difficult to find interested fabricators who had the capability to make the cylinders. After a careful survey a contract was awarded to Brooks and Perkins of Detroit, Michigan to design and build these three cylinders. Shortly thereafter this company experienced a work stoppage due to a strike. An effort was made to save time by the use of a subcontractor but this proved costly both in time and workmanship. After five months of delay and after a modest change in the required tolerances the cylinders were accepted and delivered. Test results indicate that the relaxed tolerances in Table II-1b caused no problems.

The largest cylinders (32 foot, 16 foot, 8 foot) were formed by attaching pre-rolled skins to an inner framework of circular channels. The inner framework for the 32 foot cylinder included nine 2 1/2" x 1 1/2" x 1/8" channels rolled into circles of the required diameter. The circular forms were supported by longitudinal channels and additional diagonal braces and the skin was held to the framework by a flat head rivets. The method of fabrication used for the 16 foot and 8 foot cylinders is similar except for a more simple inner framework design. For these cylinders, the rivets were countersunk into the skin in order to meet the surface roughness tolerances. The approximate weights of the 32 foot, 16 foot and 8 foot cylinders are 1300, 250 and 30 pounds respectively. Further information on the design of the cylinders is given in Figs. 2-1, 2-2, and 2-3 which are preliminary drawings of Brooks and Perkins.

TABLE II-1

CYLINDER DIMENSIONS

(a) Original Tolerances

Length	Diameter[+] (inches)	Surface Roughness (welds, rivet heads, etc) (inches)	Surface Irregularity[++] (straightness)	Skin Thickness (inches)
32' ± 1/2"	60 ± 1/4	± 0.087	± .033"/ft	0.100
16' ± 1/4"	30 ± 1/8	± 0.043	± .033"/ft	0.050
8' ± 1/8"	15 ± 1/16	± 0.032	± .033"/ft	0.050
4' ± 1/64"	7.5 ± .005	± 0.005	± .005"/ft	0.250
2' ± 1/64"	3.75 ± .005	± 0.005	± .005"/ft	0.125

[+] Cylinders are to be circular to within 0.1 percent of diameter.

[++] The axis of the cylinder is not to deviate from a straight line by more than .250, .125, .063" for the 32, 16 and 8' cylinders respectively. The ends are to be perpendicular to the cylinder axis to within $1/4^{o}$.

(b) Revised Tolerances (January 24, 1966)

	Surface Irrigularities	Circularity
32' Cylinder	± 0.06"/ft	± 0.080"
16' Cylinder	± 0.043"/ft	± 0.043"
8' Cylinder	Same as above	± 0.030"

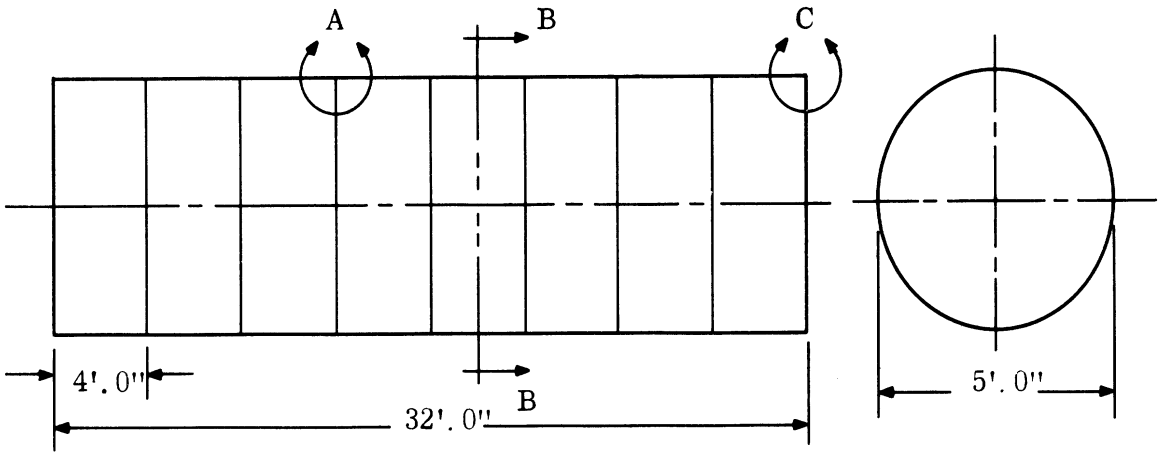

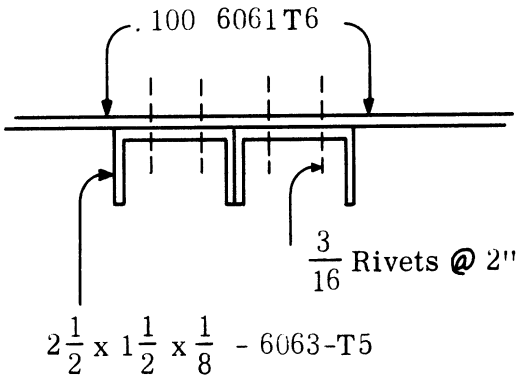

VIEW A - (Sectioned)

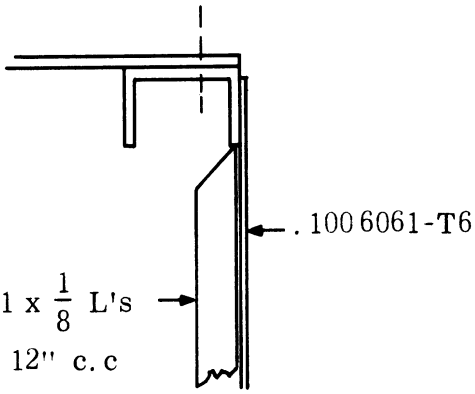

VIEW C (Sectioned)

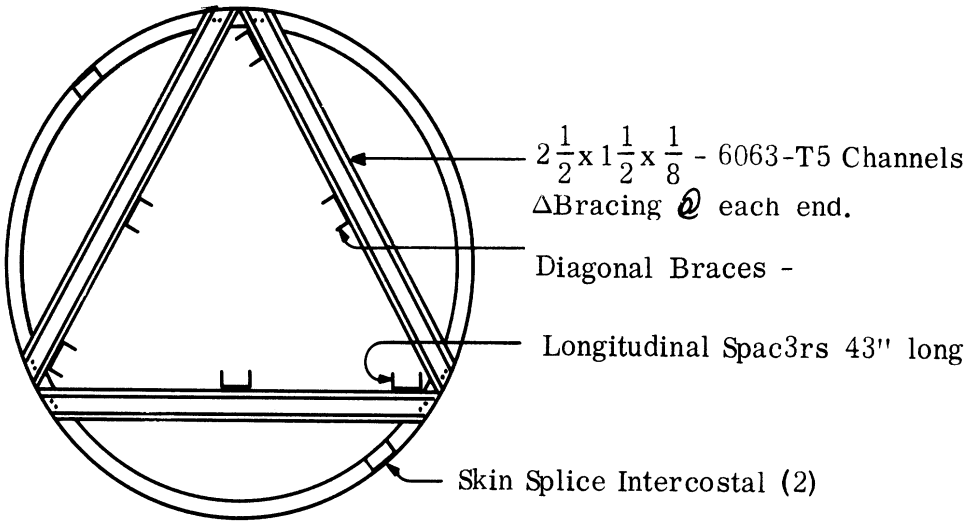

SECTION B-B

16 - 1/4 " Vent Holes Required

Est. Wt. = 1280
Scale = None

FIG. 2-1: BROOKS AND PERKINS PRELIMINARY DRAWINGS FOR 32 FOOT CYLINDER.

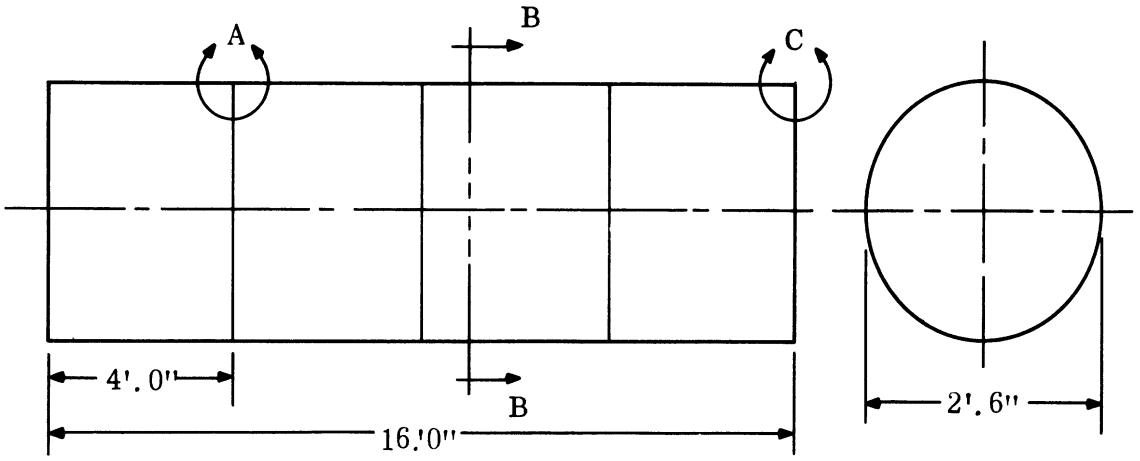

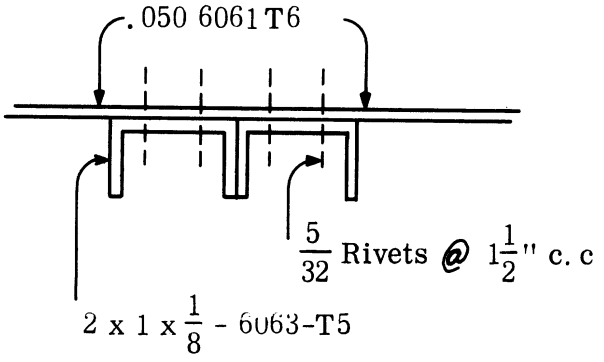

VIEW A - (Sectioned)

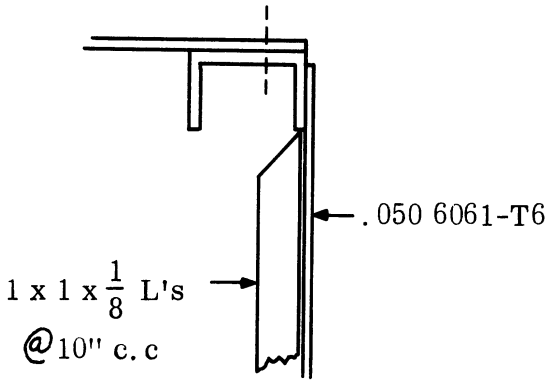

VIEW C (Sectioned)

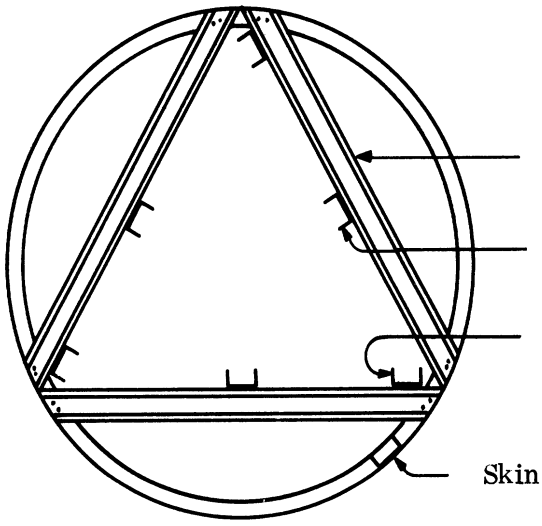

2 x 1 x 1/8 - 6063-T5 Channels

ΔBracing @ each end.

Diagonal Braces -

Longitudinal spacers 44" long

Skin Splice Intercostal

Est. Wt. = 240

SECTION B-B

Scale = None

8 - 1/4" Vent Holes Required

FIG 2-2: BROOKS AND PERKINS PRELIMINARY DRAWINGS FOR 16 FOOT CYLINDER.

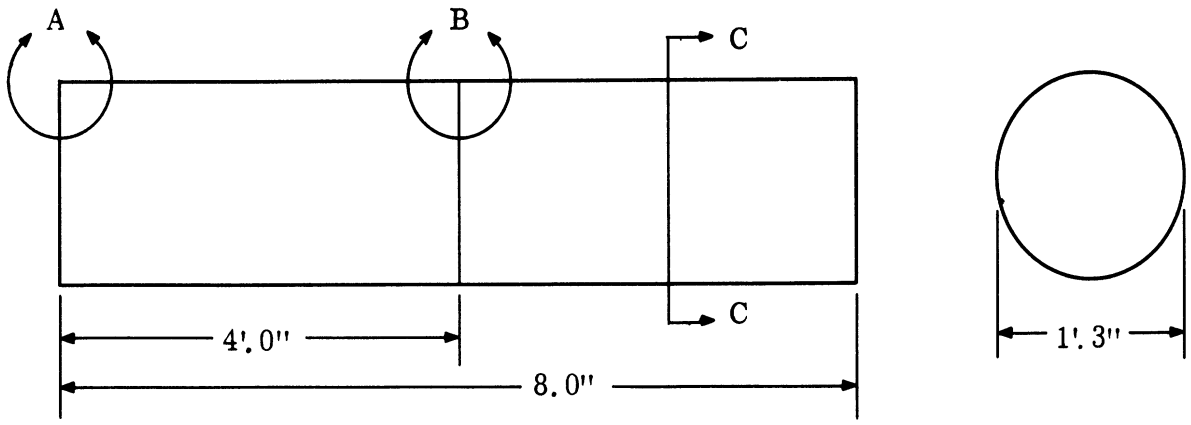

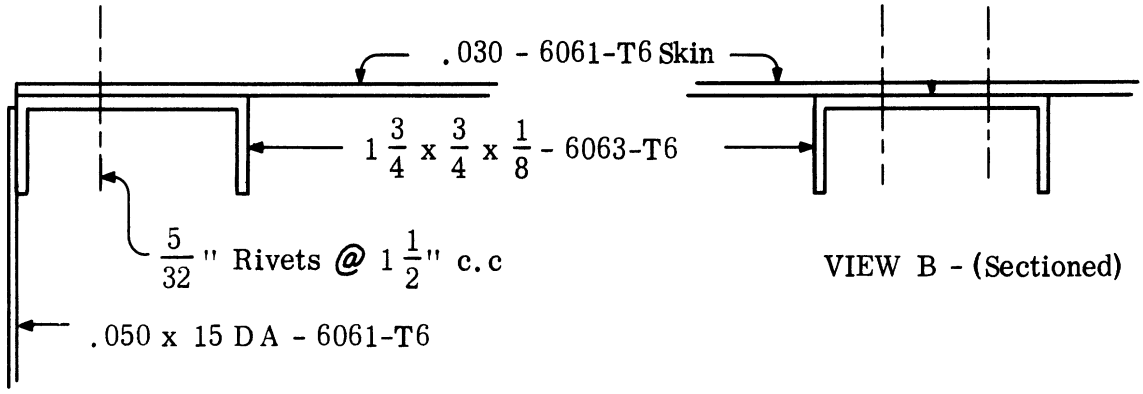

VIEW A - (Sectioned)

VIEW B - (Sectioned)

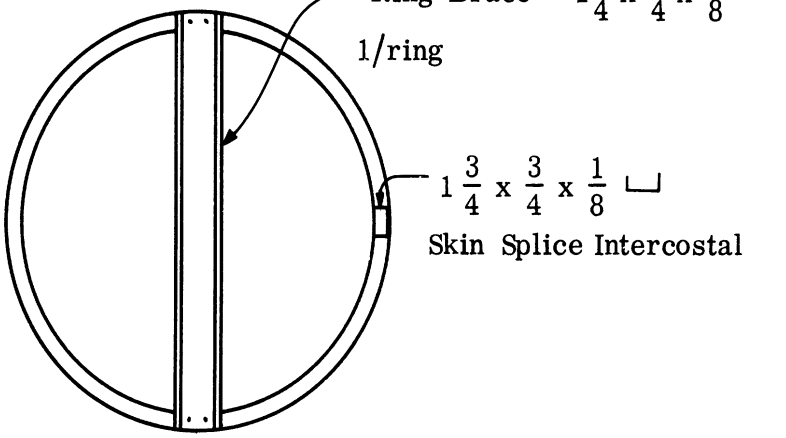

4 1/4" Vent Holes Required

Weight = 27

Scale = None

FIG. 2-3: BROOKS AND PERKINS PRELIMINARY DRAWINGS FOR 8 FOOT CYLINDER.

2.2 Range Environment

The typical model range geometry in which the targets were measured is shown in Fig. 2-4. In all the tests the cylinder was mounted on a pedestal with its axis in the horizontal plane. Rotation took place about the vertical axis with the aspect angle θ being measured relative to the end-on position. For monostatic tests the transmitter and receiver are located together a distance R from the target.

With the exception of Micronetics, all the outdoor ranges made use of the ground plane geometry in their measurements. In the typical ground plane range, the antenna and target heights are adjusted so that the target is placed at the peak of the first lobe formed by the in-phase addition of the direct and ground reflected waves as shown in Bachman et al (1963). At Micronetics (Honer and Fortner, 1964) the ground reflections are minimized by a mound of asphalt in the shape of an inverted V which extends along the path between the transmitter and the target. With this arrangement the target and antenna heights are not as critically dependent on one another as in the ground plane geometry.

Conductron Corporation (Wren, 1964) uses a CW transmitter and employs a balanced RF bridge to separate the transmitted from the received signal. The other four outdoor ranges use pulse-type radar systems with pulse widths between 1.0 and 0.1 microseconds and repetition rates on the order of a few KHz. When pulsed equipment is used the transmitted and received signals are separated in time and range, making it possible to gate out unwanted returns originating outside the target area. Blacksmith et al (1965) give more details on these types of systems and measurement techniques.

Limited tests were made at the Air Force Avionics Laboratory which has an indoor facility with a maximum range of 50 foot (Bahret, 1965). Only VV and HH polarized tests were made on the 2 foot and 4 foot cylinders at 1360 and 2720 MHz.

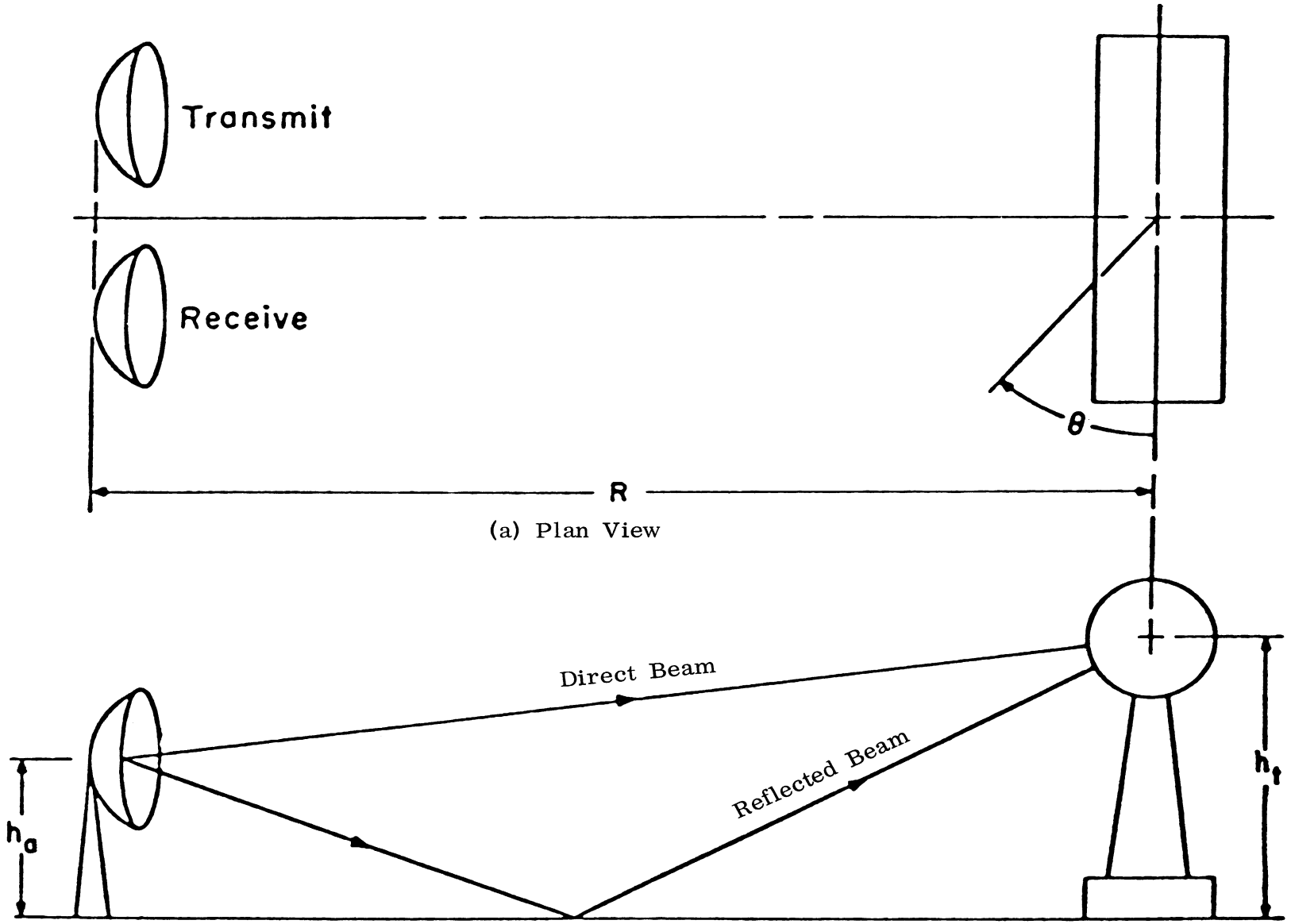

FIG. 2-4: GEOMETRY FOR TYPICAL RADAR CROSS SECTION MEASURING FACILITY.

Results from these tests are tabulated in the appropriate places, but due to the limited amount of data no final grades are assigned to this range. The overall evaluation is limited to the performance of the five outdoor facilities.

All the ranges have similar systems for recording amplitude data in analog form on rectangular pattern paper. The dynamic range of the recorders varies between 40 - 50 dB depending on the facility (see Table II-2). Digital data is also recorded and at two of the ranges phase information is recorded. The type of equipment used at each range is indicated in the same table.

In order for the target to be in the far field (Fraunhofer zone) the distance R between the transmitter and target should be $R \geq 2L^2/\lambda$ where L is the maximum dimension of the target and λ the incident wavelength. The maximum R needed for the schedule of tests given in Table II-2 is about 2900 foot for the case where the 32 foot cylinder is measured at 1360 MHz. The actual ranges used and/or available at each facility are given in the table under "Maximum Range Used". Later, an example is presented showing the effects of insufficient range on measured data.

Since complete descriptions of the ranges to be evaluated are not given in this report, it is appropriate to cite additional references which provide descriptions of all ranges. The facilities and capabilities of the Radiation Incorporated range are described by Landfried and Williamson (1964). This range is the oldest of those being evaluated and during the tests it was operated by Radiation Service Company, a subsidiary of Radiation Incorporated. This facility is now operated by Sigma Incorporated and is described in their 1968 Company Brochure. A description of the General Dynamics/Fort Worth range is given in its brochure (GD/FW 1968). The RAT SCAT range is the newest facility being evaluated and is described in some detail by Marlow et al (1965). Additional information on measurements already made and on operating procedures is given in an Air Force brochure (AFMDC 1968). For more recent information on the Conductron and the Micronetics ranges the reader is referred to 1968 Company Brochures.

TABLE II-2

SOME CHARACTERISTICS OF THE SITES

Site	Transmitter	Maximum Range Used*	Geometry	Data Recorded		Digital Equipment
				Type	Dynamic Range	
Conductron	CW	200'	Ground Plane	Amplitude	40 dB	Paper Tape
Radiation Service	Pulse	1000'	Ground Plane	Amplitude	40 dB	Punch Cards
General Dynamics	Pulse	1800'	Ground Plane	Amplitude Phase	50 dB 360°	Paper Tape
RAT SCAT	Pulse	1200'	Ground Plane	Amplitude Phase (L-band)	50 dB 360°	Paper Tape
Micronetics	Pulse	600'	Direct "Λ"	Amplitude	40 dB	Magnetic Tape
Avionics Laboratory	CW and Pulse	50'	Indoor Free Space	Amplitude	40 dB	None

* Desired Maximum range 2900'

III

THEORETICAL BACKSCATTERING MODELS

In this chapter we discuss the theoretical models that were used to study and calculate the backscattering behavior of finite circular cylinders for VV and HH polarizations. Lest anyone be led astray and believe that there is an exact mathematical formulation available for determining the expected cross section of finite cylinders, let us state most emphatically that there is no such solution for this problem. All the techniques discussed here are approximate. Since there is no exact solution, precise limits of accuracy cannot be assigned to the approximate methods. Estimates of accuracy are made for those theoretical techniques which are used to evaluate the experimental data and these estimates are based on experience in dealing with both experimental and theoretical material for finite cylinders.

Continuous patterns for aspect angles between 0 and 90^{o} are calculated for all five values of ka for the cylinders. For the two lower values (1.36 and 2.72) separate patterns for VV and HH polarization are given since for these cases the polarization differences are more noticeable. As ka grows larger, polarization differences in VV and HH patterns become smaller. For the larger values of ka (5.43, 10.86 and 21.72) the polarization differences are sufficiently small to represent the VV and HH patterns with the same theoretical pattern for most applications. Thus the physical optics model, which is developed in the Appendix, is used to determine the theoretical patterns for the three larger ka cases. This model becomes meaningful for large values of ka where the VV and HH patterns tend to look alike.

Particular emphasis is given to the calculation of the cross sections at end-on and broadside aspect positions, because these results are compared directly with experimental tests in later chapters. We estimate, based on experience, that these results should be accurate to within $\pm$ 1.0 dB. A more detailed discussion of the relationship between theory and experiment is given in the last section of Chapter IV.

3.1 Backscattering from Cylinders

The theoretical techniques used to analyze the radar cross section behavior of the cylinders are:

a) Numerical solution to the integral formulation for the scattered field (Oshiro, 1967).

b) Keller's geometrical theory of diffraction (Bechtel and Ross, 1966).

c) Traveling wave approximation (Fisher, 1967).

d) Phasor addition of physical optics contributions from a cylinder and disc.

e) Separation of variables in two dimensions for a cylinder (Mentzer, 1955).

f) Andrejewski's solution for backscattering by a conducting circular disc (Schmitt, 1959).

We employed all the models except (b) at one time or another to produce continuous patterns and/or to calculate precise cross sections at specific aspect angles. In particular, we used methods (a), (c) and (d) to generate continuous scattering patterns for aspect angles between 0 and 90^{o} and used methods (e) and (f) to calculate cross sections only at broadside and end-on aspect positions.

The integral equation approach (a) is used to calculate cross sections in the resonant region (ka=1.36, 2.72) where the differences in VV and HH polarized patterns are noticeable. This is a numerical technique for evaluating an integral equation representation for electromagnetic scattering. For ka values equal to or greater than 5.43 the computer time and memory requirements tend to become prohibitive in the numerical solution for this formulation, and other approaches to the problem such as methods (b) and (d) become more practical. Norair Division of Northrop Corporation developed the numerical technique called the Source Distribution Technique (SDT) and results from SDT were obtained for this evaluation program through the Air Force Avionics Laboratory. A description of the mathematical development and computer program can be found in a series of reports by Oshiro (1965, 1967).

Complete data from the SDT program was supplied only for VV and HH polarization for ka=1.36. Partial results were furnished for ka=2.72 and 5.43 but these datum points were not sufficiently close together to construct continuous patterns. Fortunately, Fred Fisher (1967) of Radiation Service Company developed a traveling wave model (c) for VV and HH patterns for ka= 2.72. Fisher's technique incorporates portions of methods (d) and (e) along with a traveling wave contribution for HH polarization. Although method (c) is not as accurate as the numerical approach of (a), it does show the salient features of the VV and HH patterns.

Method (d), the phasor addition of the physical optics contributions for a cylinder and disc, is discussed in detail in the Appendix. This formulation becomes more accurate for increasing values of ka (see Ch. IV). Continuous patterns for ka=5.43, 10.86 and 21.72 are obtained for this model.

The last two techniques, (e) and (f), are used to calculate cross sections for all ka values and both polarizations at broadside and end-on aspect positions. In the last section of this chapter plots of cross section versus ka curves are given for the 32-foot cylinder based on these models. The cross sections of the other four scale models are found by subtracting the appropriate number of 6dB increments from the full scale values. Broadside and end-on cross sections are displayed in tables for all the cylinder models.

3.2 Cylinder Scattering Patterns

Ordinarily ten theoretical patterns would be necessary to describe all the experimental scattering configurations for VV and HH polarizations which arise during the cylinder measurements if they are normalized to the square of the wavelength (λ^2) . Mathematically, this corresponds to casting the scattering expression into a form like that in Eq.(A-14) in the Appendix. The ten patterns consist of VV and HH data for the five ka cases. Both polarized patterns are presented for ka=1.36 and 2.72. In the cases of the three larger ka values, the physical optics formulation was used to calculate the cross section data; thus the VV and HH theoretical patterns are the same. Because of this, seven

patterns instead of ten are needed to describe the scattering behavior of the cylinder tests. One phase pattern for ka = 5.43 is shown and it was obtained from Eq. (A.16).

The parameters for the five cylinder and frequency combinations are:

Case	1	2	3	4	5
ka	1.36	2.72	5.43	10.86	21.72
$k\ell$	17.4	34.8	69.6	139.2	278.4

In all cases the cylinder dimensions are such that $k\ell$=12.8 ka. Figures 3-1 through 3-5 present the scattering functions for σ/λ^2 in dB as a function of aspect angle θ. It is sufficient to display 90^o of the pattern because of the target symmetry; $\theta = 0^o$ is the end-on and θ=90^o is the broadside aspect position.

For Case 1 the VV and HH patterns are given in Fig. 3-1. Some noticeable differences in the two polarizations are the deeper nulls in the HH pattern and 3 dB higher broadside (θ=90^o) return in that pattern. These patterns were obtained from the SDT (Oshiro, 1967) program through the Air Force Avionics Laboratory. Later experimental data from all the ranges will be superposed on these theoretical patterns.

There are still noticeable polarization differences in Case 2 (Fig. 3-2), namely the HH pattern has a significant traveling wave lobe near θ=20^o and a 2 dB higher broadside (θ=90^o) return compared to the VV pattern. These patterns are based on Fisher's work (1967), method (c). These results do not agree as well with experiment as those in Fig. 3-1.

Cases 3, 4 and 5 are given in Figs. 3-3, 3-4 and 3-5. These patterns were obtained directly from the expression (A.14) which is method (d). For these larger ka patterns, polarization differences grow smaller with increasing size. Also the pattern oscillation increases, producing more lobes to such an extent that for Case 5 in Fig. 3-5 , only the lobe peaks are shown beyond 50^o.

An example of a phase pattern is given in Fig. 3-6 for Case 3. The cross section pattern in Fig. 3-3 has been reduced to the same angular scale as the phase pattern for the sake of comparison. This example of phase data is determined by method (d) , physical optics, and is shown here to demonstrate the rapid fluctuations of a typical phase pattern.

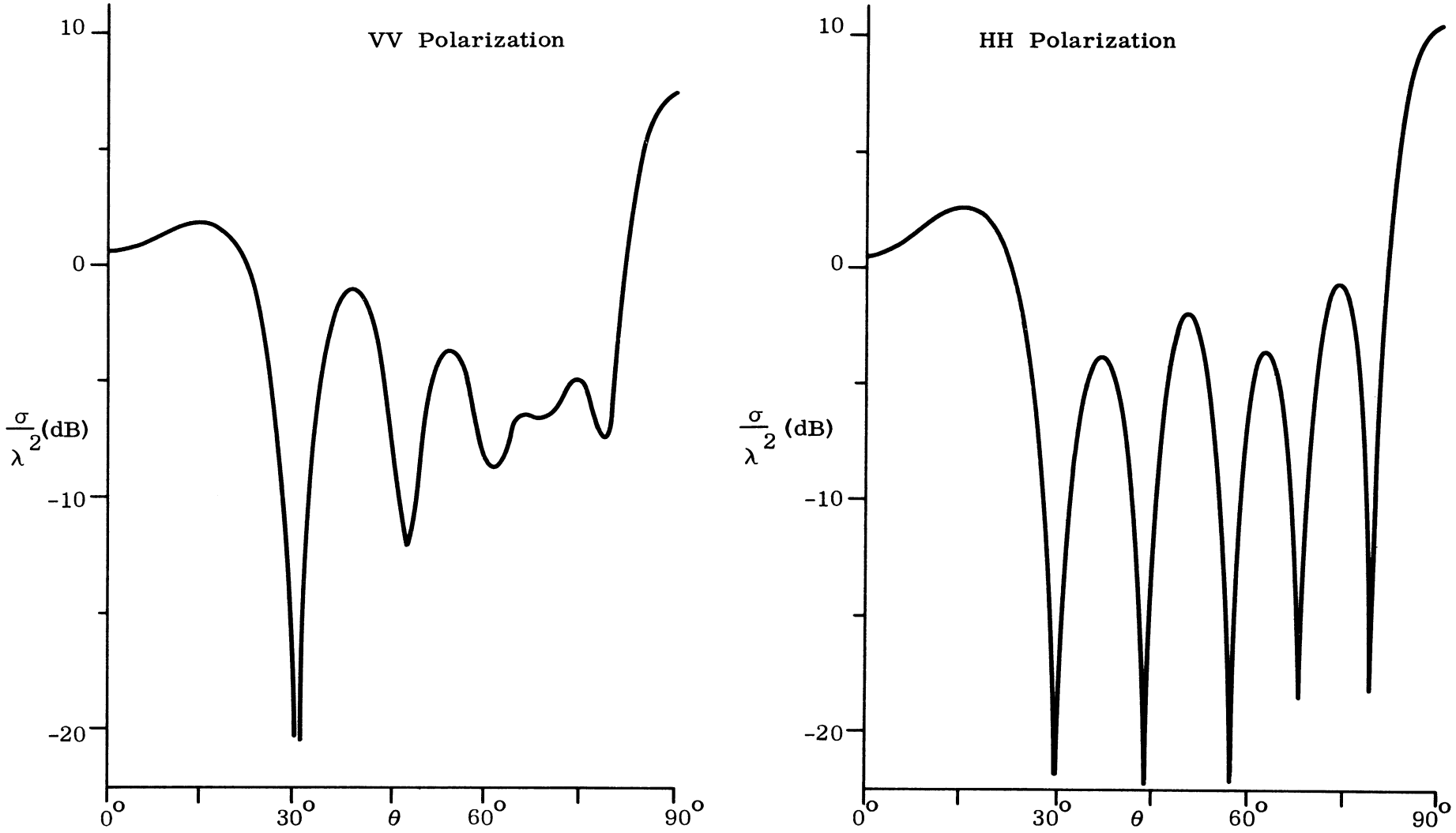

FIG. 3-1: THEORETICAL PATTERNS FOR ka = 1.36 AND kℓ = 17.4.
Calculated by Method (a) NORAIR's SDT Method.

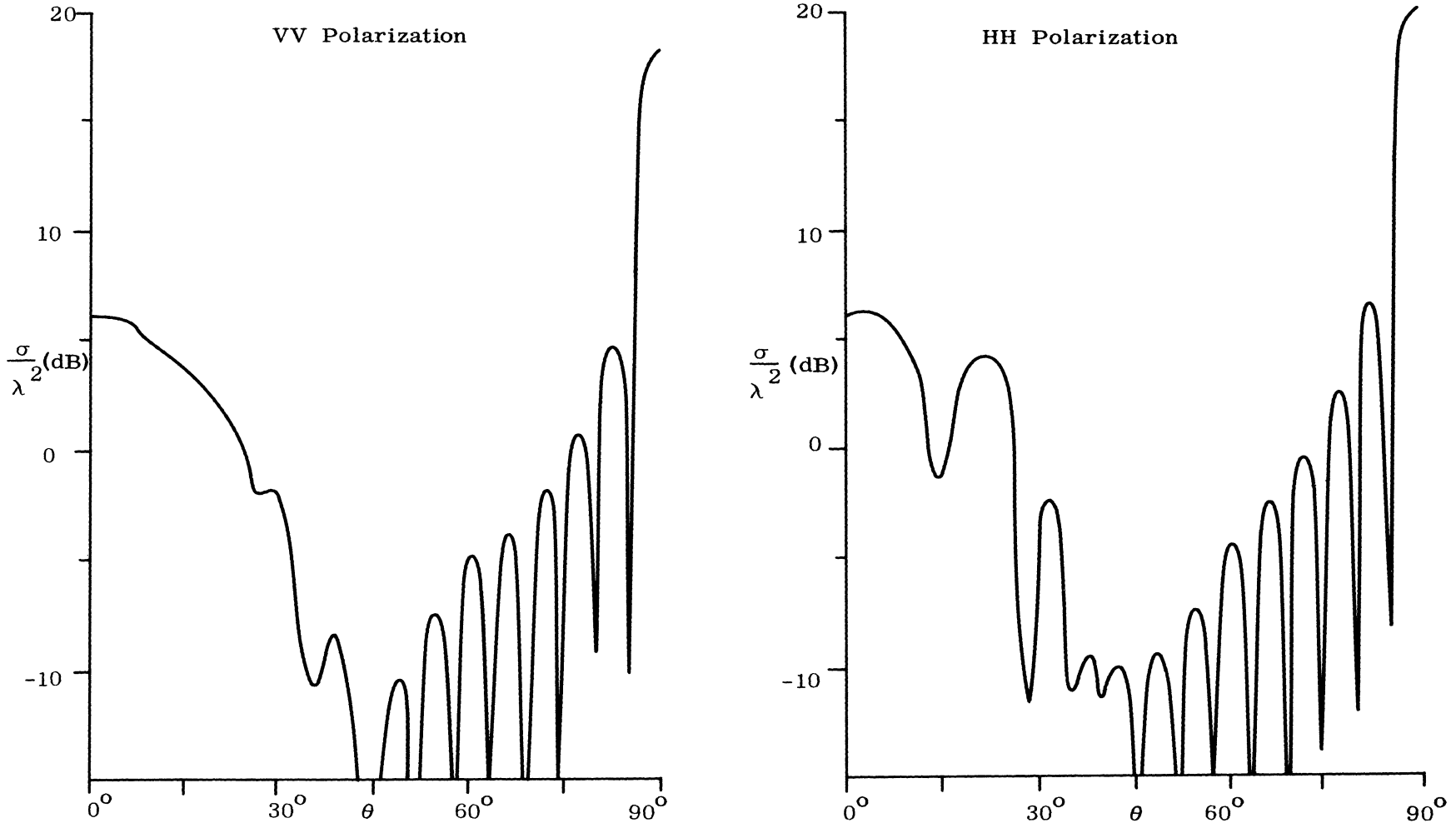

FIG. 3-2: THEORETICAL PATTERNS FOR ka = 2.72 AND kℓ = 34.8.
Calculated by Method (c), supplied by Radiation Services.

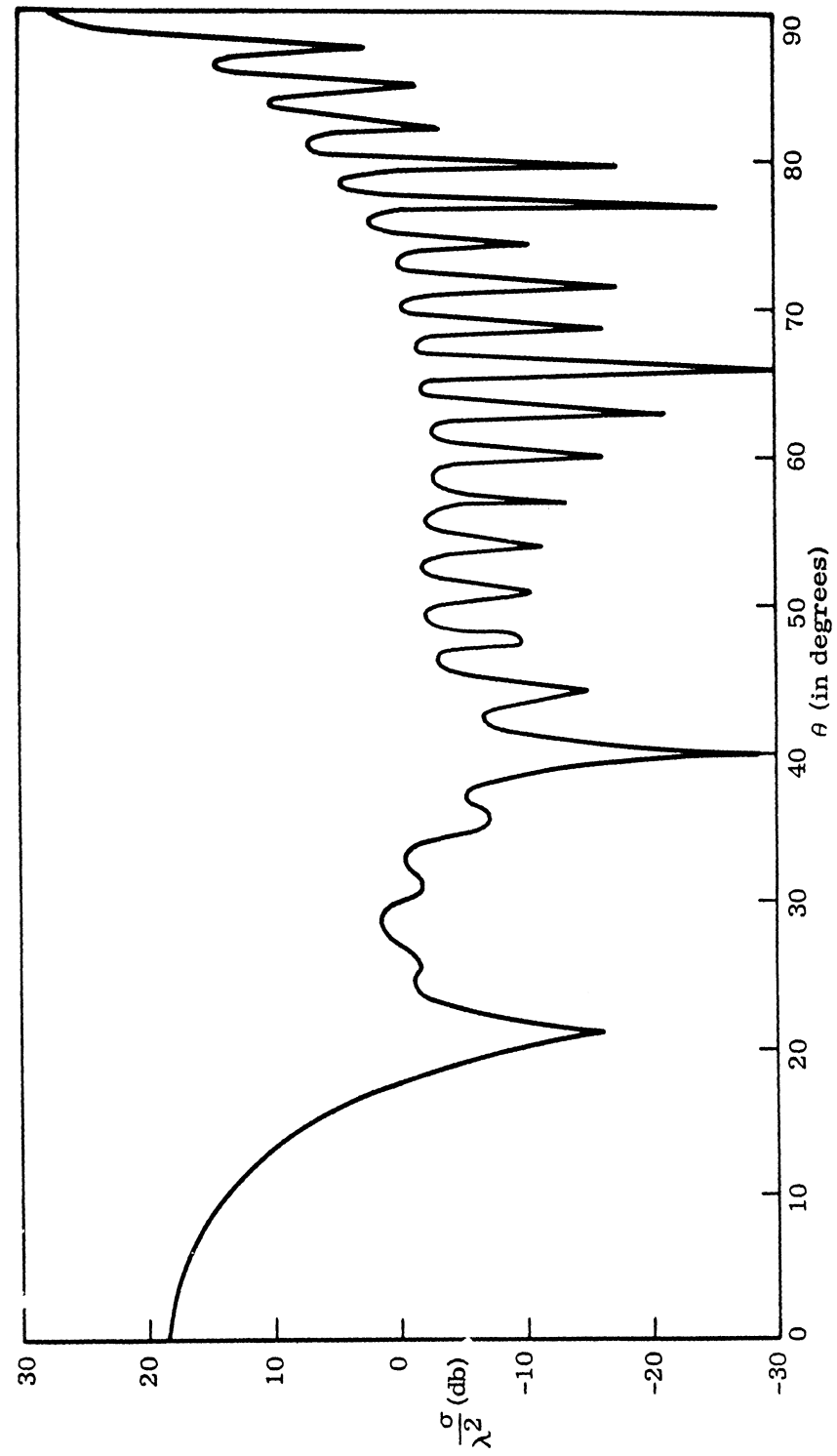

FIG. 3-3: THEORETICAL PATTERN FOR ka = 5.44 AND kℓ = 69.6. Calculated from Eq. (A.14), Method (d).

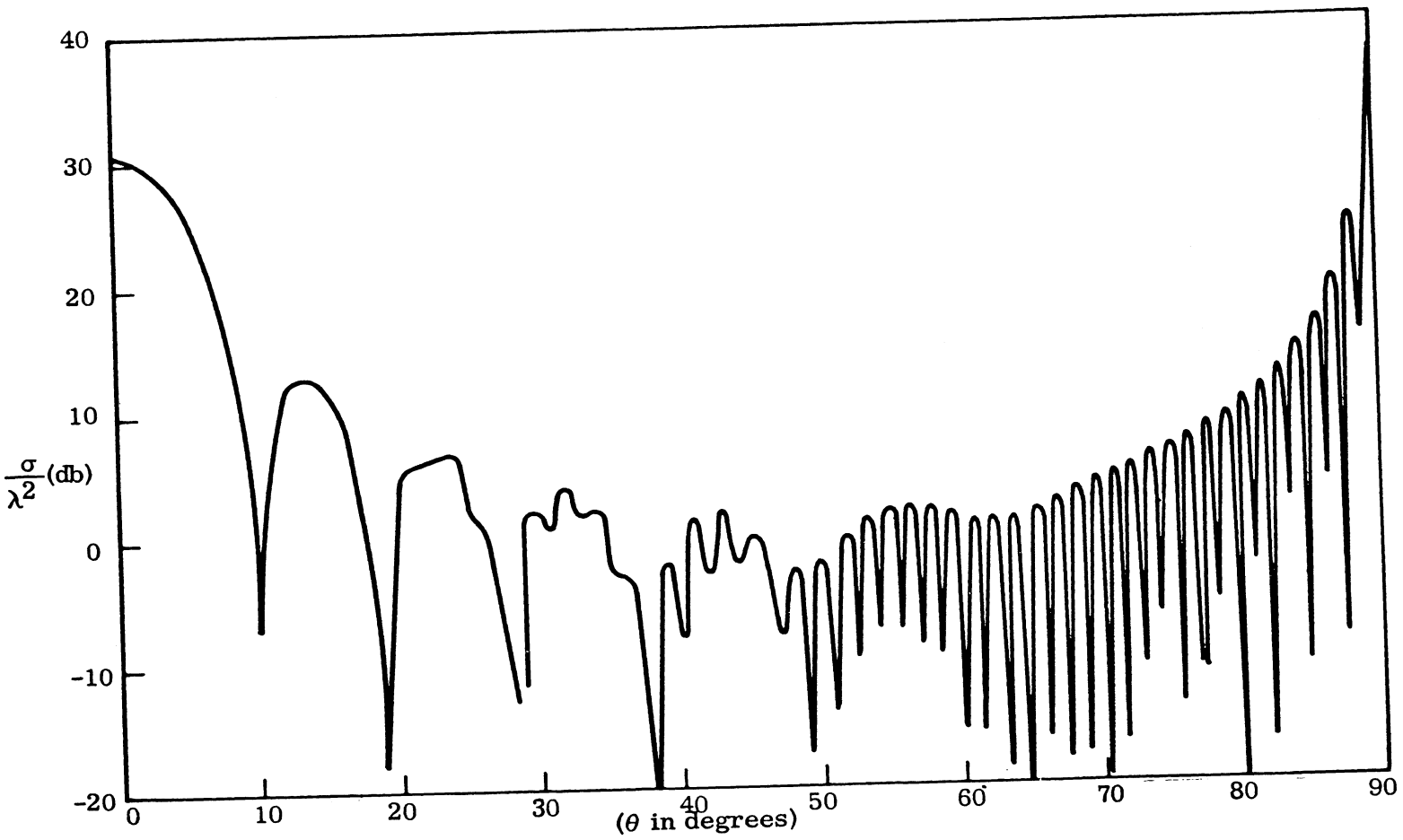

FIG. 3-4: THEORETICAL PATTERN FOR ka = 10.9 and kℓ = 139.2. Calculated From Eq. (A. 14), Method (d)

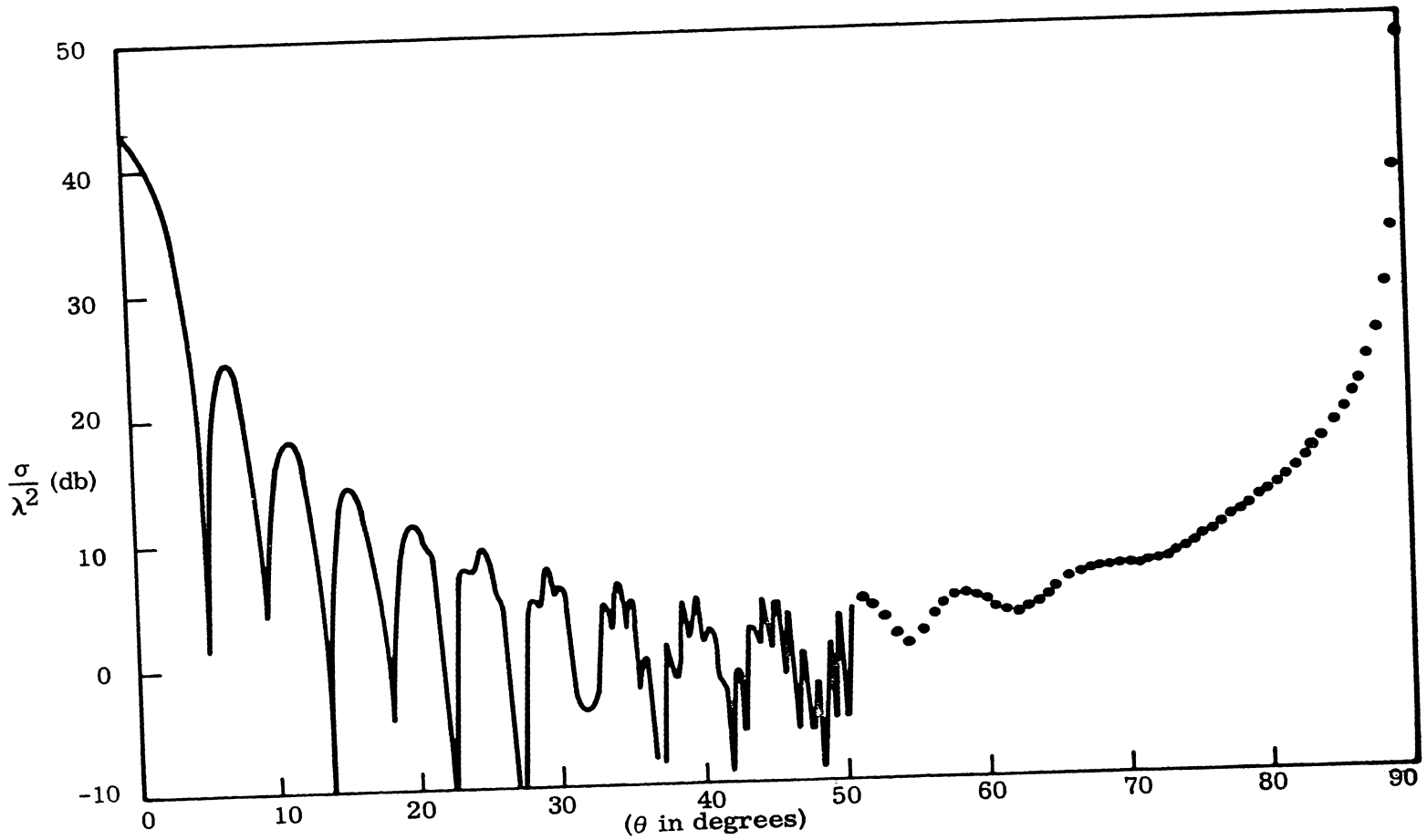

FIG. 3-5: THEORETICAL PATTERN FOR ka = 21.7 AND $k\ell = 278.4$. • Indicates peak positions for oscillations with 0.65^o period. Calculated from Eq. (A.14), Method (d) .

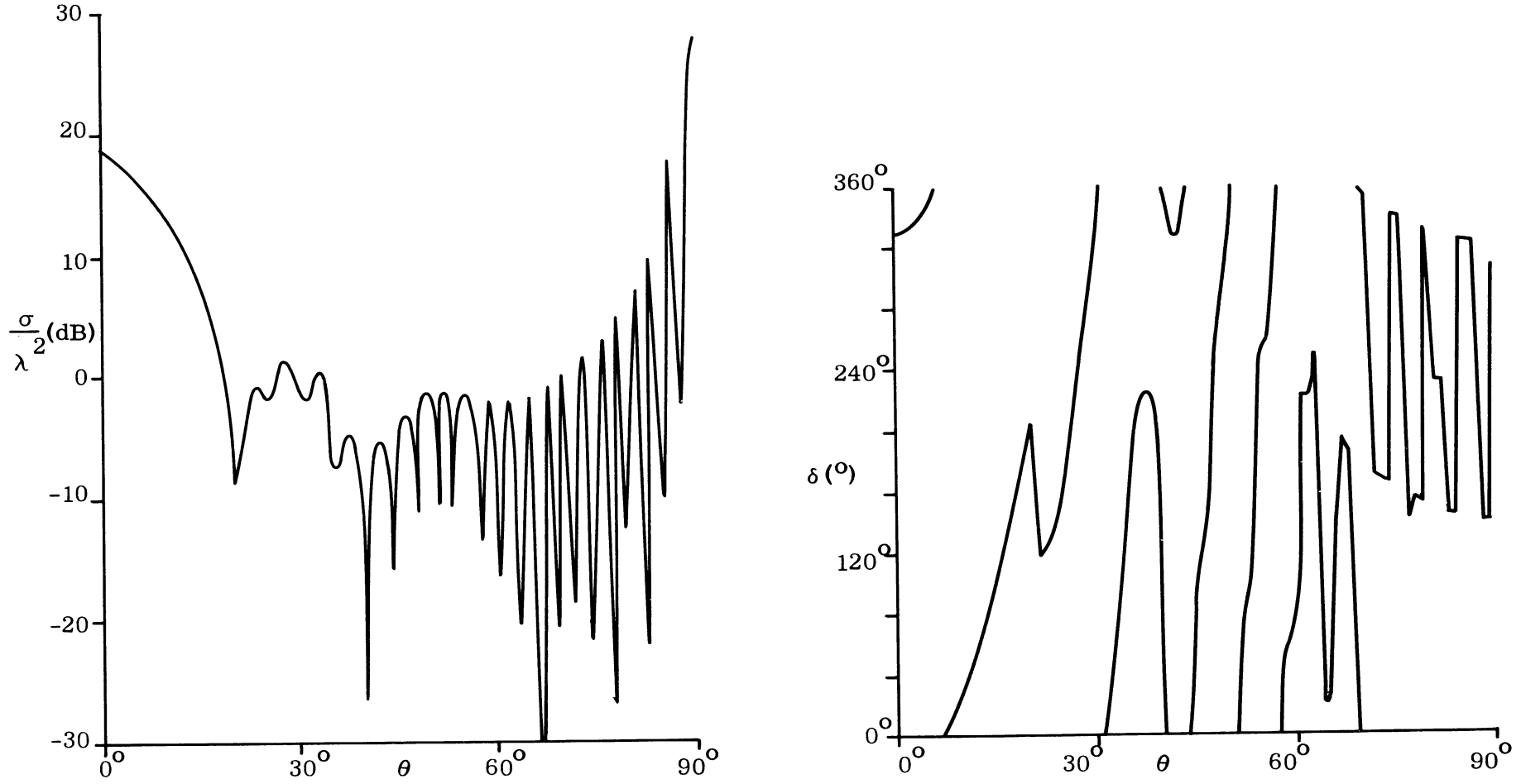

FIG. 3-6: THEORETICAL CROSS SECTION AND PHASE PATTERNS FOR ka = 5.43. Calculated from Eqs. (A.14) and (A.16), Method (d)

3.3 End-on and Broadside Cross Sections

Detailed calculations are presented here for the cross sections at broadside and end-on and are based on methods (e) and (f). Using method (e), Mentzer (1955) obtains cross section expressions for VV and HH polarizations for a finite cylinder, which for broadside incidence, reduce to

$$\sigma_{\perp} = \sigma_{VV} = \frac{4\ell^2}{\pi} \left| \sum_{-\infty}^{\infty} (-1)^n \frac{J_n'(ka)}{H_n^{(2)'}(ka)} \right|^2 \tag{3.1}$$

and

$$\sigma_{\parallel} = \sigma_{HH} = \frac{4\ell^2}{\pi} \left| \sum_{-\infty}^{\infty} (-1)^n \frac{J_n(ka)}{H_n^{(2)}(ka)} \right|^2 \tag{3.2}$$

where a and ℓ are the radius and length of the cylinder. The cylindrical functions J_n and $H_n^{(2)}$ are the Bessel functions and outgoing Hankel functions of order n. Primes in (3.2) indicate differentiation with respect to the total argument ka. As ka increases beyond 5 or 6, $\sigma_{\perp}$ and $\sigma_{\parallel}$ approach the physical optics form

$$\sigma(90^o) = ka\,\ell^2 \tag{3.3}$$

which is (A.13) with $\theta=90^o$.

Plots of the expressions in (3.1) - (3.3) are shown in the upper curve of Fig. 3-7. $\sigma_{\parallel}$ (90^o) and $\sigma_{\perp}$ (90^o) differ in the region for ka < 10. When ka > 10 they are the same as shown by the circle portion of the curve. The curves in Fig. 3-7 are cross sections in dB relative to a square meter (dBsm) as a function of ka for the 32'x5' cylinder. All other cross sections for the smaller cylinders can be derived from these curves and this will be done shortly.

The lower curve of Fig. 3-7 is the cross section of a circular flat plate or disc obtained from method (f) by Schmitt (1959). It is noted that the end-on view ($\theta=0^o$) of the finite cylinder is a disc connected to the cylinder, whereas the theoretical curve in Fig. 3-7 is for a disc alone. For the smaller ka values it is to be expected that the disc model is less accurate than the broadside cylinder model, but it is the best theoretical method available for the end-on view.

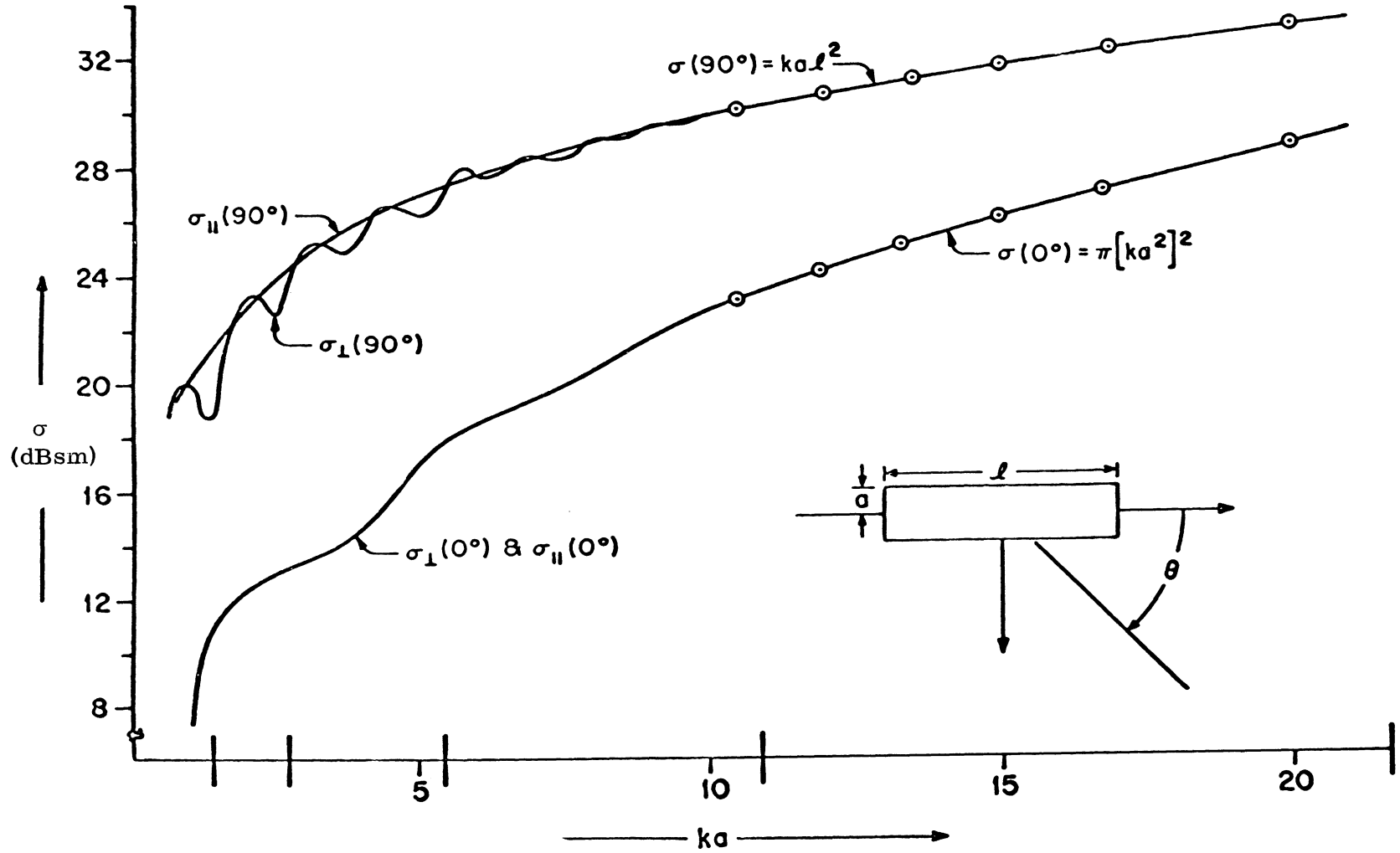

FIG. 3-7: THEORETICAL RADAR CROSS SECTION VALUES AT END-ON AND BROADSIDE FOR 32' x 5' CYLINDER.
Method (e) was used to obtain the upper curve and Method (f) the lower curve.

Schmitt's technique is an extension of Andrejewski's thesis done at Technische Hochschule in Aachen, Germany in 1952. The form of the solution is uncommon and complicated; only the curve in Fig. 3-7 is presented here. The interested reader is referred to the article by Schmitt (1959). For the entire range of ka, the end-on cross section is independent of polarization: $\sigma_{VV} = \sigma_{HH}$. When ka is large enough (ka>10) the physical optics ($\theta=0^o$ in Eq. A. 13) expression is valid

$$\sigma(0^o) = \pi a^2 (ka)^2 \quad . \tag{3.4}$$

This portion of the curve is indicated by the circles.

A display of all the theoretical cross sections for the cylinder models at end-on and broadside for VV and HH polarizations is given in Table III-1. The display is arranged as a function of frequency and model size with constant ka along the diagonal lines connecting the boxes. The full scale values are the same as those in Fig. 3-7 which were obtained from methods (e) and (f). Although the 32-foot model (1/1 scale) was not tested for ka=1. 36, these values were also noted. The cross sections for the 16-foot model (1/2 scale) are found by subtracting 6 dB from the full scale cross sections with the same ka. This procedure holds for going from the 1/2 to the 1/4 scale and so on. Thus, as one moves down a constant ka line there are successive 6 dB reductions in the cross sections for each smaller model.

It would be reasonable to ask why both polarizations for end-on were listed in the table if they are always equal. This was done here because later the same type format will be used to display the experimental data in the intra-range test. By introducing the form of Table III-1 at this time, we allow the reader to become familiar with it. It will be seen that in the experimental results, the end-on cross sections for VV and HH differ by varying amounts which, of course, is an indication of error.

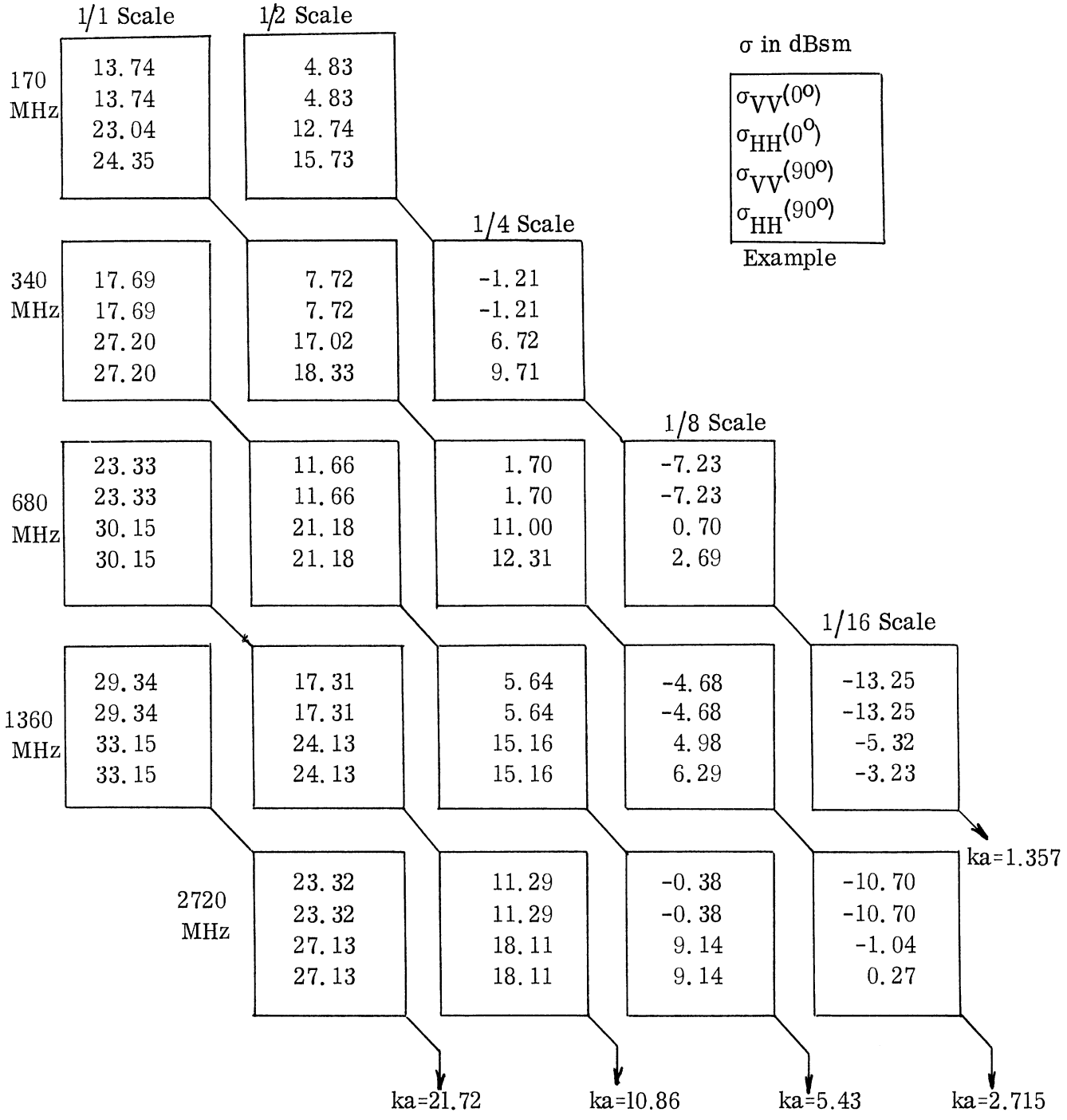

TABLE III-1: INTRA-RANGE DATA DISPLAY FOR THEORETICAL CROSS SECTIONS AT END-ON AND BROADSIDE.

The data in Table III-1 is presented in still another form to give the reader a preview of the inter-range data display. Figures 3-8 through 3-10 are plots of cross section (dBsm) versus frequency of the end-on, broadside VV, and broadside HH theoretical values. Note that the frequency scale is compressed in these figures. The cylinder size and constant ka lines are labeled in the figures. This form of display will be used for the comparison of experimental data from all the ranges and for comparison of experimental data with theory.

In this chapter all the necessary theoretical models were described to give the proper physical picture of the scattering behavior of cylinder targets and to obtain accurate cross section values for evaluating the experimental data in later chapters.

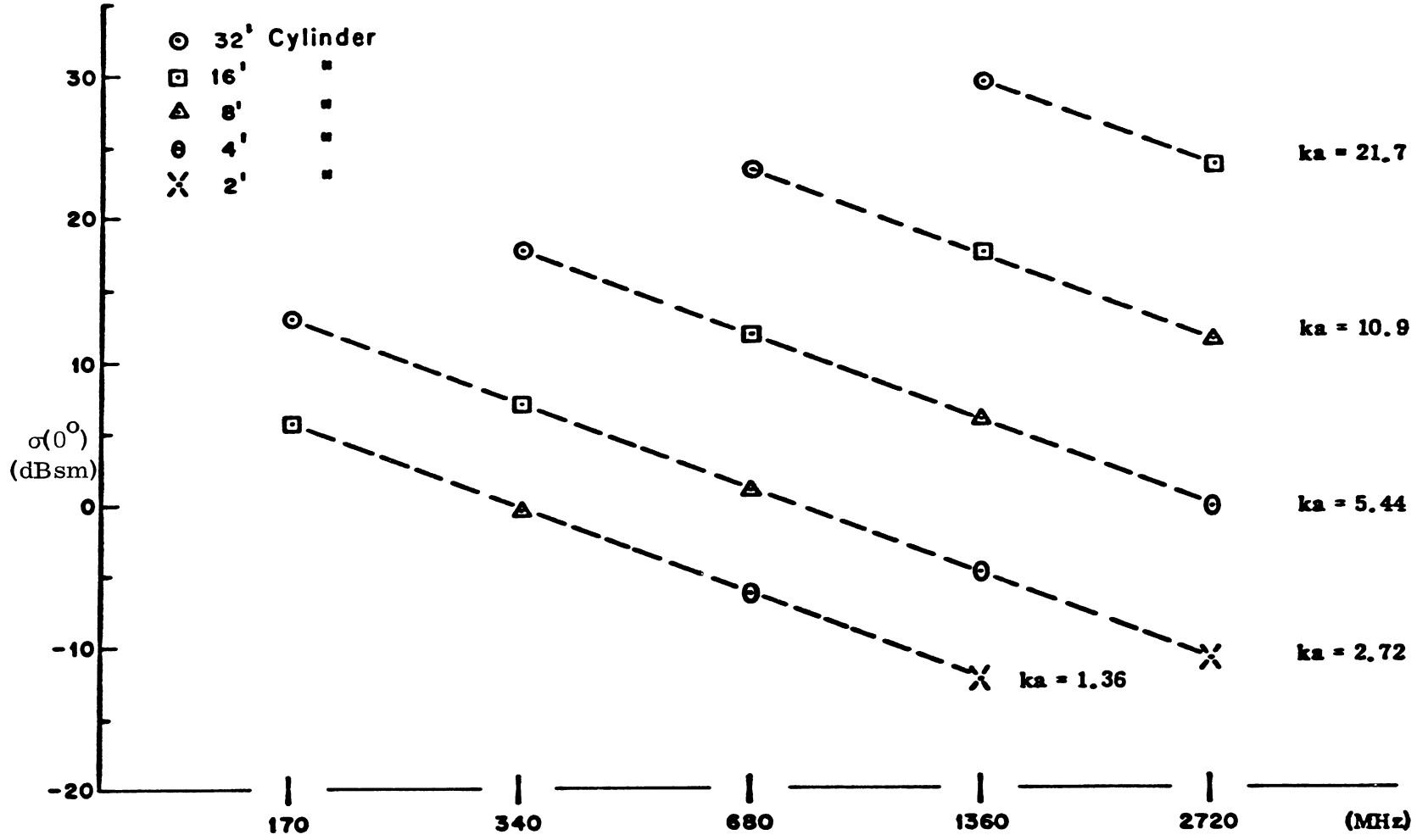

FIG. 3-8: THEORETICAL RCS OF CYLINDERS AT END-ON FOR VV AND HH POLARIZATIONS, INTER-RANGE DISPLAY.

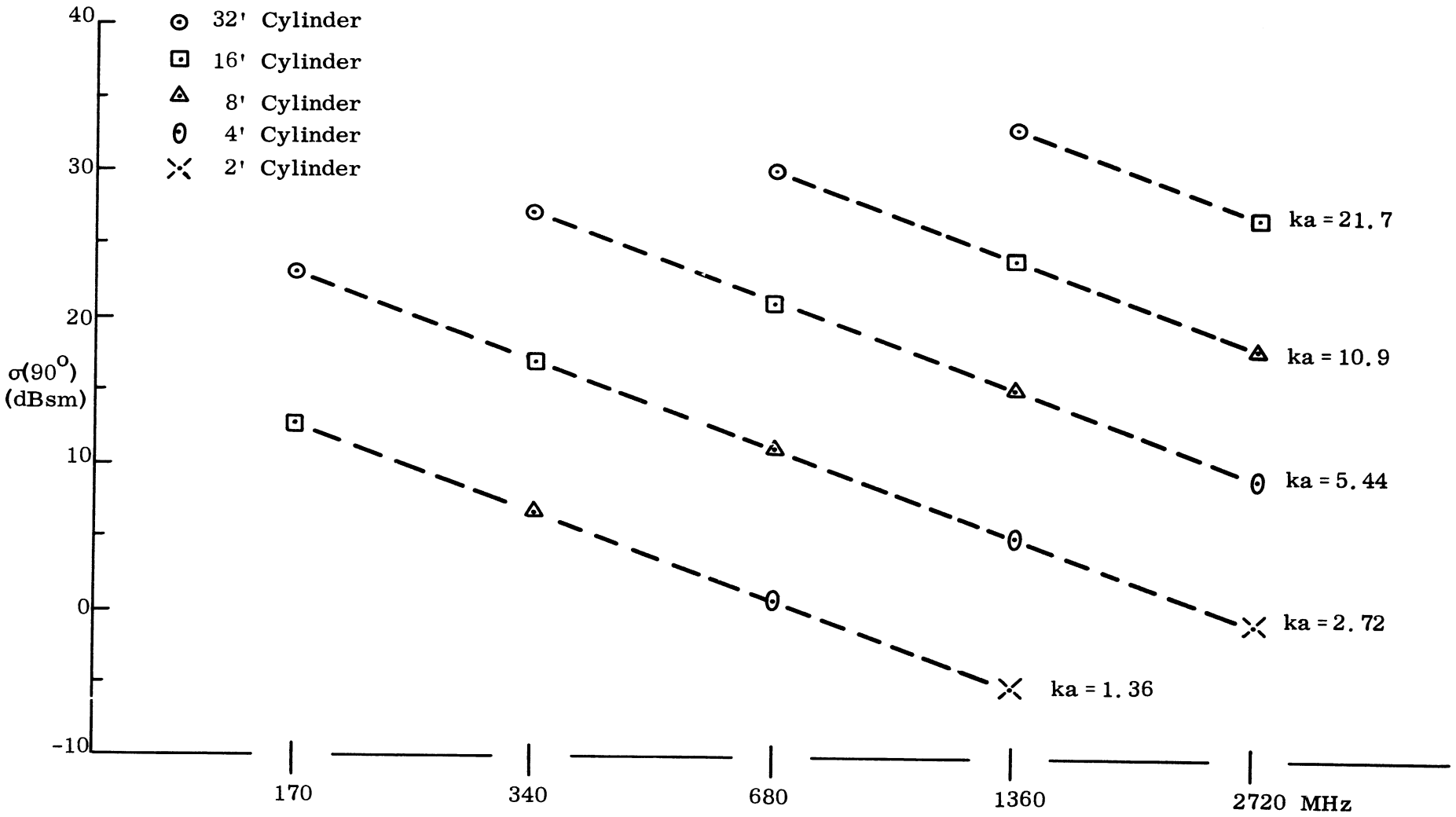

FIG. 3-9: THEORETICAL RCS OF CYLINDERS AT BROADSIDE FOR VV POLARIZATION; INTER-RANGE DISPLAY.

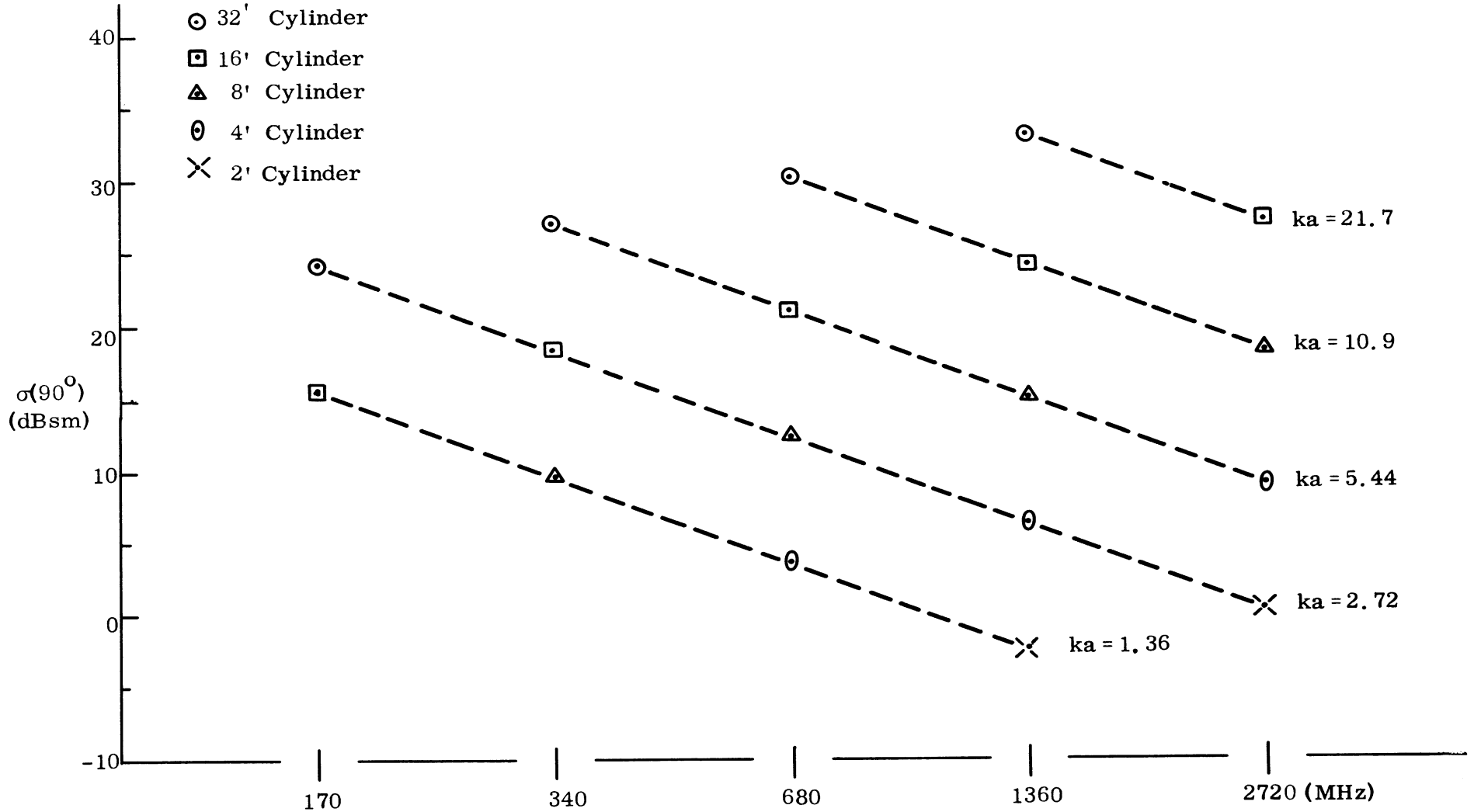

FIG. 3-10: THEORETICAL RCS OF CYLINDERS AT BROADSIDE FOR HH POLARIZATION; INTER-RANGE DISPLAY.

IV

CO-POLARIZED EXPERIMENTAL DATA

In the last chapter we saw how the data should appear by examining theoretical models; in this chapter we see how the measurements actually appear by examining experimental patterns. First, a group of ten patterns are examined including all ka co-polarized cases (VV and HH). Then a second group of ten patterns are presented to show samples from each of the five outdoor ranges for tests on the same target. The third topic is a discussion of near field distortions caused by insufficient distance between the target and radar locations. The fourth and last section describes a comparison between theory and experiment for ka = 1.36.

4.1 Patterns for all ka Cases

Figures 4-1 through Fig. 4-5 are examples of all the test pattern shapes which occur for the VV and HH cylinder measurements and correspond to the theoretical patterns in Figs. 3-2 through 3-6. These ten experimental patterns, which were recorded at Radiation Service in Melbourne, Florida, show radar cross sections for the aspect region between $\pm$ 120^{o} in dBsm. Results are calibrated relative to a square meter rather than to a square wavelength as in the last chapter. All of the patterns are for the 16 foot (1/2 scale) cylinder starting with ka = 1.36 (170 MHz) in Fig. 4-1 and ending with ka = 21.7 (2720 MHz) in Fig. 4-5. Polarization, size, frequency, and range R are indicated in each figure. Data for the 16 foot model was chosen because it is the only one measured at every frequency and ka; thus it is the only model for which there is a complete set of experimental results. Radiation Service data was chosen for this display because a uniform set of patterns (all from the same range) was desirable for comparison purposes and this data was available early in the program.

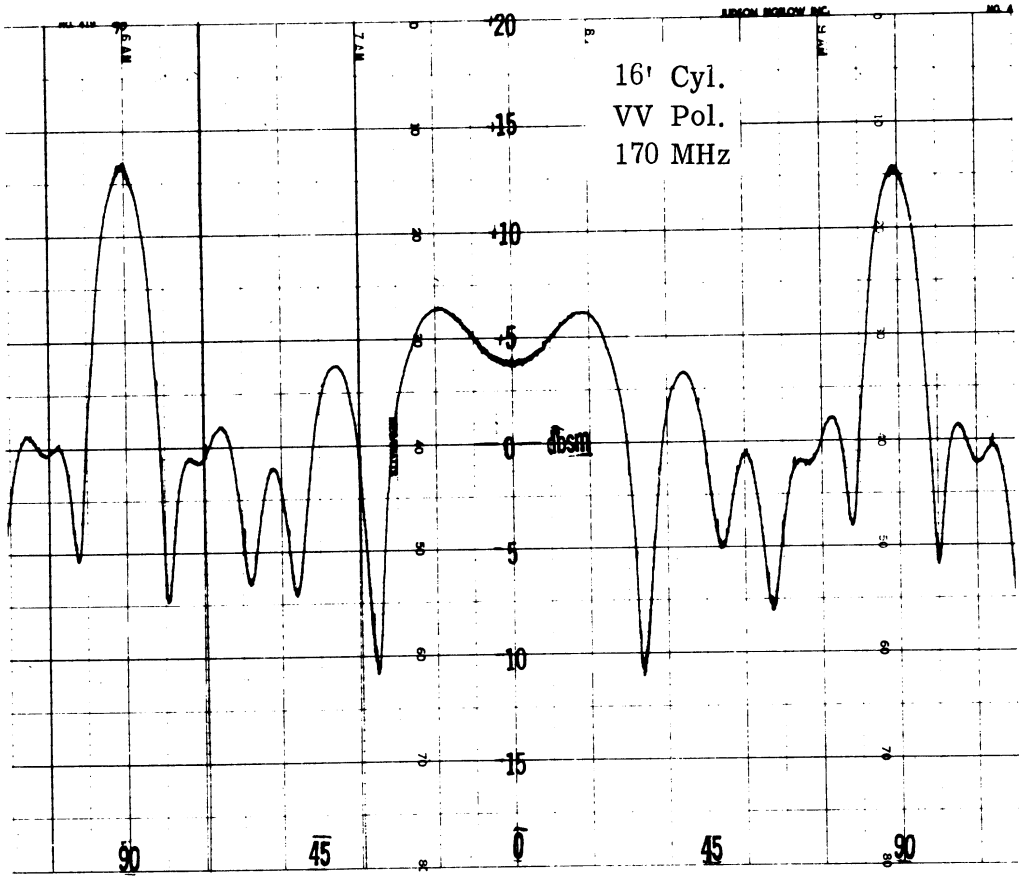

(a) VV Polarization

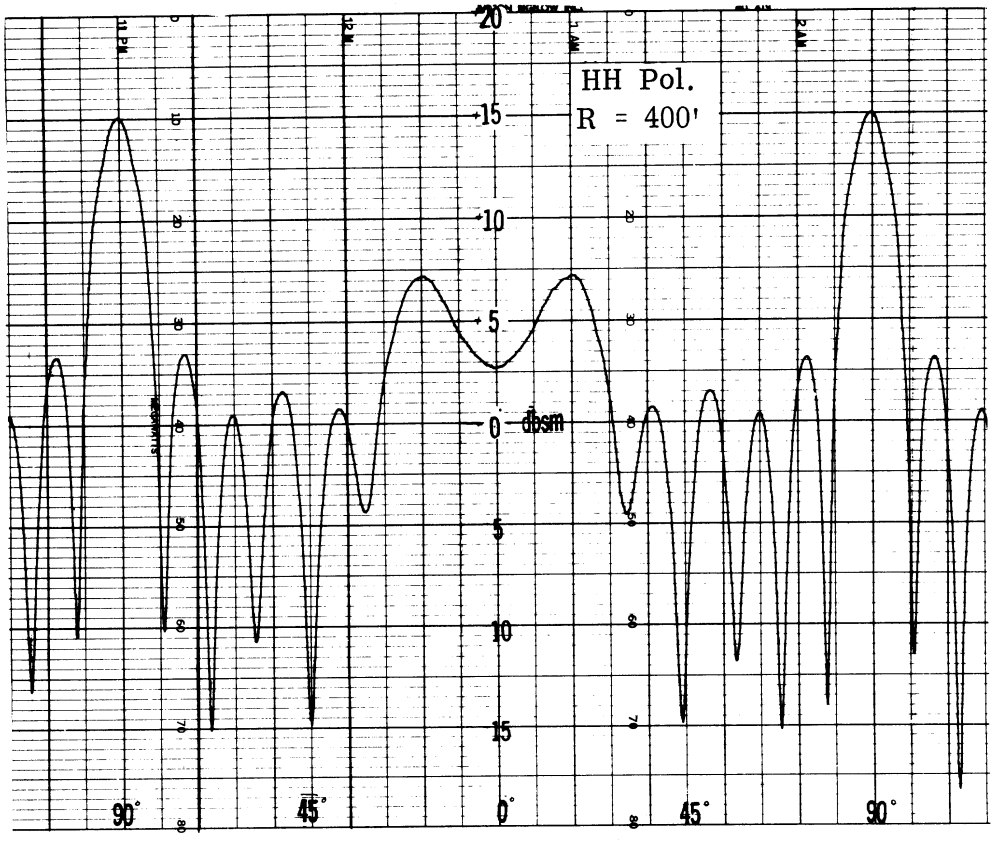

(b) HH Polarization

FIG. 4-1: EXPERIMENTAL PATTERNS FOR ka = 1.36, 170 MHz, RANGE 400 FEET, 16 FOOT CYLINDER.

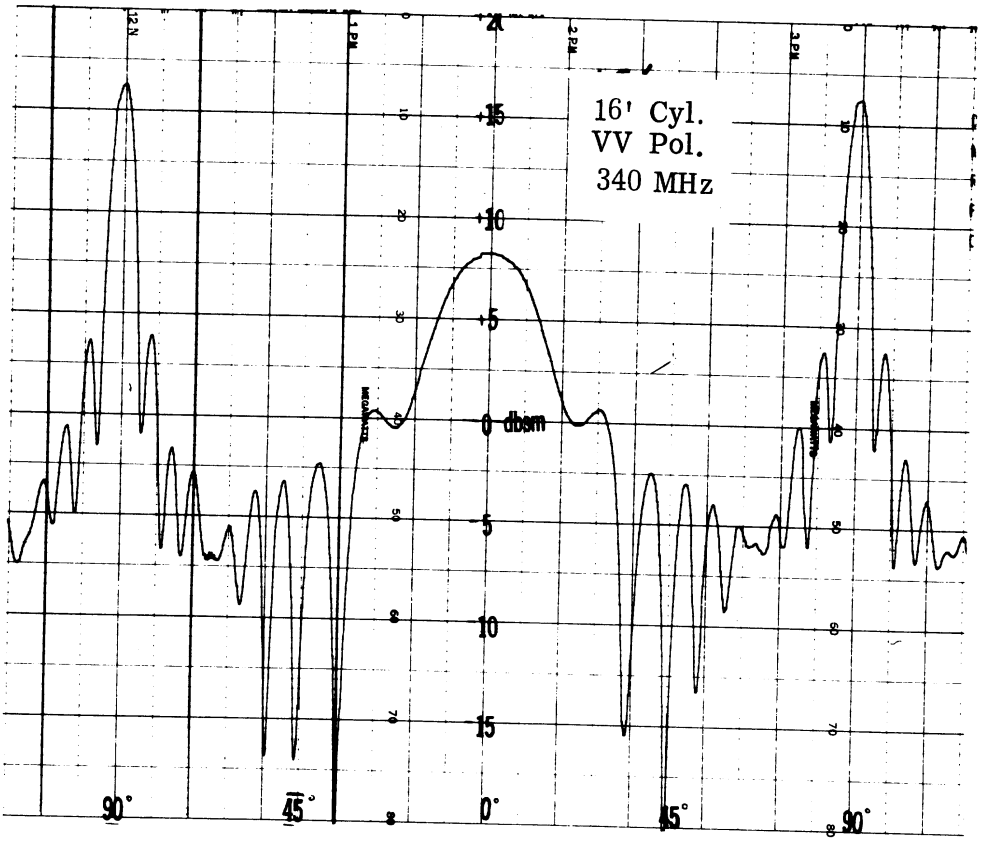

(a) VV Polarization

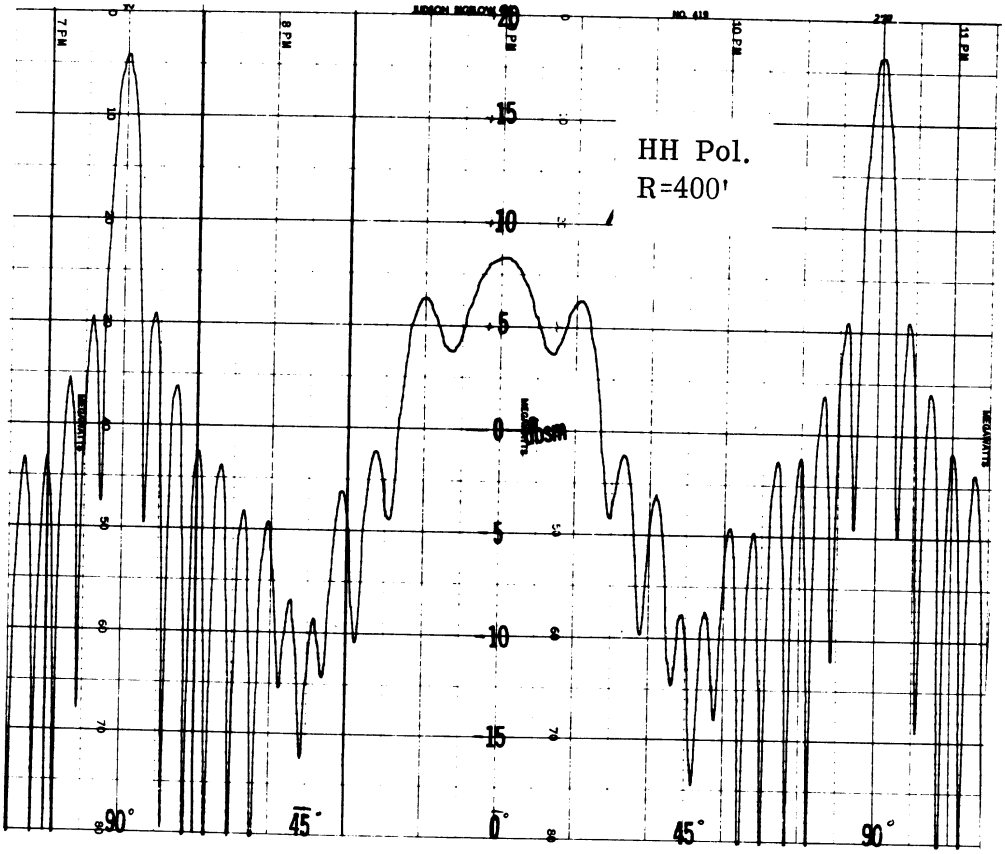

(b) HH Polarization

FIG. 4-2: EXPERIMENTAL PATTERNS FOR ka = 2.72, 340 MHz, RANGE 400 FEET, 16 FOOT CYLINDER.

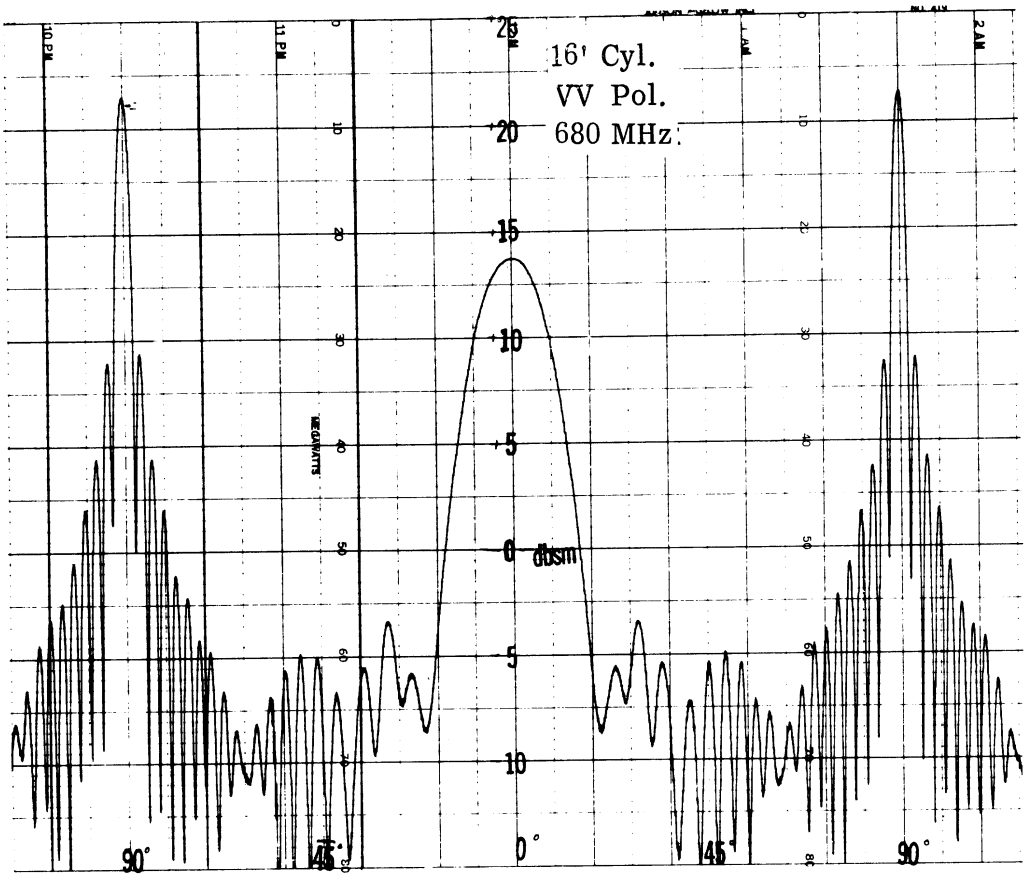

(a) VV Polarization

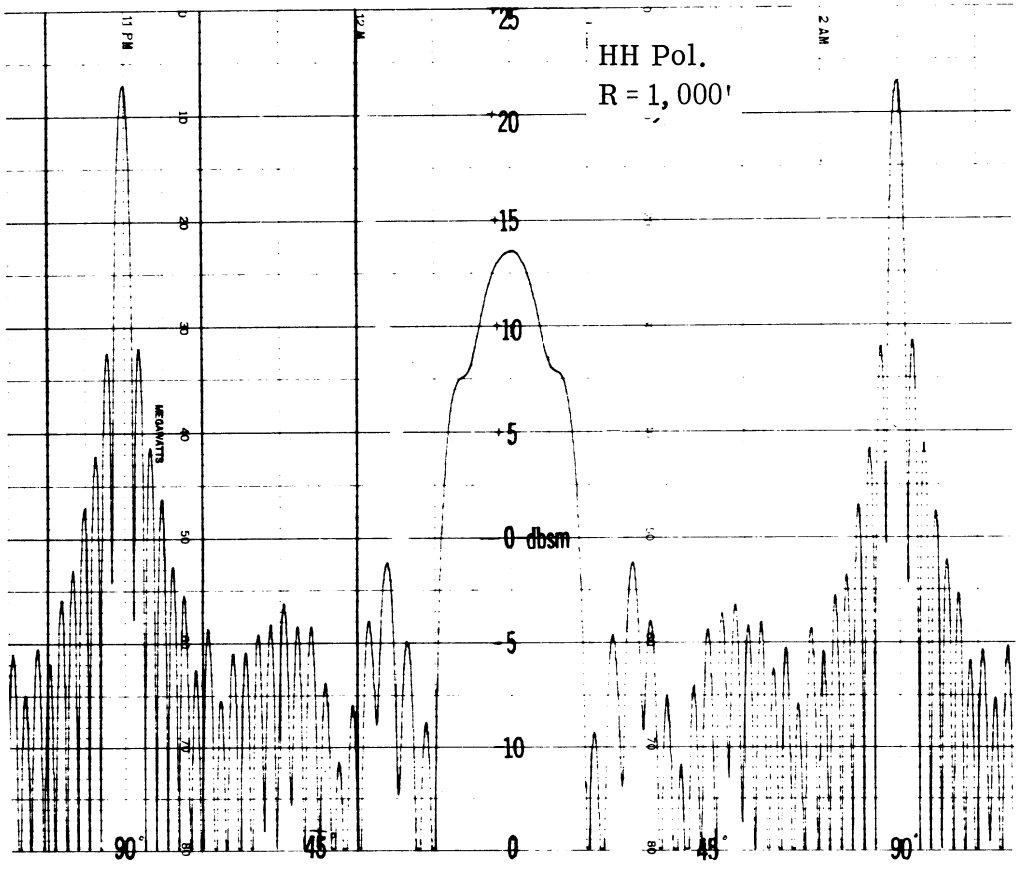

(b) HH Polarization

FIG. 4-3: EXPERIMENTAL PATTERNS FOR ka = 5.44, 680 MHz, RANGE 1000 FEET, 16 FOOT CYLINDER.

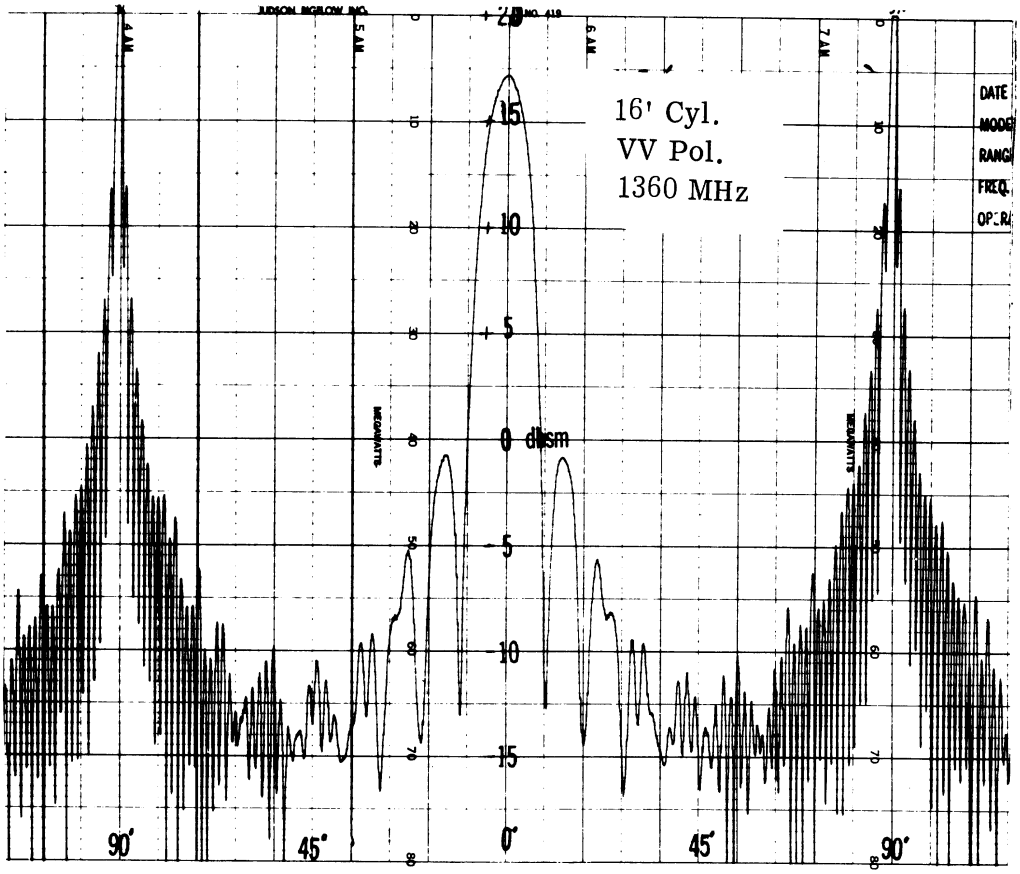

(a) VV Polarization

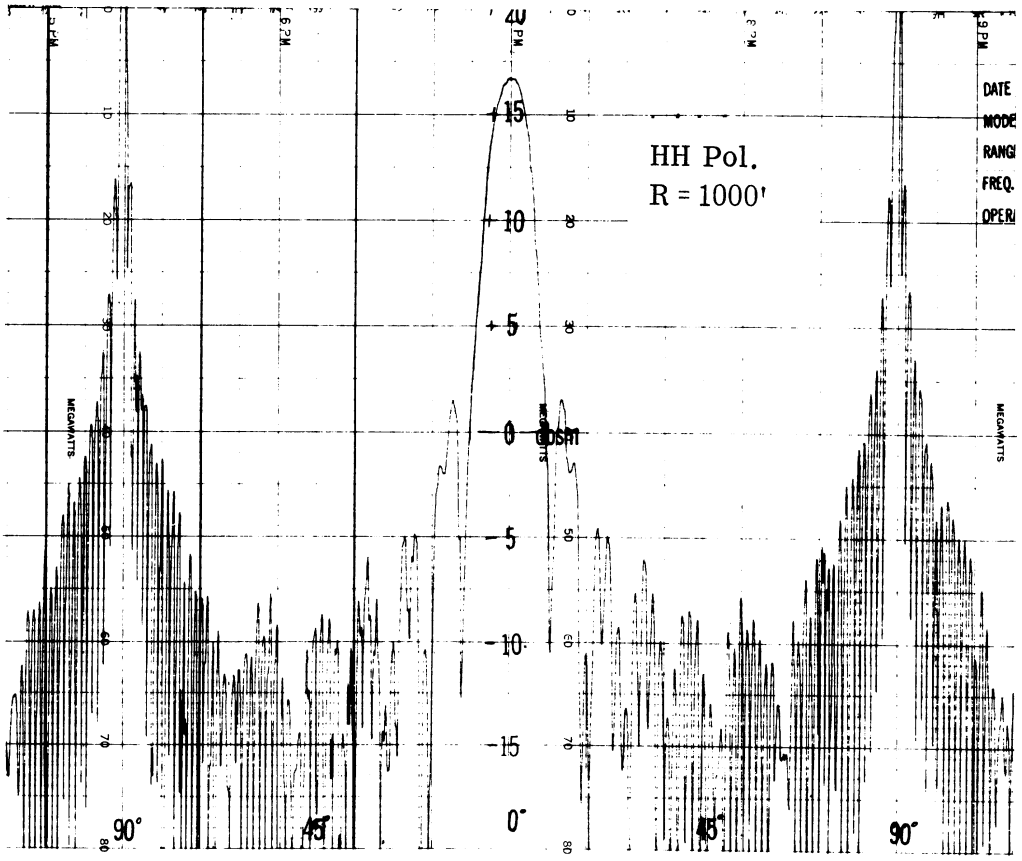

(b) HH Polarization

FIG. 4-4: EXPERIMENTAL PATTERNS FOR ka = 10.9, 1360 MHz, RANGE 1000 FEET, 16 FOOT CYLINDER.

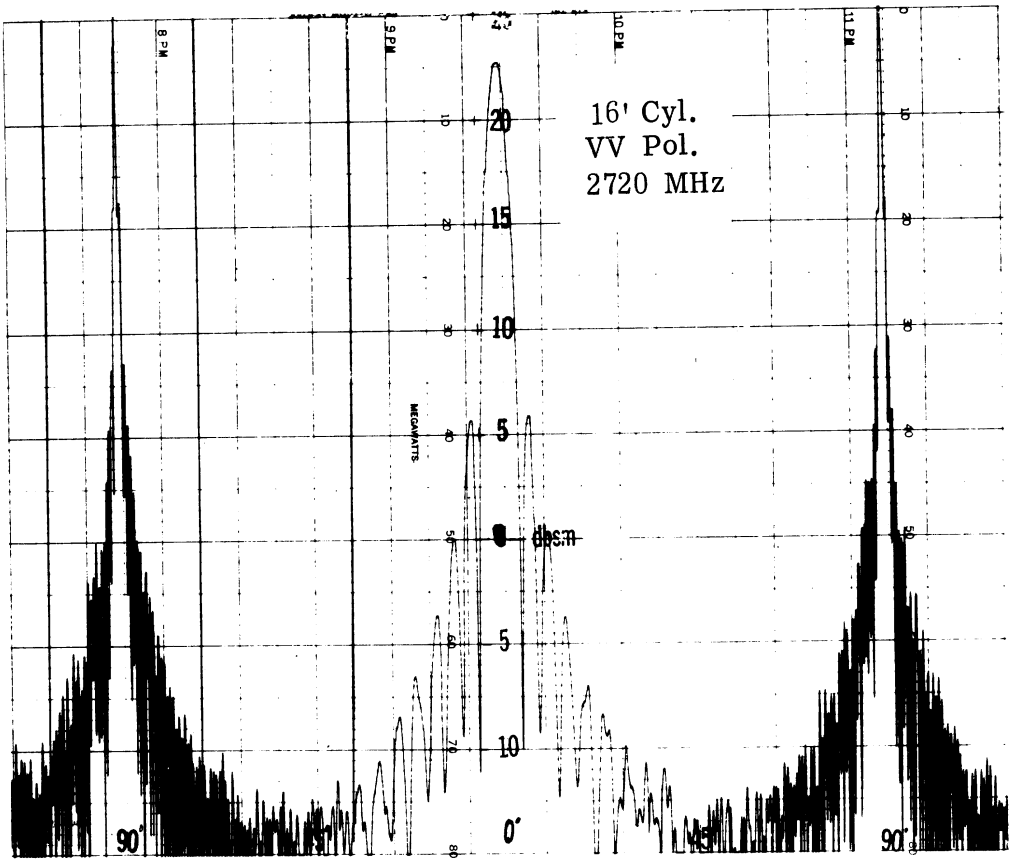

(a) VV Polarization

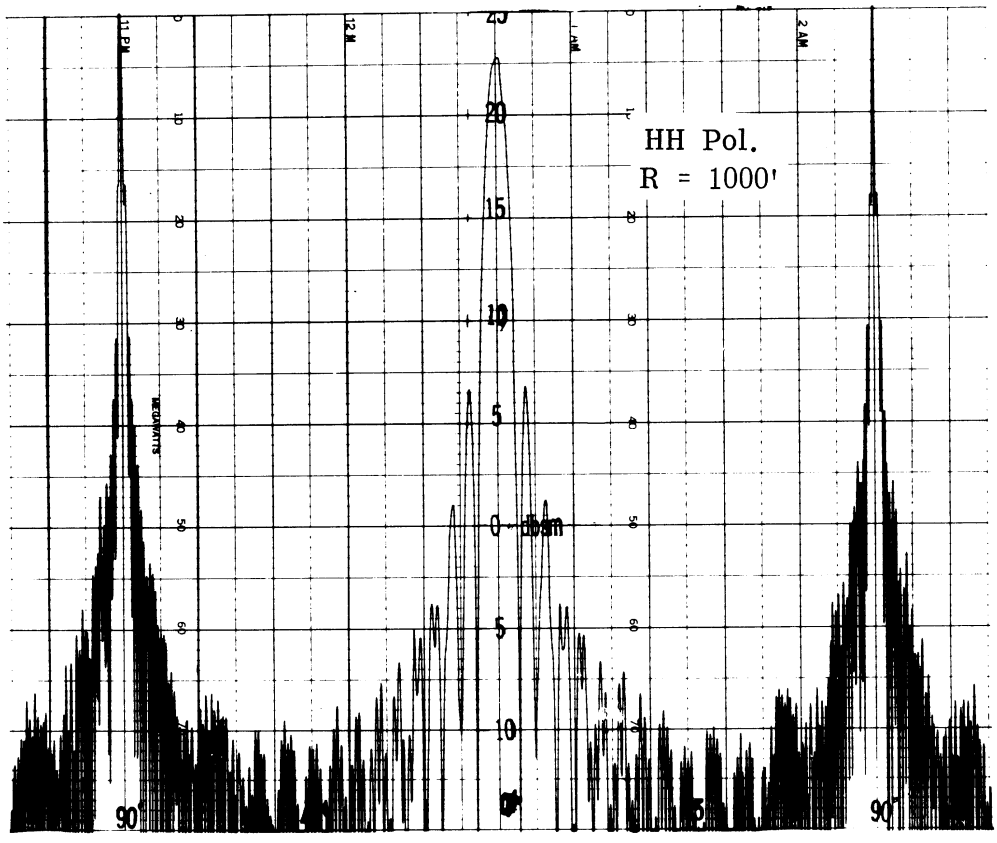

(b) HH Polarization

FIG. 4-5: EXPERIMENTAL PATTERNS FOR ka = 21.7, 2720 MHz, RANGE 1000 FEET, 16 FOOT CYLINDER.

If one compares these measured patterns with the corresponding theory in the last chapter it is seen that Figs. 4-1 and 4-5 (ka = 1.36 and 21.7) agree in more detail with theory than the other three ka values, but that, in general, there is a reasonable amount of agreement between all theoretical and experimental cases. For the most part differences in pattern shape between theory and experiment are attributed to theoretical rather than experimental deficiencies. As will become evident in later discussions, the precise dBsm level for the experimental patterns may not be as accurate as the pattern shape due to experimental errors.

One criterion for judging range performance is pattern symmetry. That is, how close are lobe amplitude and shape features about points of symmetry such as end-on ($\theta = 0^{o}$) and broadside ($\theta = \pm 90^{o}$) for these cylinder models? In general all the ranges performed well in this respect. When poor symmetry was noticed it was usually accompanied by other errors. Some symmetry difficulties are noted in the VV polarizations near $\pm 72^{o}$ for the first two cases, Figs. 4-1 and 4-2, although these are not serious. Other than for these instances, the symmetry for these ten patterns should be rated as excellent.

In Fig. 4-4 and 4-5 the broadside peaks run off the top of the recording paper. This occurs often and is done deliberately to show more of the details in the lower portion of the pattern. In most cases, as in the present one, additional patterns are recorded showing the complete broadside peaks moved down on the record. The second patterns are not included here but we note that the level of the broadside peaks for both the VV and HH patterns are tabulated in Table V-2.

In the highest ka pattern, Fig. 4-5, the pattern oscillations are so rapid that it is not possible to resolve the lobe width beyond $\pm 45^{o}$ aspect angle. This difficult was indicated in the theoretical pattern, Fig. 3-6,

where only the peak locations were given for θ greater than 50^{o}. All the ranges have the capability to avoid this problem by expanding the aspect scale on their records, but since the contract with each of these ranges did not call for expanded patterns, it was not done. This example points out the importance of adequate recording scales if the pattern lobe structure is to be examined in any detail.

4.2 Patterns from Each Outdoor Range

Examples of measurements made at each of the outdoor ranges on the 32 foot cylinder at 340 MHz (ka = 5.44) are shown in Figs. 4-6 through 4-10 for VV and Figs 4-11 through 4-15 for HH polarizations. Like all the experimental patterns these cross sections are given in dBsm but here the complete aspect region, $\pm 180^{o}$ is shown rather than just $\pm 120^{o}$ as in the previous ten patterns. Though all the patterns were recorded on 10 inch by 20 inch chart paper, GD/FW and RAT SCAT have a 50 dB range over 10 inches while the other three facilities have 40 dB over 10 inches. Also it should be noted that during the photographic reduction, the angular scales were reduced by slightly different amounts. These discrepancies make it difficult to perform accurate, direct comparisons between the patterns from different ranges. Nevertheless it is informative to make cursory comparisons for this set of data.

On first inspection of these patterns one is probably aware of the noticeable distortion and asymmetry in the broadside region in the Conductron patterns, Fig. 4-6 and 4-11. This is caused by near field distortion, the largest single cause of errors in the patterns. Further discussion on this topic follows in the next section.

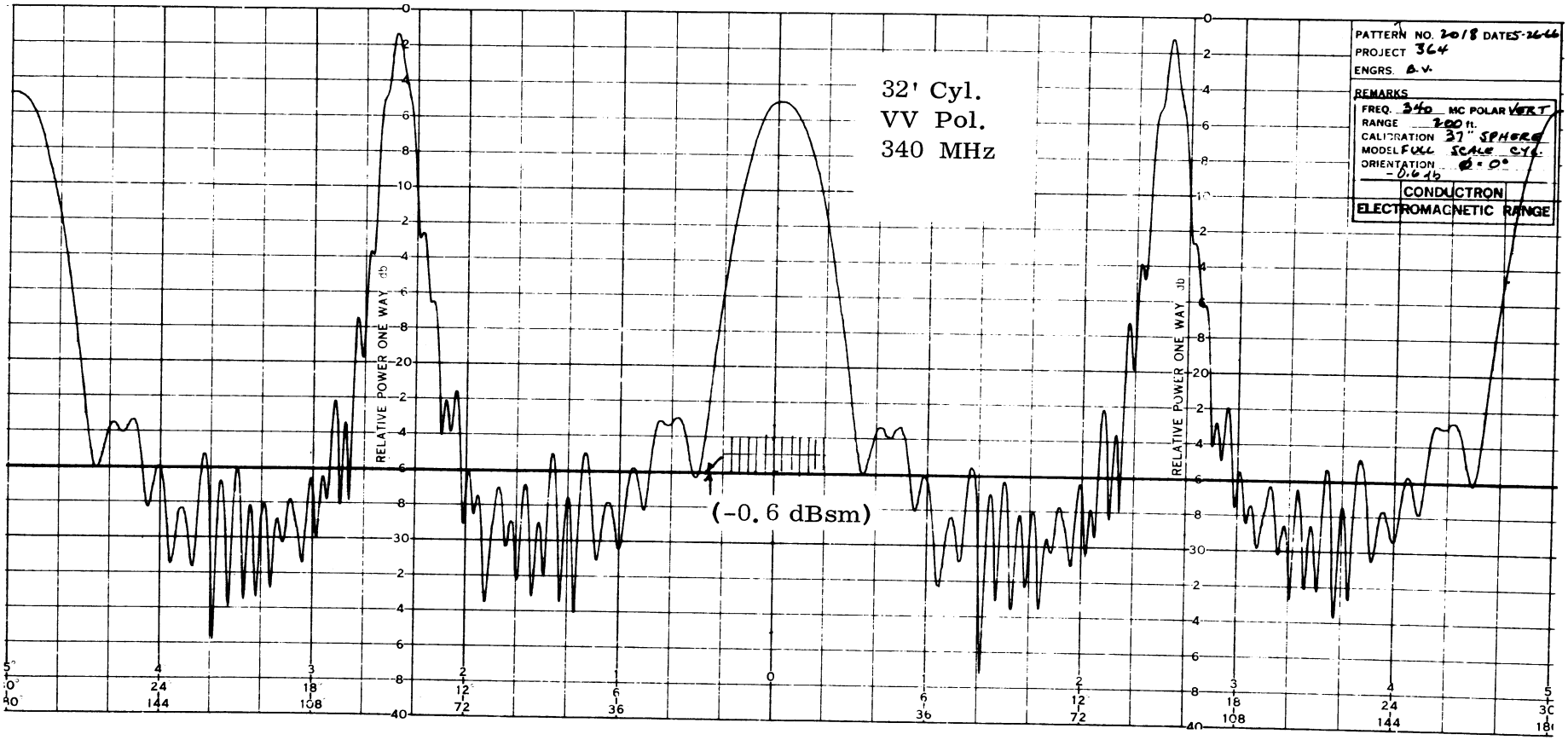

FIG. 4-6: CONDUCTRON PATTERN FOR 32 FOOT CYLINDER, VV POLARIZATION, 340 MHz.

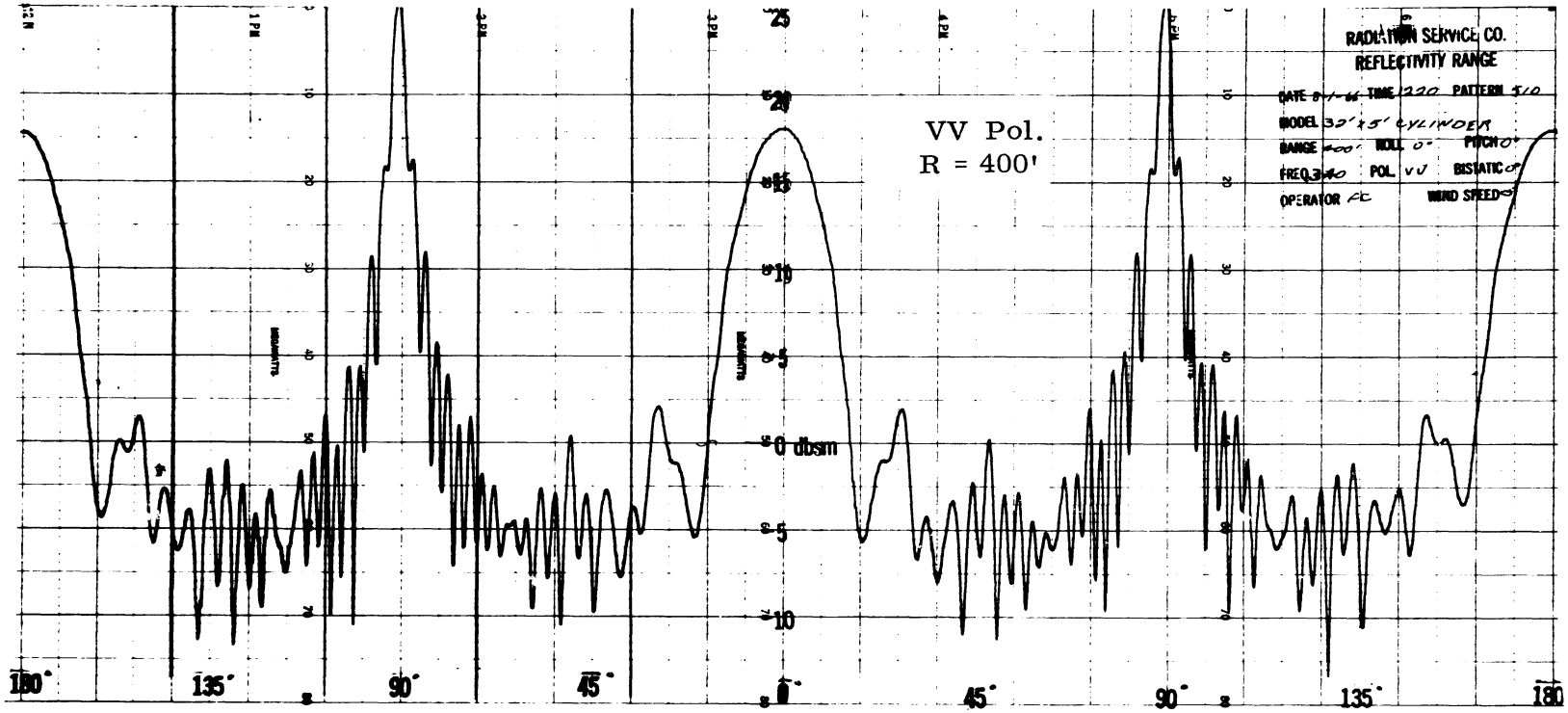

FIG. 4-7: RADIATION SERVICE PATTERN FOR 32 FOOT CYLINDER VV POLARIZATION, 340 MHz.

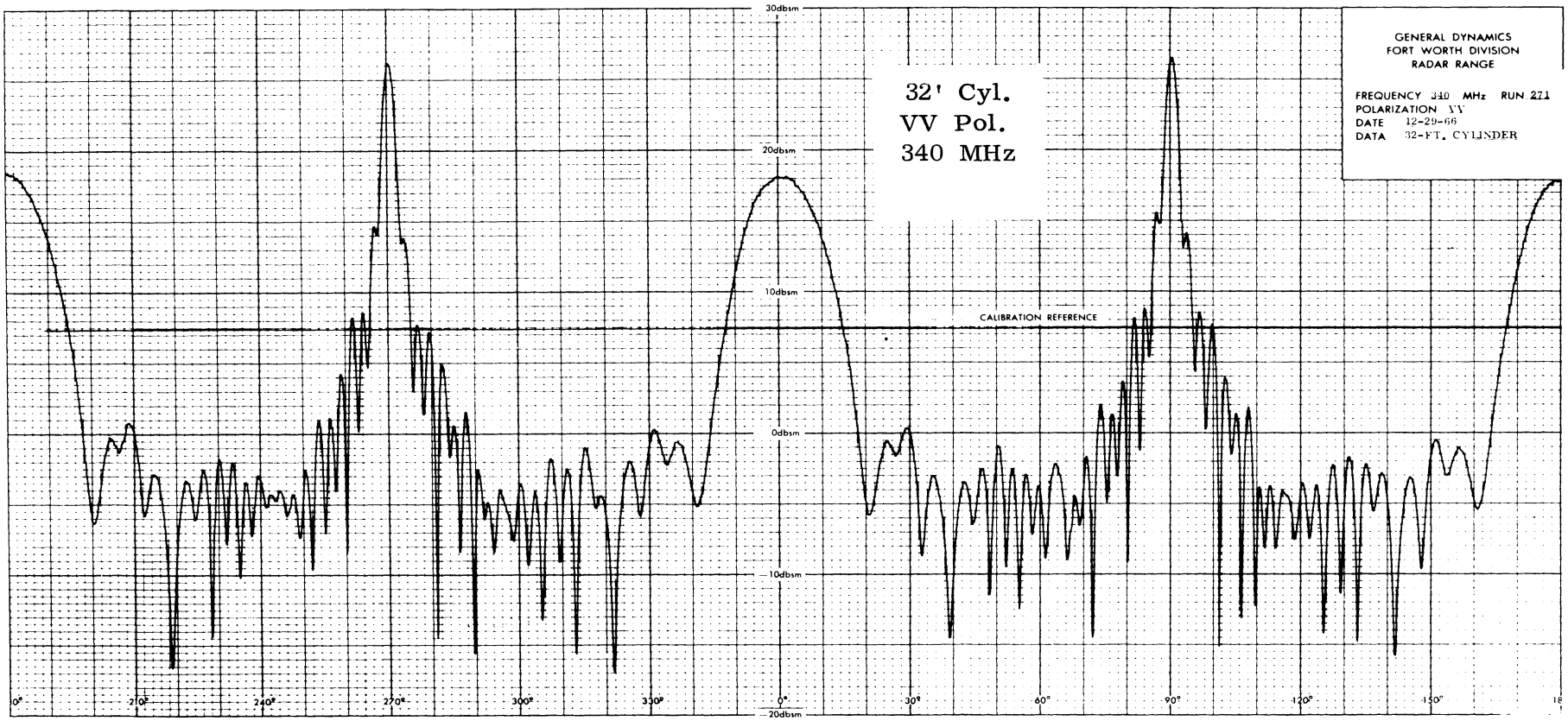

FIG. 4-8: GENERAL DYNAMICS PATTERN FOR 32 FOOT CYLINDER, VV POLARIZATION, 340 MHz.

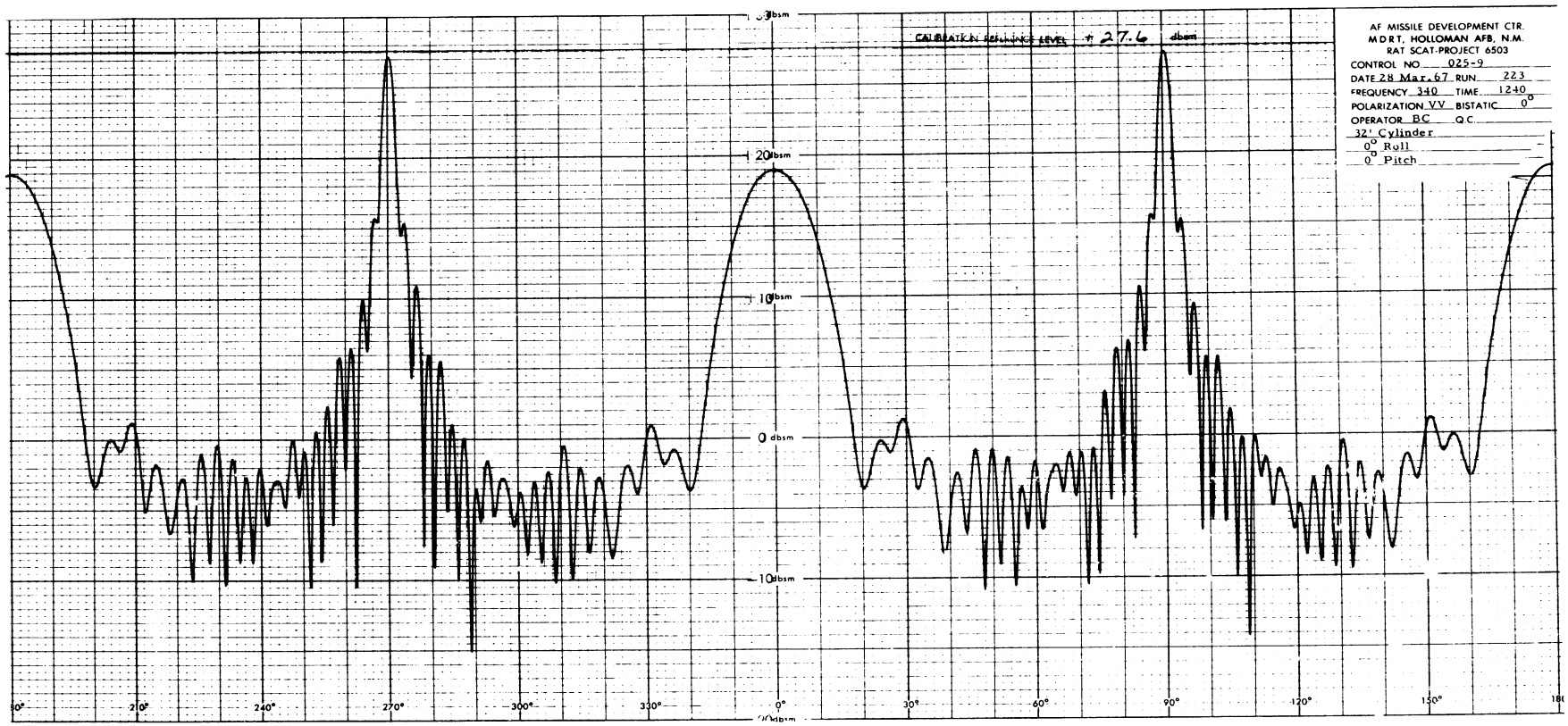

FIG. 4-9: RAT SCAT PATTERN FOR 32 FOOT CYLINDER, VV POLARIZATION, 340 MHz.

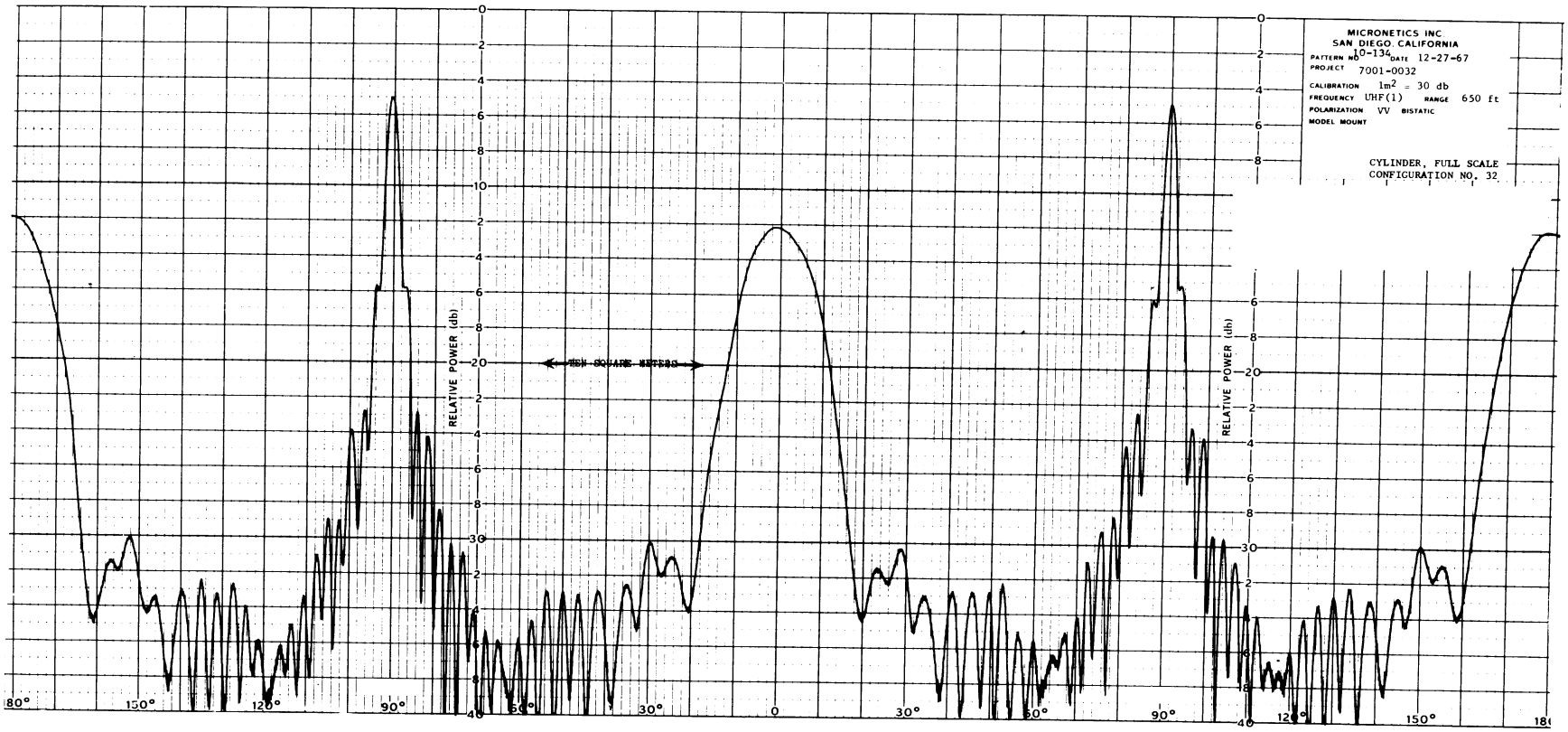

FIG. 4-10: MICRONETICS PATTERN FOR 32 FOOT CYLINDER, VV POLARIZATION, 340 MHz. (The horizontal arrows indicate the + 10 dBsm level).

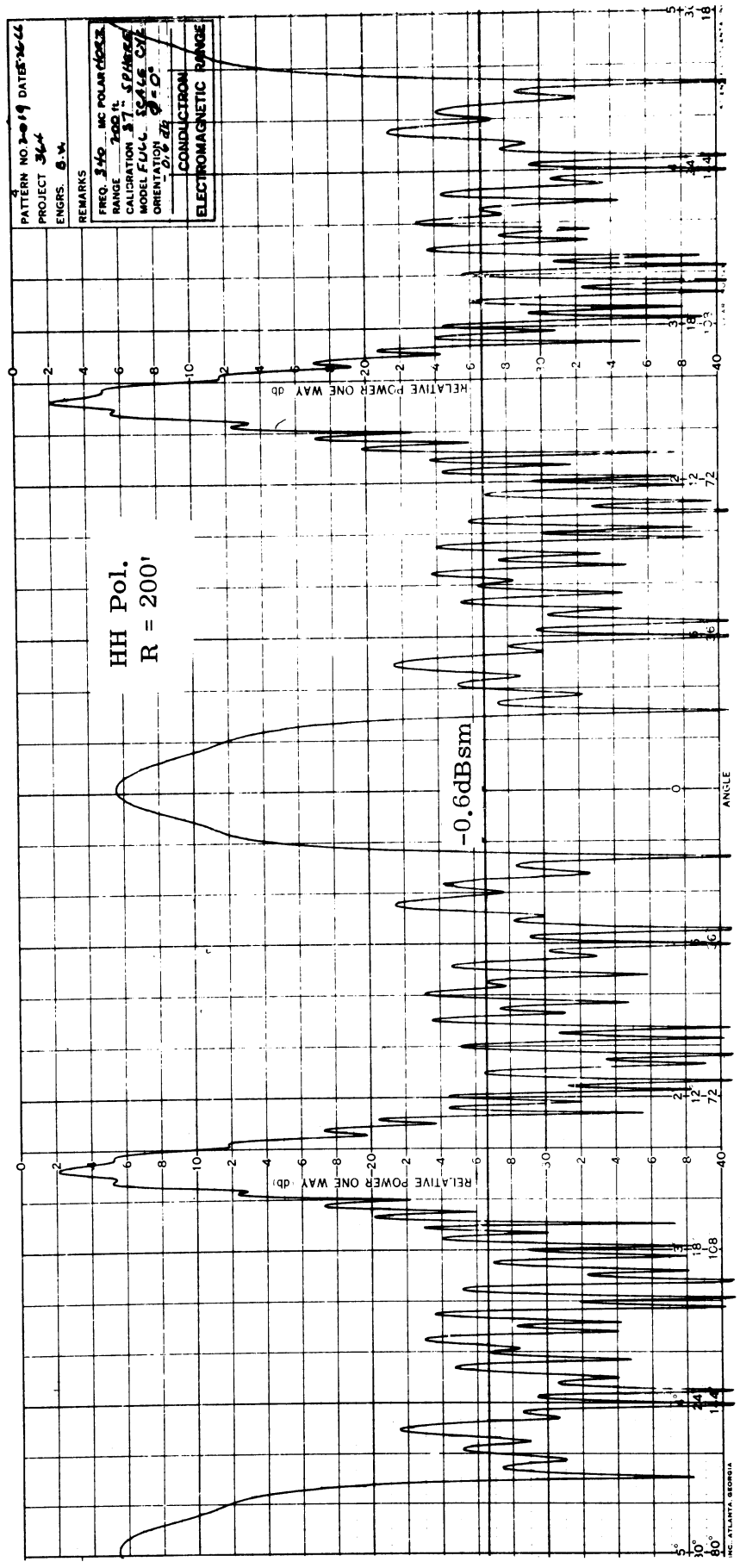

FIG. 4-11: CONDUCTRON PATTERN FOR 32 FOOT CYLINDER, HH POLARIZATION, 340 MHz.

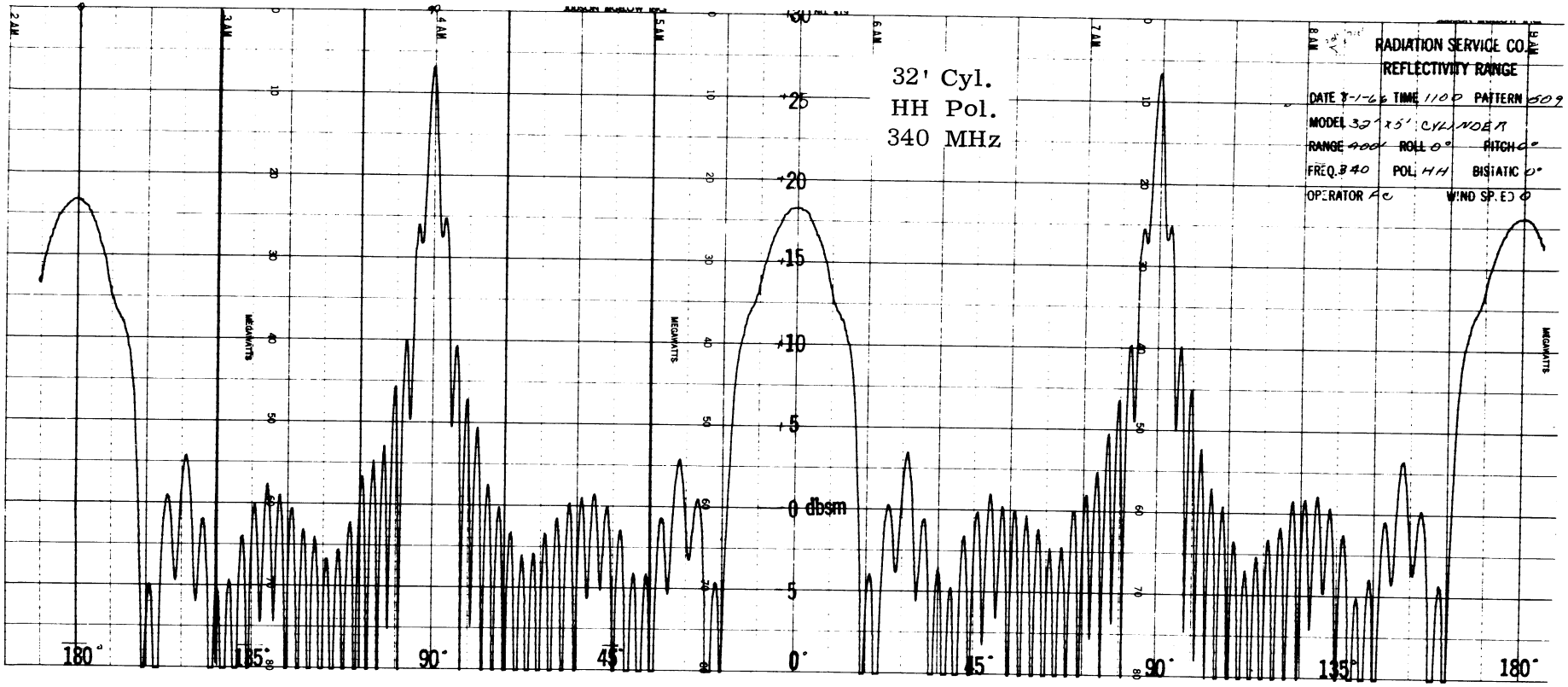

FIG. 4-12: RADIATION SERVICE PATTERN FOR 32 FOOT CYLINDER, HH POLARIZATION, 340 MHz.

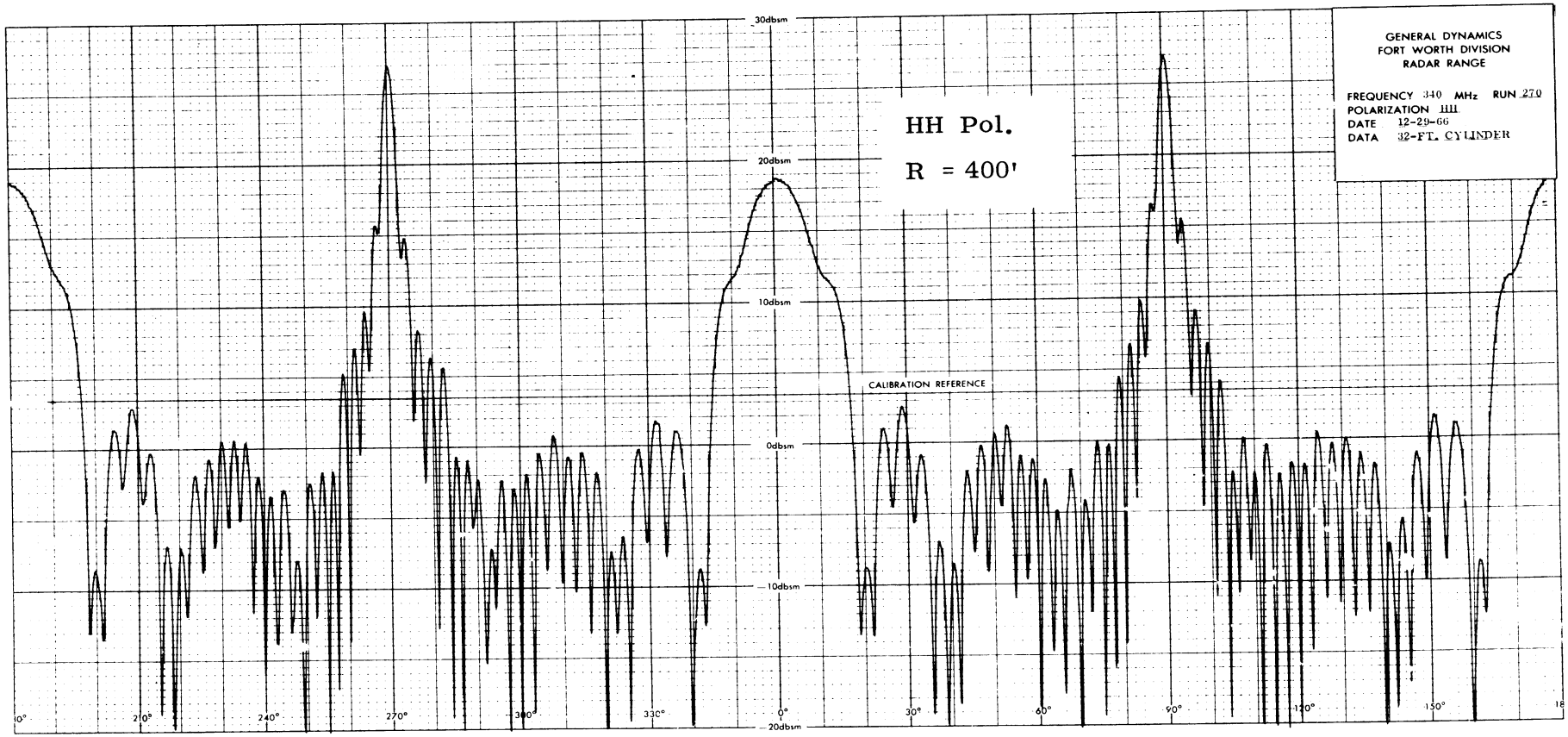

FIG. 4-13: GENERAL DYNAMICS PATTERN FOR 32 FOOT CYLINDER, HH POLARIZATION, 340 MHz.

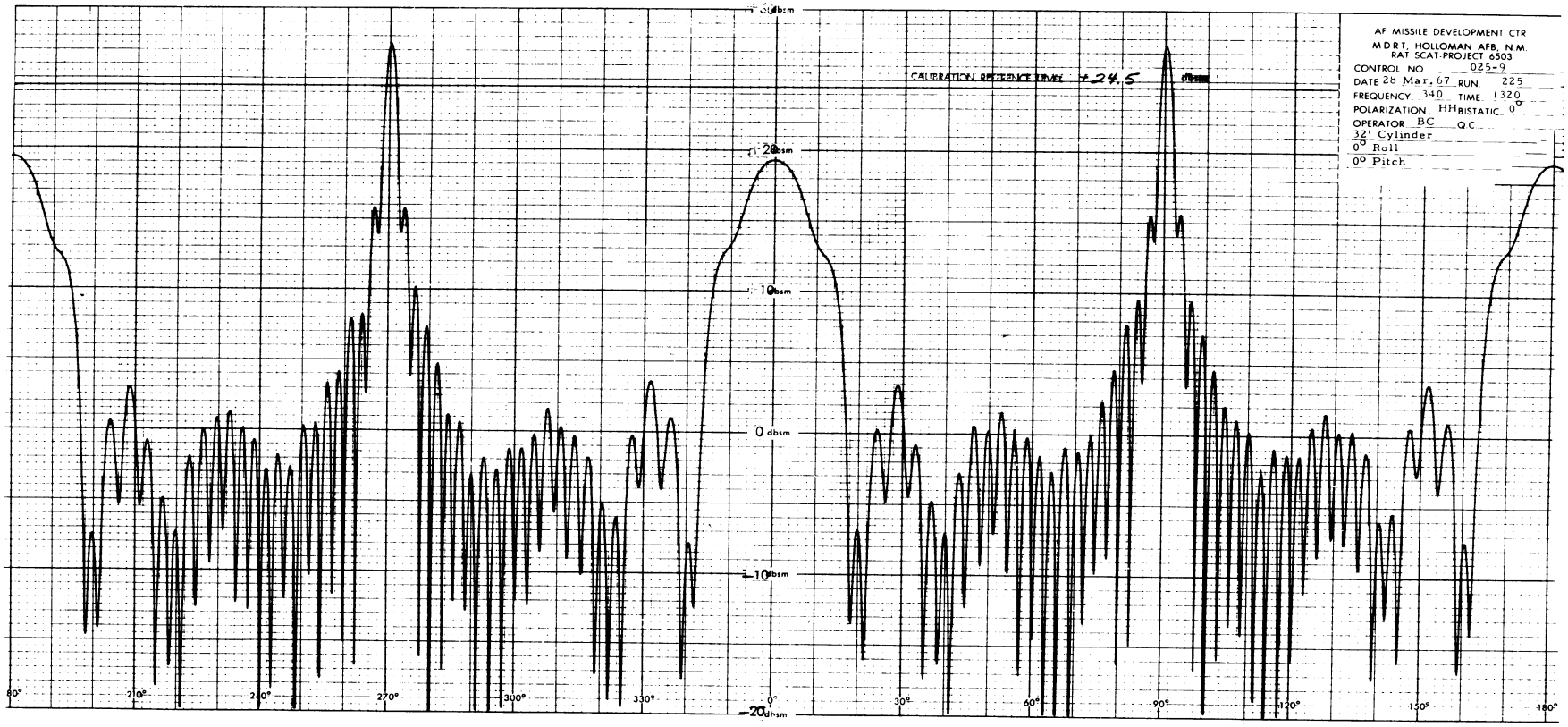

FIG. 4-14: RAT SCAT PATTERN FOR 32 FOOT CYLINDER, HH POLARIZATION, 340 MHz.

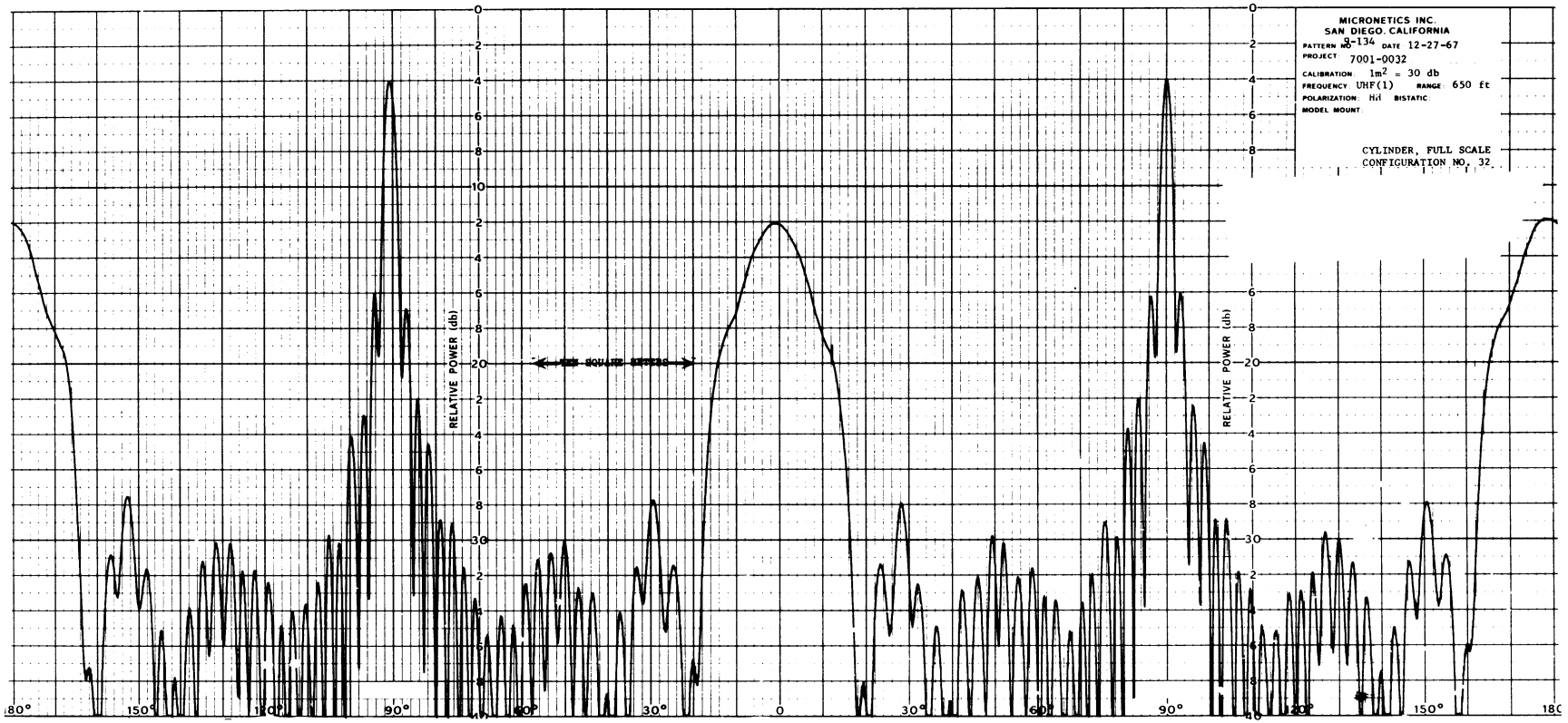

FIG. 4-15: MICRONETICS PATTERN FOR 32 FOOT CYLINDER, HH POLARIZATION, 340 MHz. (The horizontal arrows indicate the + 10 dBsm level).

An annoying feature of the Conductron pattern is that there is no convenient relation between the dBsm values and the dB level on the chart grid. This is a result of making pattern calibrations after the target pattern is measured, instead of before, and the format is clearly not as easy to read as is the pre-calibrated patterns of the other ranges. CW ranges can pre-calibrate their work like pulse ranges do with very little extra effort and we recommend that this be done.* The pattern traces on the Avionics Laboratory data (not shown here) are placed on the recording paper in a manner similar to Conductron's but in addition their angular locations appear to be randomly placed on the recording paper, disregarding the angular markings, hence making their patterns even more difficult to read.

Additional comparisons can be made on the 32 foot cylinder data by referring to the 1/2 scale data for ka = 5.44 in Fig. 4-3; this should have the same shape but be 6 dB less than the full scale data. A quick examination shows actual differences closer to 5 dB between the broadside peak for the full scale and the half scale patterns. The approximate 1 dB error is in the full scale data and is due to near field effects also.

4.3 Near Field Distortion

Noticeable near field distortions have been pointed out in Figs. 4-6 and 4-11, but a further examination indicates that all of the patterns in Figs. 4-6 through 4-15 are beginning to show near field effects compared to the patterns in Fig. 4-3. The first indication of insufficient range between the target and radar (near field effects) is that the nulls in the

---

* After working with post-calibrated data on this contract, we are convinced of the convenience of this format and have changed our own calibration technique at the Radiation Laboratory, University of Michigan accordingly.

lobes just off broadside ($\theta = 90^{o}$) become shallow. Compare Fig. 4-3 with any of the full scale data to see this behavior. As the range is further reduced, the target passes from the Fraunhofer (far) zone to the Fresnel (near) zone. This progressive degeneration in range requirements is exemplified by passing from Fig. 4-3 (Fraunhofer pattern) to Figs. 4-7 or 4-2 and 4-6 or 4-11 (transition region) and then to Fig. 4-16 (Fresnel pattern). The second effect which becomes noticeable in the near field is the amplitude reduction in the broadside peak. This was mentioned indirectly at the close of the last section where it was noticed that there was closer to a 5 dB rather than 6 dB difference in the full and 1/2 scale data for ka = 5.44.

Ideally, it is desirable to have the target illuminated by a plane wave when its cross section is being measured because then the shape and form of the scattering pattern are constant and only the power level varies as $1/R^4$. The illumination is considered to be sufficiently plane when there is less than $\lambda/16$ phase variation over the target at the time its maximum dimension L is exposed to the radar. To satisfy this phase requirement the range R must be (Kouyoumjian and Peters, 1965)

$$R \geq \frac{2\,(D + L)^2}{\lambda}$$

where D is the maximum dimension of the radar antenna. If D is small compared to L, it may be ignored and the above expression reduces to the $2L^2/\lambda$ criteria introduced in Chapter II. Disregarding D which varies from one facility to another the necessary ranges R for the various cylinder models are listed in Table IV-1.

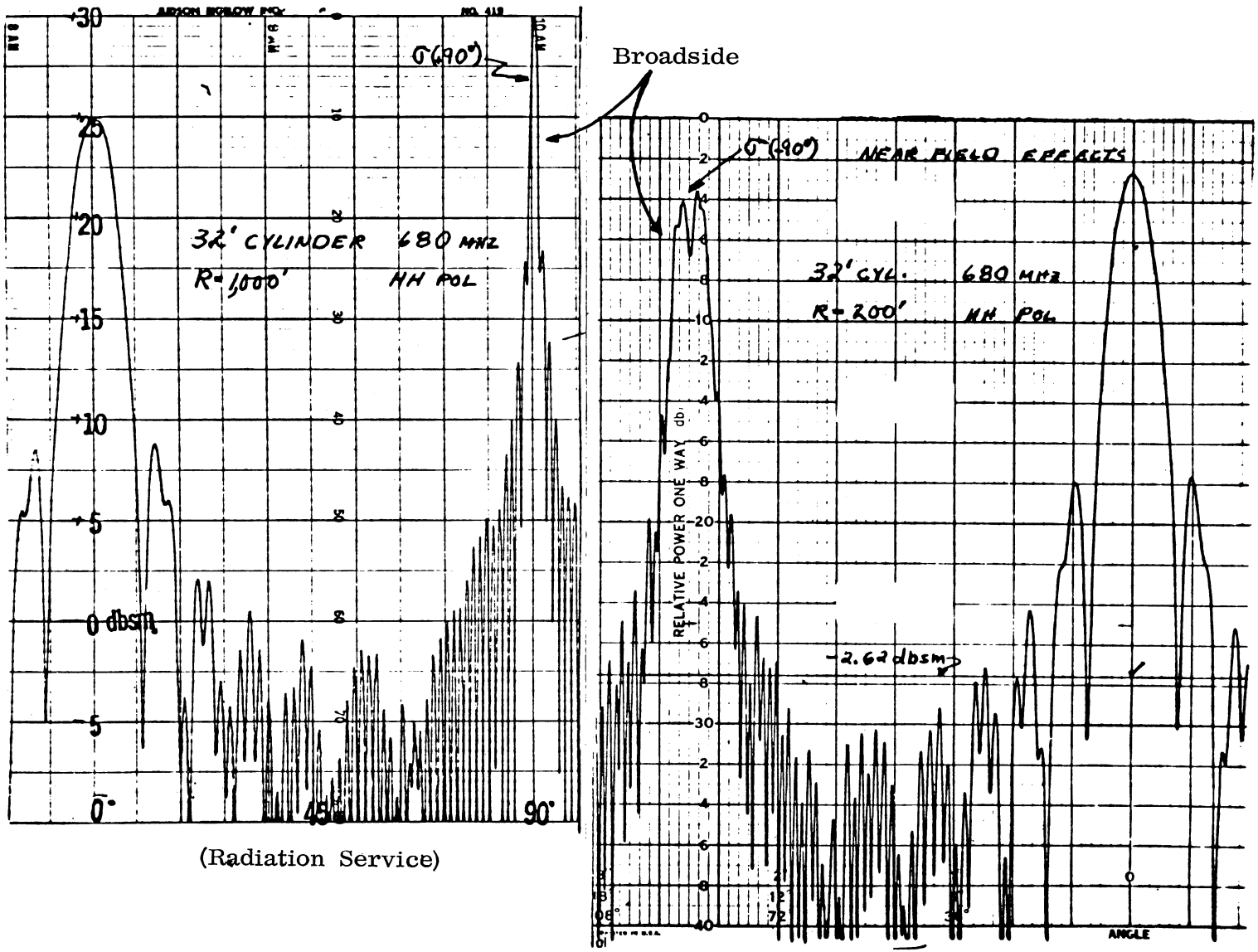

(Radiation Service)

(Conductron)

FIG. 4-16: NEAR FIELD DISTORTIONS FOR HH POLARIZATION AT ka = 10.9. THE PATTERN ON THE RIGHT SHOW THE EFFECT OF BEING IN THE FRESNEL ZONE NEAR $\theta = 90^{o}$.

TABLE IV-1

REQUIRED RANGE DISTANCE (FEET) AS DETERMINED BY $2L^2/\lambda$

Frequency MHz	Model Length (feet)				
	32	16	8	4	2
170	354	88	-	-	-
340	708	177	44	-	-
680	1416	354	88	22	-
1360	2832	708	177	44	11
2720	-	1416	354	88	22

Further explanation is needed for Fig. 4-16 which is an example of severe near field distortion. These are experimental patterns for the full scale cylinder measured at 680 MHz (ka = 10.9) and HH polarization. The pattern on the left was measured at a range of 1000 feet ($1.4\ L^2/\lambda$) while the one on the right was measured at 200 feet ($0.3\ L^2/\lambda$). According to Table IV-1 the minimum range should have been 1,416 feet. Note that these two patterns are arranged with their broadside returns in the center of the figure; the left pattern covers the aspect range between 0 and + 90^o while the right one covers between - 90^o and 0^o. The vertical placement of the two patterns in Fig. 4-16 is such that equal dBsm levels are aligned. In this example near field distortion caused about a 12 dB difference in the broadside return. There is a 2.5 dB difference in the end-on region ($\theta = 0^o$). As it turns out the Radiation Service pattern (left) is about 1.5 dB high and Conductron (right) pattern 1.0 dB low compared to theory at $\theta = 0^o$, so discrepancies in this region are not near field errors.

Near field errors as serious as those shown in the right hand portion of Fig. 4-16 occurred in eight patterns (six from Conductron and two from Micro-netics). Errors due to this cause are the largest and occur most frequently in this test program. Their occurrence is, however, predictable in that an examination of the maximum target dimension, the incident wavelength and the antenna-to-target separation distance indicates whether or not this problem will exist. More suggestions and discussion concerning the near field effects are found in Volume I.

4.4 Comparison Between Theory and Experiment

In this section we make some selected comparisons between theory and experiment, and although we use four distinct theories, the comparisons are summarized in three figures. Table IV-2 lists the figures and ka values for which the various theories apply.

TABLE IV-2: LIST OF CONDITIONS IN WHICH THEORY IS COMPARED WITH EXPERIMENT.

Fig. No.	Theory Used	Aspect Angle at Which Comparison is Made .	ka Values for Which Comparison is Made.
4-17, 4-18	Norair SDT	End-on, broadside, and at peaks of five other lobes.	1.36
4-19	Schmitt-Andrejewski	End-on.	1.36, 2.72, 5.43
4-19	Infinite Cylinder (exact)	Broadside.	1.36, 2.72, 5.43
4-19	Physical Optics	End-on, broadside.	10.86, 21.72

Although there were 18 cylinder-frequency combinations measured by each range, these data can all be collected into five groups according to ka. In order to make the best use of all the data, we reduced the radar cross sections from dBsm to $dB\lambda^2$ by simply adding or subtracting a correction factor (in dB). This resulted in a large number of samples, producing, for example, as many as 52

values for analysis of the end-on return for ka = 2.72. For each comparison we draw in Figs. 4-17 through 4-19 we show the mean value of the data and the standard deviation. If the individual deviations are assumed to be entirely random, the standard deviation represents a confidence level of 68.3 percent; that is to say, if ten more measurements are made, and if the errors are truly random, seven of them will fall within the range bracketed by the mean value plus or minus the standard deviation.

Norair's SDT prediction is shown in Fig. 4-17 for HH polarization and ka = 1.36, the smallest electrical size involved in the measurements program. Note that the worst disagreement is about 1.1 dB and it occurs at end-on and 63^{o} aspect. The broadside return is predicted within 0.3 dB and the standard deviations are usually less than 1 dB. The Norair theory for VV polarization is shown in Fig. 4-18. Note that the standard deviations are much greater for this than HH polarization, reaching a value of nearly 2.5 dB at the 66.5^{o} aspect angle. The experimental end-on return is precisely the same as for HH polarization, and again the broadside return is within 0.3 dB of the theoretical prediction. The point of poorest agreement lies at 54.5^{o} and the difference between theory and experiment is 1.6 dB. For both polarizations the experimental data lie consistently below the theory (except for VV polarization at broadside). At best we can say the Norair SDT theory does well or it does poorly, depending what aspect angle is of interest.

We have not made any comparisons of null depth or null locations, and there is no reason to believe the theory will predict these returns any better than it does the lobe amplitudes in Figs. 4-17 and 4-18. (Inspection of Figs. 6-5 through 6-6 show that range performance becomes progressively worse away from the peaks of the lobes, especially for this low ka.) It is apparently more difficult to produce accurate VV patterns than HH patterns, presumably because the ground reflects this polarization more readily into the target area

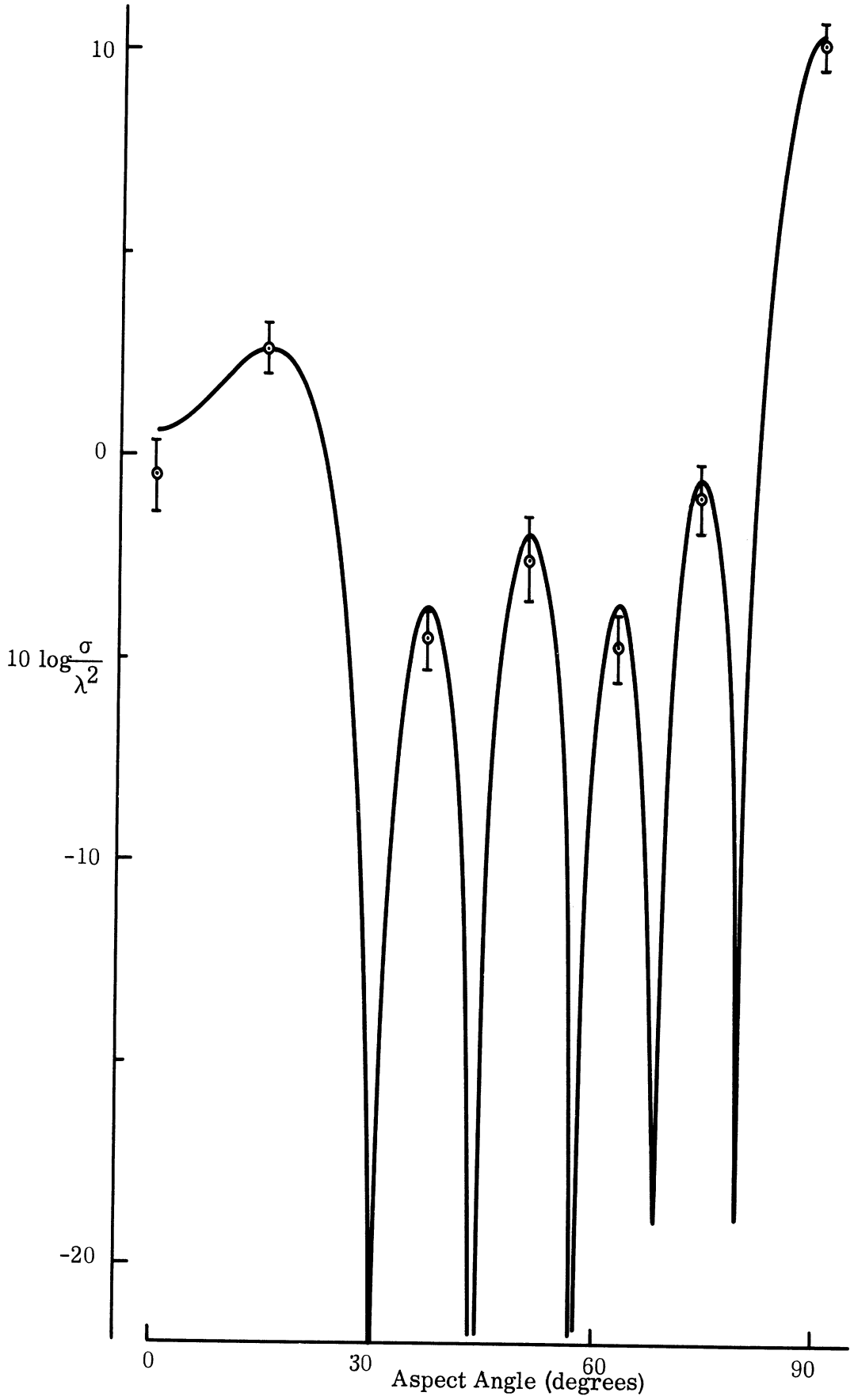

FIG. 4-17: COMPARISON OF NORAIR SDT THEORY WITH RANGE DATA FOR HH POLARIZATION (ka=1.36). Each mean value and standard deviation is based on 21 data samples.

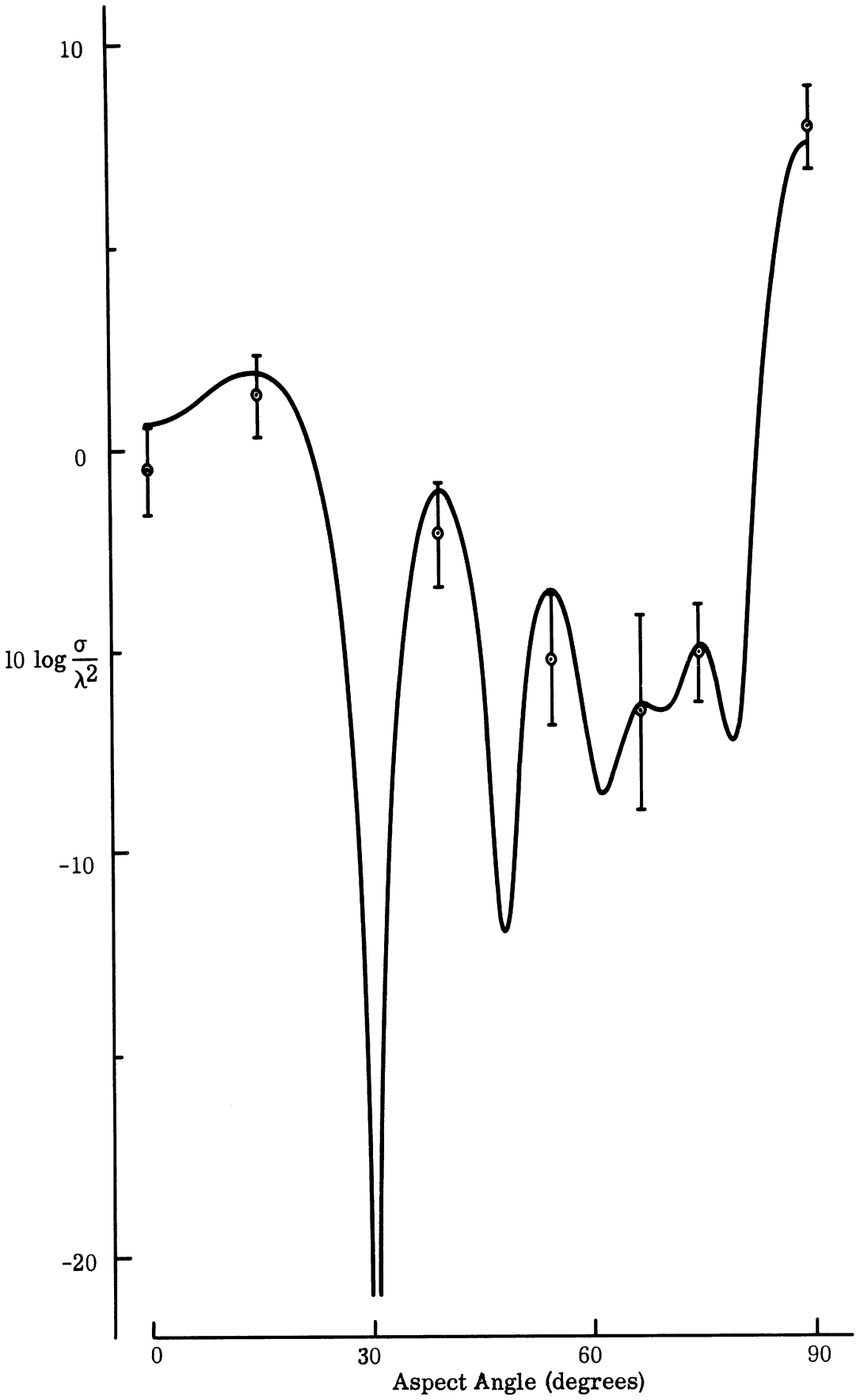

FIG. 4-18: COMPARISON OF NORAIR SDT THEORY WITH RANGE DATA FOR VV POLARIZATION (ka=1.36). Each mean value and standard deviation is based on 21 data samples.

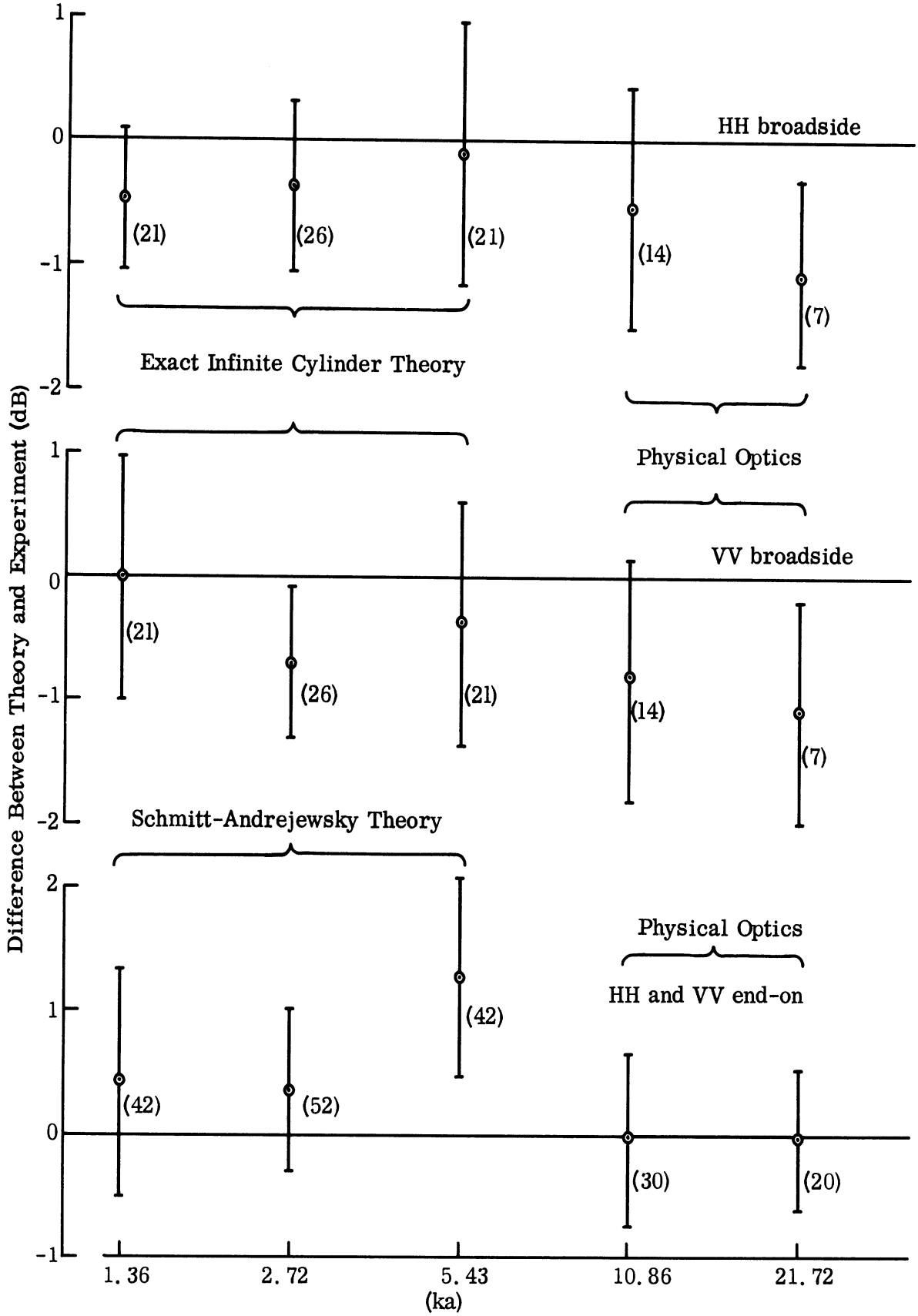

FIG. 4-19: DIFFERENCES BETWEEN THEORY AND EXPERIMENT ARE SUMMARIZED FOR END-ON AND BROADSIDE ASPECT ANGLES. The quantities in parentheses show the number of data samples used to obtain the means and standard deviations.

as an interference signal. As we will point out later, the ranges turned in poorer performances on the larger cylinders than the smaller ones for ka = 1.36.

Turning now to Fig. 4-19, we present a comparison of three theoretical methods with experiment, this time for all five values of ka, but only for end-on and broadside viewing angles. The exact infinite cylinder solution was used to predict the theoretical broadside returns for both polarizations for the first three ka values. For end-on incidence, the Schmitt-Andrejewski theory was used, again for the first three ka values. Beyond ka = 10, both theories become indistinguishable from physical optics theory and the latter was used for both broadside and end-on incidence for the two highest ka values. Note that the differences between theory and experiment are plotted in Fig. 4-19.

For broadside incidence, the theory seems to be no better than 1 dB for either polarization, and this occurs, moreover, for the highest ka. Since physical optics becomes progressively more successful as ka increases, and since the frequency was high, we believe it is the experiment that should be doubted. Near field effects were particularly severe for this high ka and the theory should be accurate within 0.5 dB here. By discounting the high ka experimental data, we venture to state that the exact infinite cylinder theory predicts the broadside return within $\pm$ 1.4 dB with a confidence level of about 70 percent.

For end-on incidence, physical optics does very well for higher ka (10.86 and 21.72). There was no near field problem in this case and the mean values lie less than 0.05 dB from the physical optics prediction. For ka = 1.36 and 2.72, the Schmitt-Andrejewski theory lies less than 0.5 dB below the experimental mean, but at ka = 5.43, it fails by 1.3 dB. Based on Fig. 4-19, we contend that the theory will be no more than 2 dB greater, nor 0.8 dB less, than experiment with a confidence of 68 percent.

None of the mean experimental values presented in Figs. 4-17 through 4-19 lie more than 1.6 dB from the various theories used for comparison and we would like to attribute the theory with more accuracy than we have stated. Indeed, we will take the liberty of endowing the theory with absolute truth in Chapter VI, but Figs. 4-17 through 4-19 do not tell us if theory or experiment is in error; they merely say there is a difference.

V

INTRA-RANGE EVALUATION TESTS

Having considered the background material in the first four chapters, we now turn our attention to the reduction and evaluation of the VV and HH measured data. In this chapter we examine the measurements by the intra-range technique which is independent of theory, and is a comparison of separate data (from the same range) that have some relationship to one another through scaling or symmetry. In the following chapter (Chapter VI) data from all the ranges are compared directly with theory.

Earlier in Chapters I and IV we noted how the test data would be reduced and evaluated. Reduction of the data has consisted of recording the amplitude of lobe peaks and the angular location of nulls from each scattering pattern in tables like that shown in Table V-1. The locations of the numbered peaks and the lettered nulls in Table V-1 are indicated on the sample pattern in Fig. 5-1. This pattern is for the lowest ka, 1.36. As ka grows, evaluation points 8, 9 and 10 and letters E and F migrate closer to $\theta = 90^{o}$ and numbers 4, 5 and 6 and letters A, B, C and D move closer to $\theta = 0^{o}$, but lobe peak 7 remains in the aspect region near 45^{o}. In the reduction method data recorded for smaller ka values are equally distributed throughout the region for θ between 0^{o} and 90^{o}. As ka increases the recorded points begin to cluster about the 0^{o} and 90^{o} regions and only one point is recorded in the mid region near 45^{o}. This is an acceptable approach since, as ka increases, the lobe peaks in the mid region become small in amplitude compared to those at 0^{o} and 90^{o}.

Because our method of reducing and recording the measurements tends to accent the end-on and broadside regions, it follows that our evaluation and grading of the data is based primarily on the performance in these same regions. After recording and examining 60 percent of all the data and knowing that the remaining 40 percent would not be available until the last few days before the final reports would be due, we were forced to further limit the number of points that we could formally evaluate and grade. We concluded that the most efficient

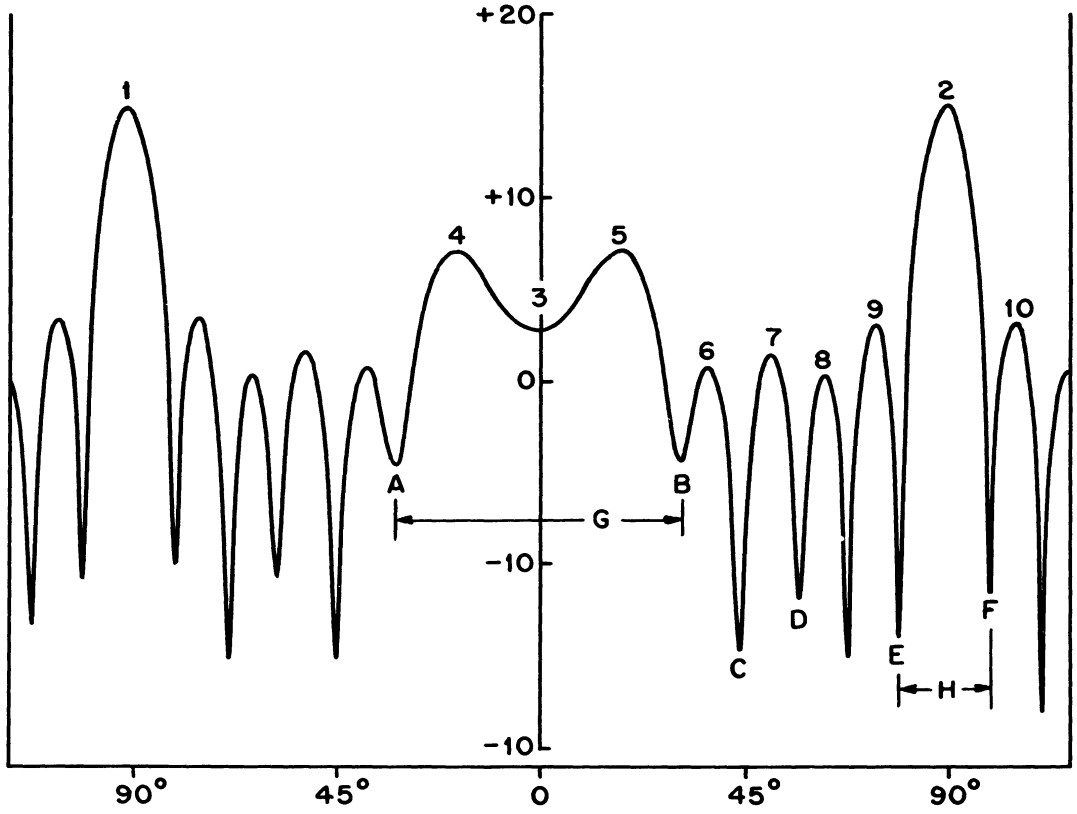

FIG. 5-1: SCATTERING PATTERN SHOWING THE POINTS RECORDED IN TABLE V-1.

TABLE V-1: EXAMPLE OF HOW DATA WAS REDUCED FOR EACH PATTERN FROM EACH RANGE. Scale: 1/2, Frequency 170 MHz, Polarization, HH, ka = 1.36. See Fig. 5-1 for the location of the points given here.

(dBsm)

Location	1	2	3	4	5	6	7	8	9	10
CC	+15.5	+15.5	+3.0	+6.75	+6.75	0.0	+4.25	+1.0	+2.75	+3.0
RSC	+15.0	+15.0	+2.75	+7.25	+7.25	+0.75	+1.5	+0.5	+4.0	+3.25
GD/FW	+15.5	+15.5	+3.5	+6.0	+6.0	+0.5	0.0	+1.0	+4.0	+3.75
RSS	+15.0	+15.0	+4.2	+7.2	+7.2	+0.1	+2.5	-0.7	+3.5	+3.5
MC	16.75	17.0	5.0	8.7	8.8	1.3	4.3	1.0	6.0	6.0
THEO	15.6	15.6	5.6	8.1	8.1	1.6	3.1	1.6	4.6	4.6

Lobe Amplitude

(Degrees)

Location	A	B	C	D	E	F	G	H
CC	-33.5	+29.5	+41	+57	+77.5	+99	63	21.5
RSC	-34	+31	+44	+57	+79	+100	65	21
GD/FW	-30	+30.5	+44.5	+56.5	+79.5	+102	60.5	24.5
RSS	-31.0	+31.7	+44.5	+68.4	+80.0	+101	62.7	21
MC	-31	+32	45	+68.2	80.0	100.5	63	20.5
THEO	-30	+30	44	57	79	101	60	22

Null Positions - A through F

Angular Widths - G and H

approach would be to limit our attention to points 2 and 3 in Fig. 5-1. Preliminary examination of these two points indicated that a meaningful insight into the performances of the ranges can be obtained from these samples. At the same time this limitation in our analysis would prevent us from being overwhelmed with too many details. After analyzing the ranges based on the data at end-on and broadside, we believe that we have displayed the weak and strong attributes of the ranges.

The intra-range evaluations consist of constant ka tests and end-on polarization comparisons. In the constant ka tests the VV and HH experimental cross sections at end-on and broadside are tabulated in a frequency-model scale display similar to that in Table III-1. The data from each range are presented in a separate table. Comparisons are made within each table along diagonal (constant ka) lines; thus the name "constant ka test" has been assigned to this form of evaluation.

In the end-on polarization comparison the cross section values at θ=0 are displayed on a graph like that in Fig. 3-8. Measurements from all the ranges are presented in the same graph. In this test, differences are noted between the VV and HH returns at end-on incidence. Theoretically these two values should be equal.

All the measurements involved in the evaluation were read directly from the test patterns submitted by the ranges. No corrections, additions or deletions have been introduced. The estimated accuracy for reading the patterns is $\pm$0.25 dB or better, depending on the recording paper submitted to us. The raw data listed in Tables V-2 through V-7 contain the entire family of sample points that will be used in all subsequent evaluations.

5.1 Constant ka Tests

Constant ka displays are shown in Tables V-2 through V-6 for the outdoor ranges and a small display for the indoor range in Table V-7. Four cross section values in dBsm are given in each box, these are VV and HH cross sections for end-on and broadside as indicated in the example below.

$\sigma_{VV}(\theta=0^o)$	End-on
$\sigma_{HH}(\theta=0^o)$	End-on
$\sigma_{VV}(\theta=90^o)$	Broadside
$\sigma_{HH}(\theta=90^o)$	Broadside

In these tables the frequency is constant across each row and is given along the left margin. Model size is constant in each column and is indicated at the top of the columns.

The diagonal lines connect boxes with the same ka. Cross sections in the same position in adjacent boxes along the same diagonal should differ by 6 dB while those separated by one or two boxes should differ by 12 and 18 dB respectively.

As an example, consider Table V-2 (Conductron data) for the 1/8 and 1/16 scale models when ka=1.36. Here $\sigma_{VV}(\theta=0^o)$ and $\sigma_{HH}(\theta=0^o)$ both differ by 7 dB, $\sigma_{VV}(\theta=90^o)$ by 6.5 dB, and $\sigma_{HH}(\theta=90^o)$ by 6.0 dB. For the same case in Table V-3 (Radiation Service data) the corresponding differences are 6.5, 6.25, 5.5 and 5.25 dB . Similar comparisons may be made between the 1/8 and the 1/4; then 1/4 and the 1/2 scale measurements, and so on for each line of equal ka. Deviations from the expected 6 dB difference are noted as errors.

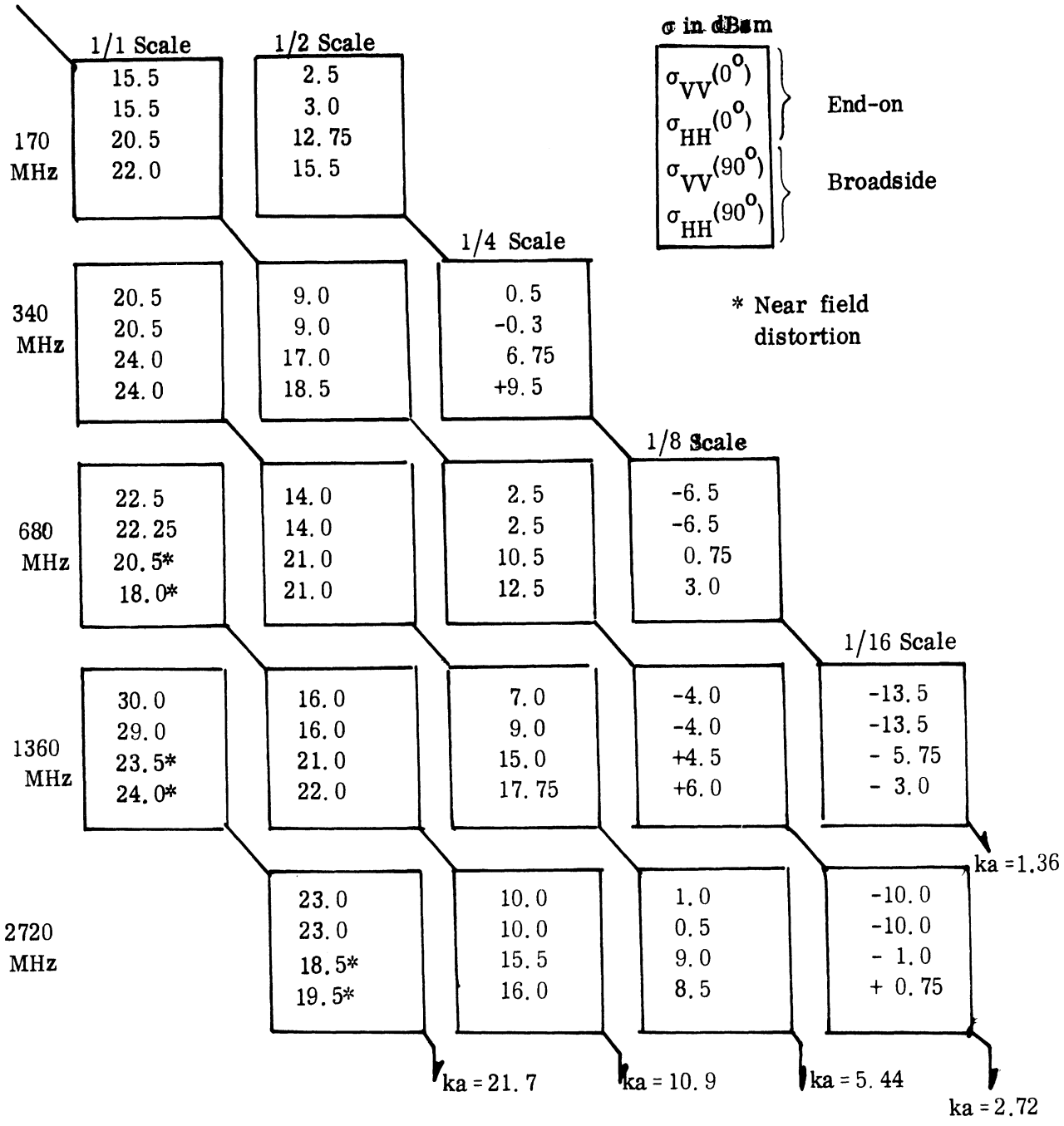

TABLE V-2: CONDUCTRON CONSTANT ka TEST.

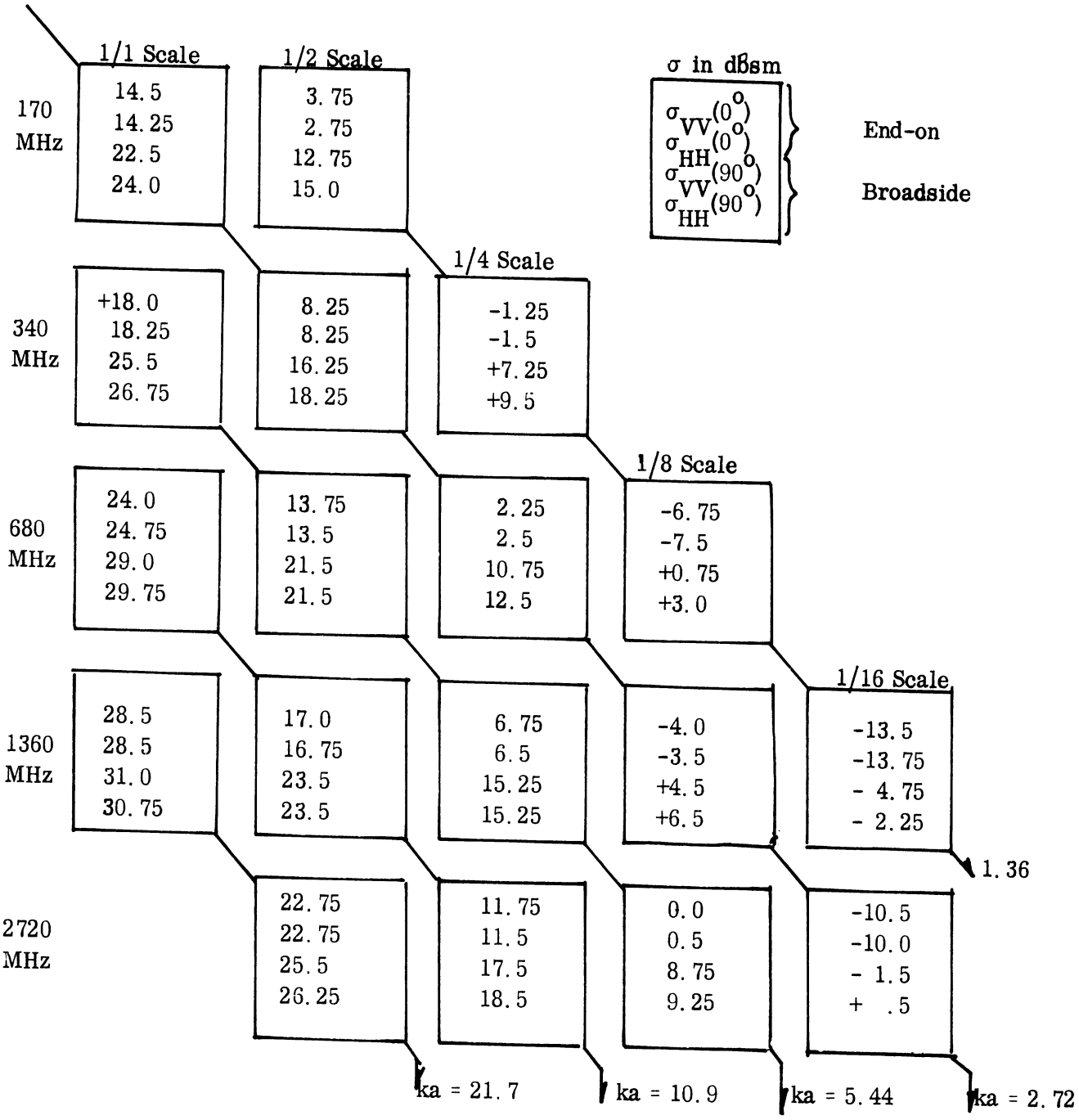

TABLE V-3: RADIATION SERVICE CONSTANT ka TEST.

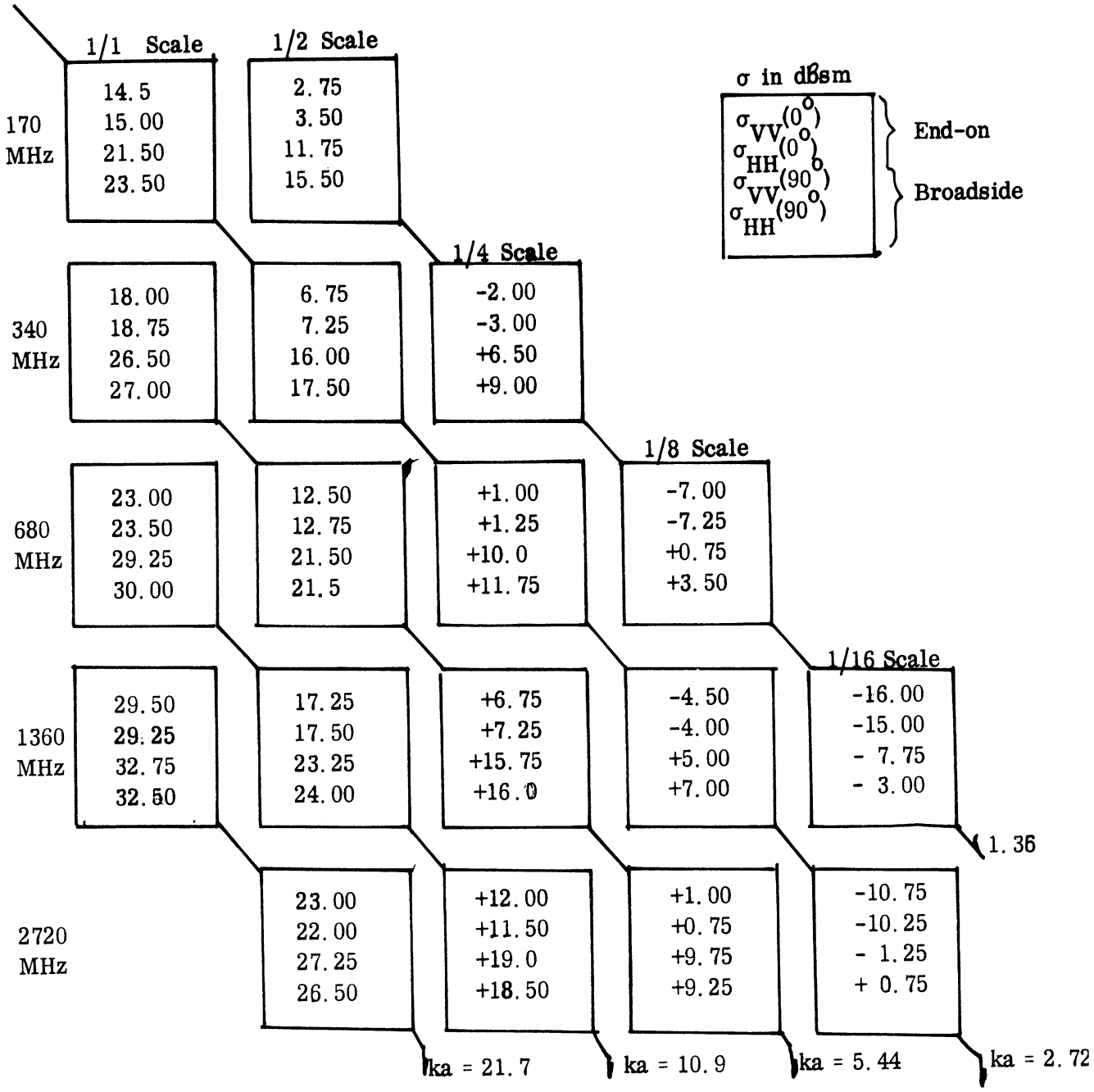

TABLE V-4: GD/FW CONSTANT ka TEST.

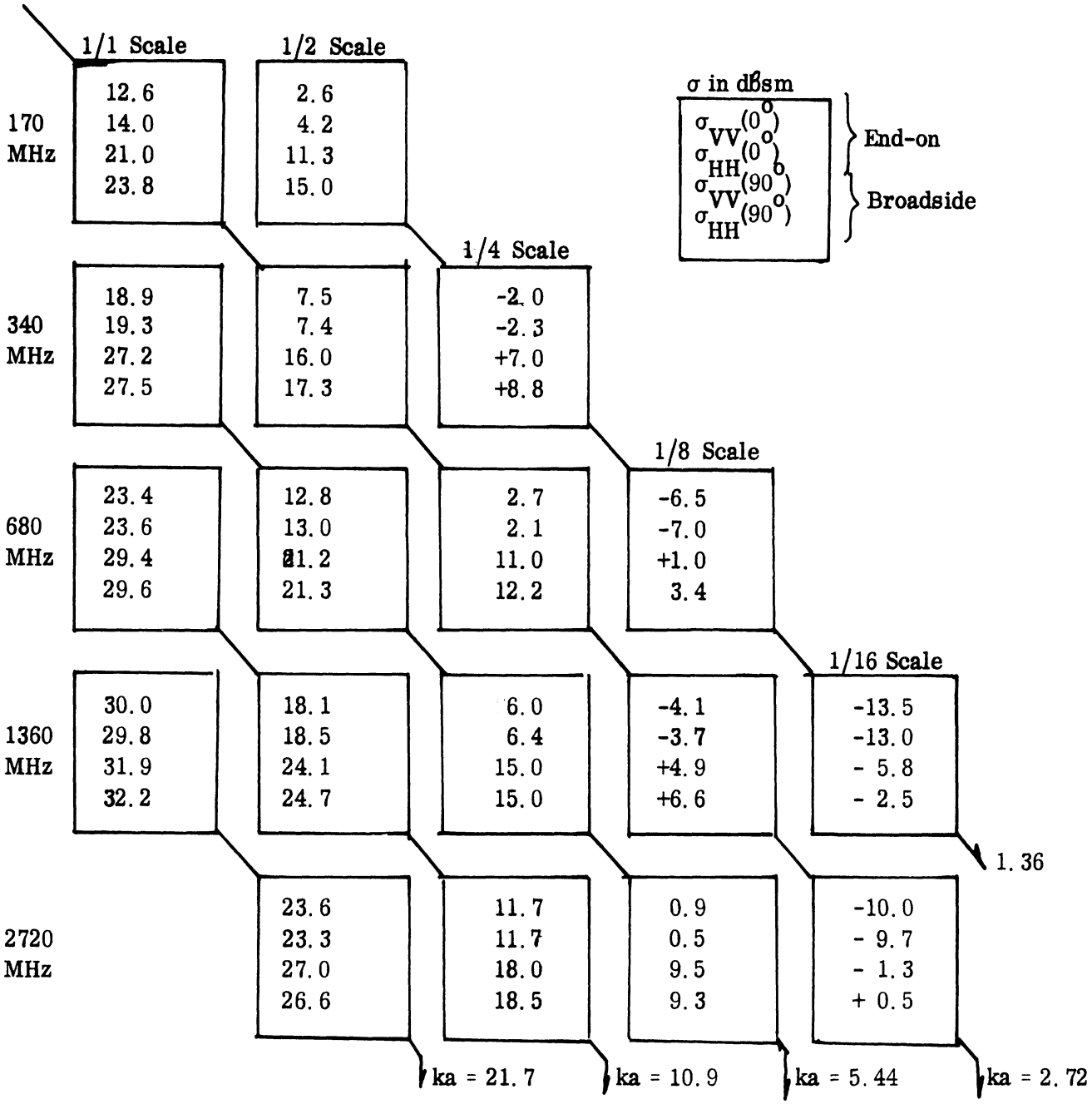

TABLE V-5: RAT SCAT CONSTANT ka TEST.

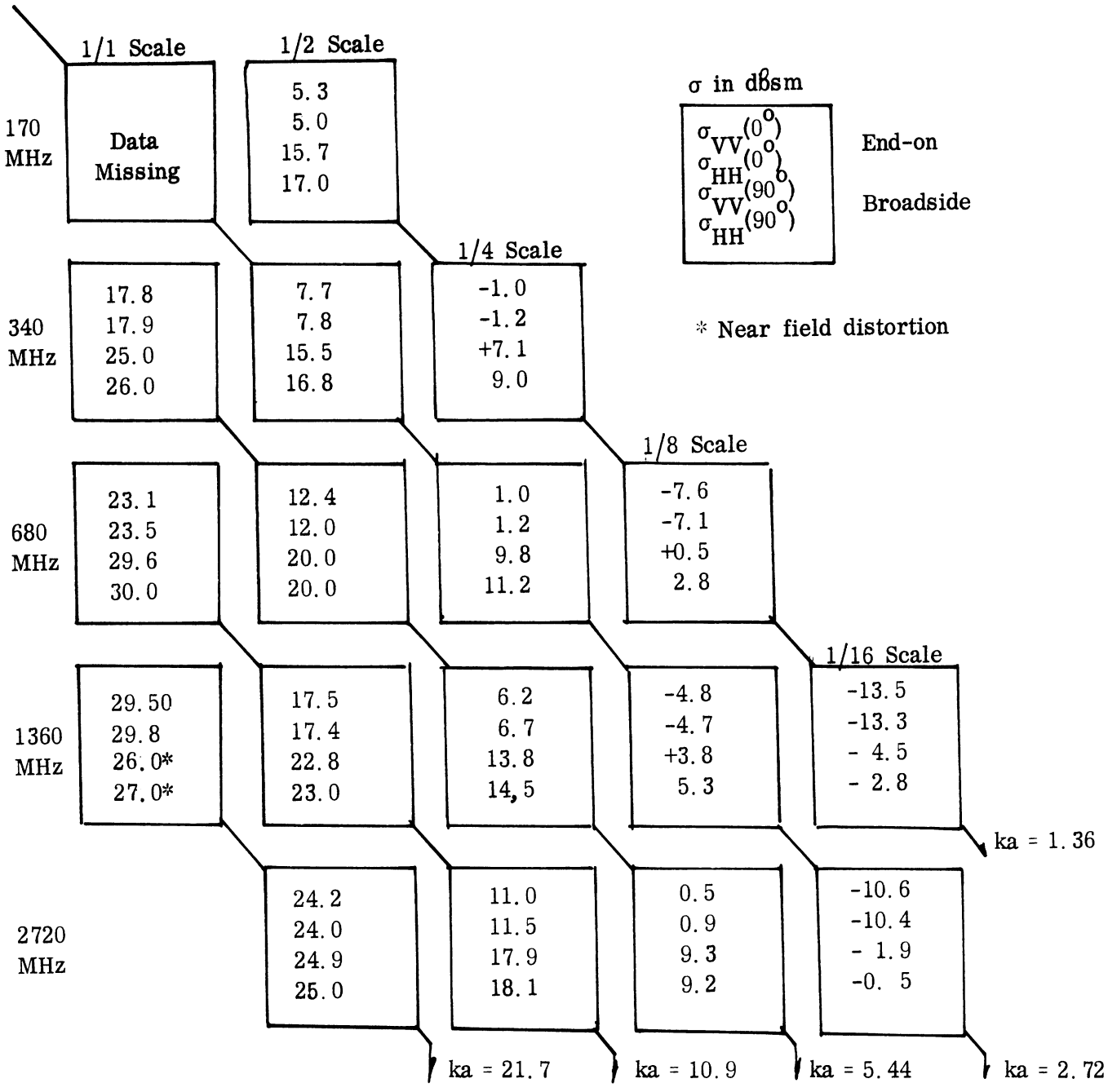

TABLE V-6: MICRONETICS CONSTANT ka TEST.

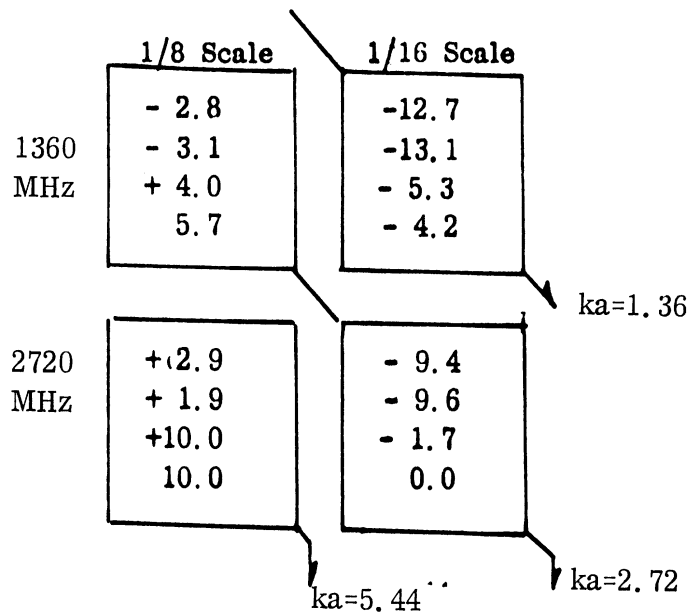

TABLE V-7: AVIONICS LABORATORY CONSTANT ka TEST.

Figure 5-2 shows the distribution of errors for the constant ka tests. In this figure the number of errors is given as a function of error size. For the upper three cases the errors are more discrete in their spread than in the lower two cases. This represents a difference in reading accuracy. Early in the program we read data to the nearest $\pm$ 1/4 dB while later on we attempted to read it to the nearest $\pm$ 1/10 dB. This change is due in part to the finer graduation on the recording paper used by some of the ranges.

The final tally for the errors found in the constant ka tests for Tables V-2 through V-7 are given in Table V-8. A total of 52 comparisons were made for each table except Table V-7. Extreme near field errors in the Conductron and Micronetics data are indicated by an asterisk (*). Although these errors may be between 6 and 12 dB in size, we treat them as any other error which exceeds 1 dB. Micronetics is missing data for the full scale model at 170 MHz because this target was dropped from the pedestal during its last test at this range. This missing data is also treated as an error of greater than 1 dB and therefore reduces this range's performance.

TABLE V-8: CONSTANT ka TEST RESULTS

Range	Errors 1dB and Less		Grade
	Total No. 52	Percent	
CC	39	75	C
RSC	46	88	B
GD/FW	43	84	B
RSS	45	87	B
MC	41	79	C
AL	4	100	A

Displays like Table V-8 above are used to summarize the evaluation results for other tests also. In these tables and some of the graphs the range names are abbreviated; CC (Conductron), RSC (Radiation Service) GD/FW (General Dynamics, Fort Worth), RSS (RAT SCAT Site), MC (Micronetics)

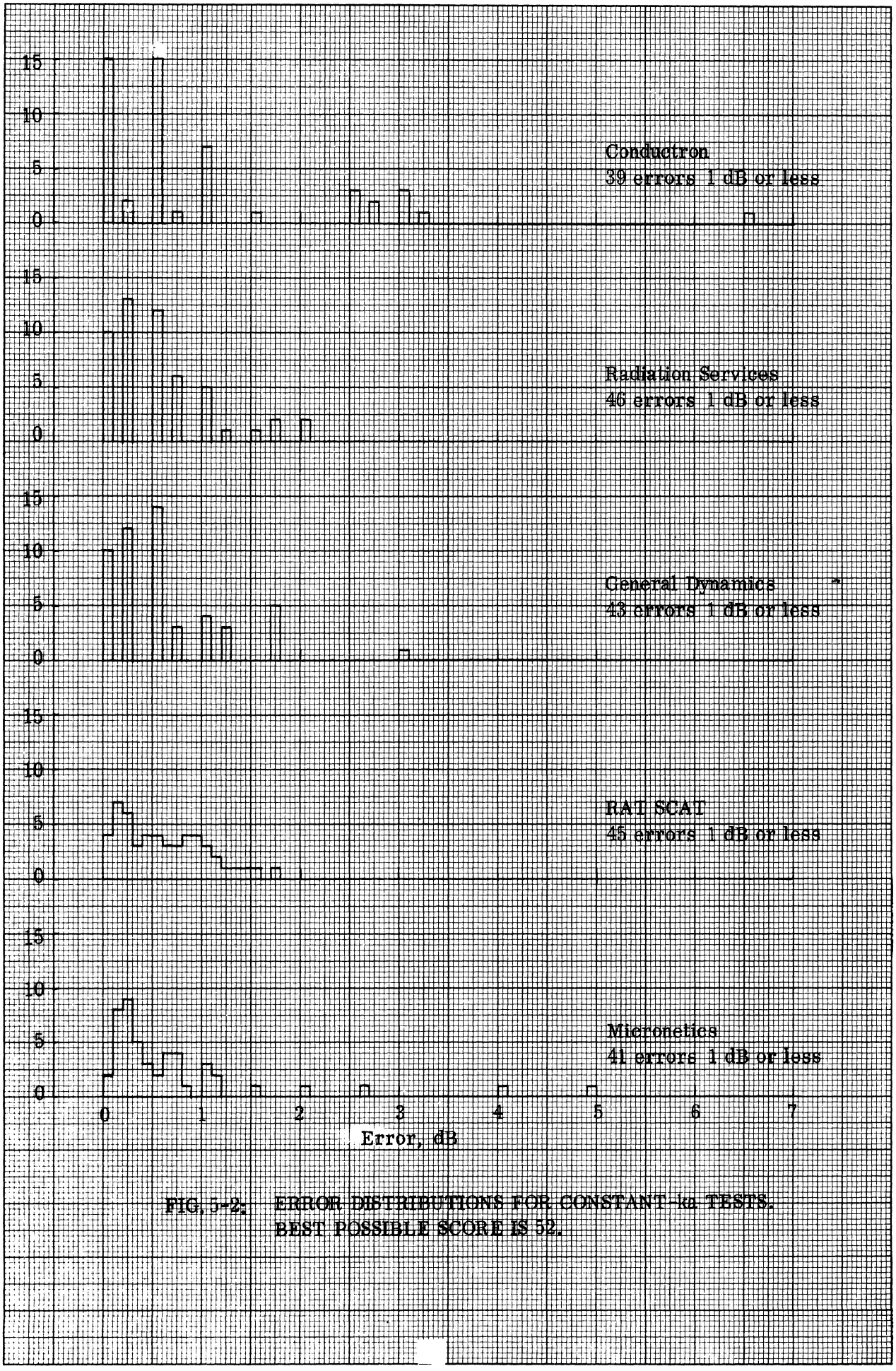

FIG. 5-2: ERROR DISTRIBUTIONS FOR CONSTANT-ka TESTS. BEST POSSIBLE SCORE IS 52.

and AL for Avionics Laboratory. The number of errors and the corresponding percentage of the total number of cases are listed according to range. A letter grade is found on the far right and is based on the percentage of errors 1 dB or less. As in Volume I the letter grades are defined as:

A	Very Good	(90 to 100 percent)
B	Good	(80 to 89 percent)
C	Acceptable	(70 to 79 percent)
D	Barely Acceptable	(60 to 69 percent)
E	Intolerable	(0 to 59 percent)

The constant ka test is independent of theoretical calculations and it seems reasonable to expect that no errors in scaled measurements should exceed 1 dB. Generally speaking, we found that most of the errors greater than 1 dB were due to near field distortion. In these cases the errors would be located in the lower left portion of the constant ka test tables where the measurements for the larger models at higher frequencies are found.

There are other errors which are not due to near field effects; most noticeable in this regard is the difference between the 1/2 and 1/4 models for ka=1.36 for all the ranges but particularly for GD/FW and RAT SCAT. GD/FW had one 3 dB error between the 1/8 and 1/16 scale data for $\sigma_{VV}(0^o)$. This was the largest error in this test not due to near field effects. It is hard to find a reason for such a large error other than carelessness. With the exception of the cases just mentioned, the performances of the ranges in this test are satisfactory, but are far from outstanding as reflected in the grades of Table V-8 .

5.2 End-on Polarization Comparison

The end-on cross sections for VV and HH polarization given in the tables of the last section are now arranged in another form in Fig. 5-3. At first glance this dense collection of data may be hard to digest, but after referring back to Fig. 3-8, this display hopefully will become more meaningful. Constant ka lines are labelled in Fig. 3-8 but have been omitted from Fig. 5-3 to reduce conjestion. The one inch long horizontal lines in Fig. 5-3 are the same

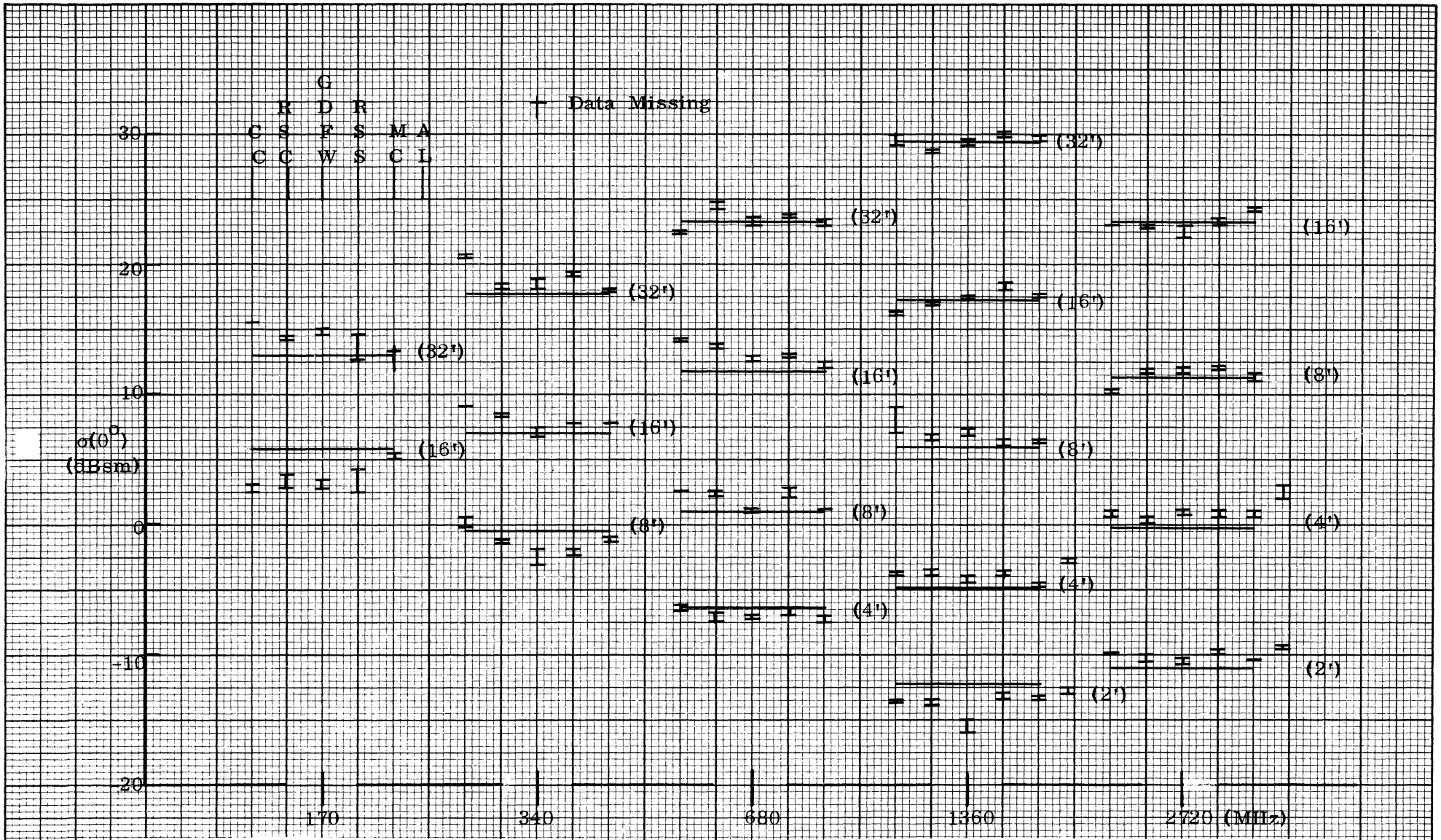

FIG. 5-3: COMPARISON BETWEEN THEORY AND EXPERIMENT AT END-ON FOR CYLINDERS, VV AND HH POLARIZATIONS (I): Theoretical results (——) taken from Fig. 3-9.

theoretical values denoted by points in Fig. 3-8. The short pairs of horizontal lines connected by a vertical line (generally there are five pairs per theoretical line) show the level of the experimental data from the ranges. In each case they are listed from left to right as Conductron, Radiation Service, General Dynamics, RAT SCAT, Micronetics, and in four instances, Avionics Laboratory.

The lengths of the vertical lines in this display are equal to the error between the VV and HH end-on returns but no attempt is made to show which of the short horizontal lines is VV and which is HH. Although the theoretical, as well as experimental, results are shown in Fig. 5-3, the evaluation test is like the constant ka test in that it is essentially independent of theory. For the present case we depend upon theory only for the proof that for end-on incidence the VV and HH polarized returns are equal. If one accepts this statement there is no further need for any theoretical arguments for the polarization comparison tests.

Therefore, for the present test we should concern ourselves only with the length of the vertical line connecting the VV and HH cross sections in Fig. 5-3. The distribution for the polarization errors shown in Fig. 5-3 are displayed in bar graph form in Fig. 5-4. This display has the same format as Fig. 5-2. Note that Micronetics has a very good cluster of errors less than 1 dB but failed to score perfectly because of missing data. Errors 1 dB and less are tabulated in Table V-9 along with the percentages and grades.

TABLE V-9: END-ON POLARIZATION TEST RESULTS

	Errors 1 dB and Less		
Range	Total No. 18	Percentage	Grade
CC	17	95	A
RSC	18	100	A
GD/FW	18	100	A
RSS	16	89	B
MC	17	95	A
AL	4	100	A

So far as grades are concerned this test produced the highest marks of all the evaluation tests, with three ranges registering errors of 1 dB or less

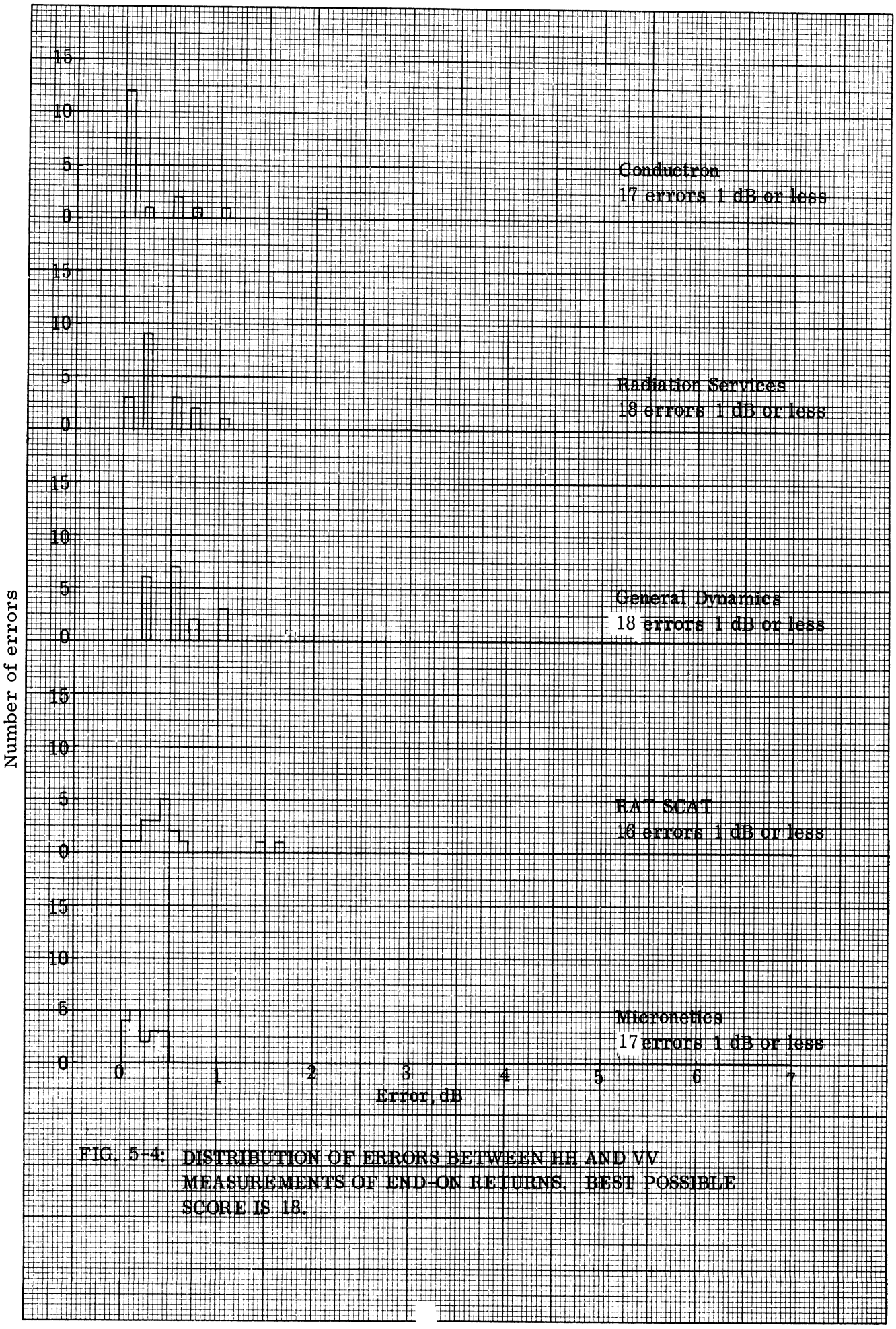

FIG. 5-4: DISTRIBUTION OF ERRORS BETWEEN HH AND VV MEASUREMENTS OF END-ON RETURNS. BEST POSSIBLE SCORE IS 18.

for all the comparisons. The four cases in which errors exceeded 1 dB stand out in Figs. 5-3 and 5-4. At 170 MHz RAT SCAT had two errors of 1.75 dB and Micronetics was missing the full scale measurements. At 1360 MHz for the 1/4 scale model Conductron achieved the low point with a 2 dB error.

It is to be expected that for this type of evaluation all the ranges should do well. The agreement between VV and HH polarization for an aspect view with total roll symmetry should be one of the first things checked by the range operator when he is analyzing cross section data. Another reason for the good performance in this test is that near field effects are not present at end-on incidence because at this aspect angle the target always exposes a sufficiently small view of itself to the radar so that it is in the far field. We should emphasize, perhaps, that this has been a test for consistency by making use of a well known theoretical fact. Results which rate high in this test may have an inferior rating when we examine the absolute level of the end-on cross section in the next chapter.

This concludes the intra-range tests where data from each range were compared and judged by themselves, independently of theory and the other ranges. The separate results for each range were then compared with one another in Tables V-8 and V-9. For the inter-range tests in the next chapter, bar graphs like that in Fig. 5-3 are used to compare measurements with theory.

VI

INTER-RANGE EVALUATION TESTS

In the inter-range evaluation tests, cross section measurements for end-on and broadside aspect angles are compared with one another and with theory. These comparisons are presented in the same form as in Fig. 5-2, in fact the data in this figure is one of the cases analyzed in these tests. Data for broadside (VV and HH) are grouped in the form shown in Figs. 3-10 and 3-11. Also included here are VV and HH measurements for the sidelobe peaks next to broadside.

If near field distortions are excluded, we find that broadside measurements agree better with theory than do the end-on measurements. For a fixed frequency-model size situation there is also better agreement for broadside than end-on measurements when related experimental data are compared. As should be expected, near field distortions become even more pronounced in the data for the first sidelobe away from broadside than for the specular flash.

6.1 End-on Data

To rate the ranges on the basis of the measured end-on returns, we computed the differences between the theory and the experiment for both polarizations. These differences can be inspected in the graphical presentation of Fig. 5-2 or they can be calculated from the raw and theoretical data presented in Tables III-1 and V-2 through V-7. The distribution of the errors is displayed in Fig. 6-1 and, as in the error distributions shown in Chapter V , we make no distinction between positive or negative errors. Notice that Micronetics' errors were all clustered below 1.3 dB and that this range did better than all the other ranges in spite of its failure to measure the full scale cylinder at 170 MHz. Conductron shows the largest spread in errors and turned in the poorest performance, while the remaining three lie between these extremes.

The Avionics Laboratory error distribution is not included in Fig. 6-1 because it performed far fewer tests. Its performance is tabulated, however, along with those of the other ranges, in Table VI-1. Because AL turned in only

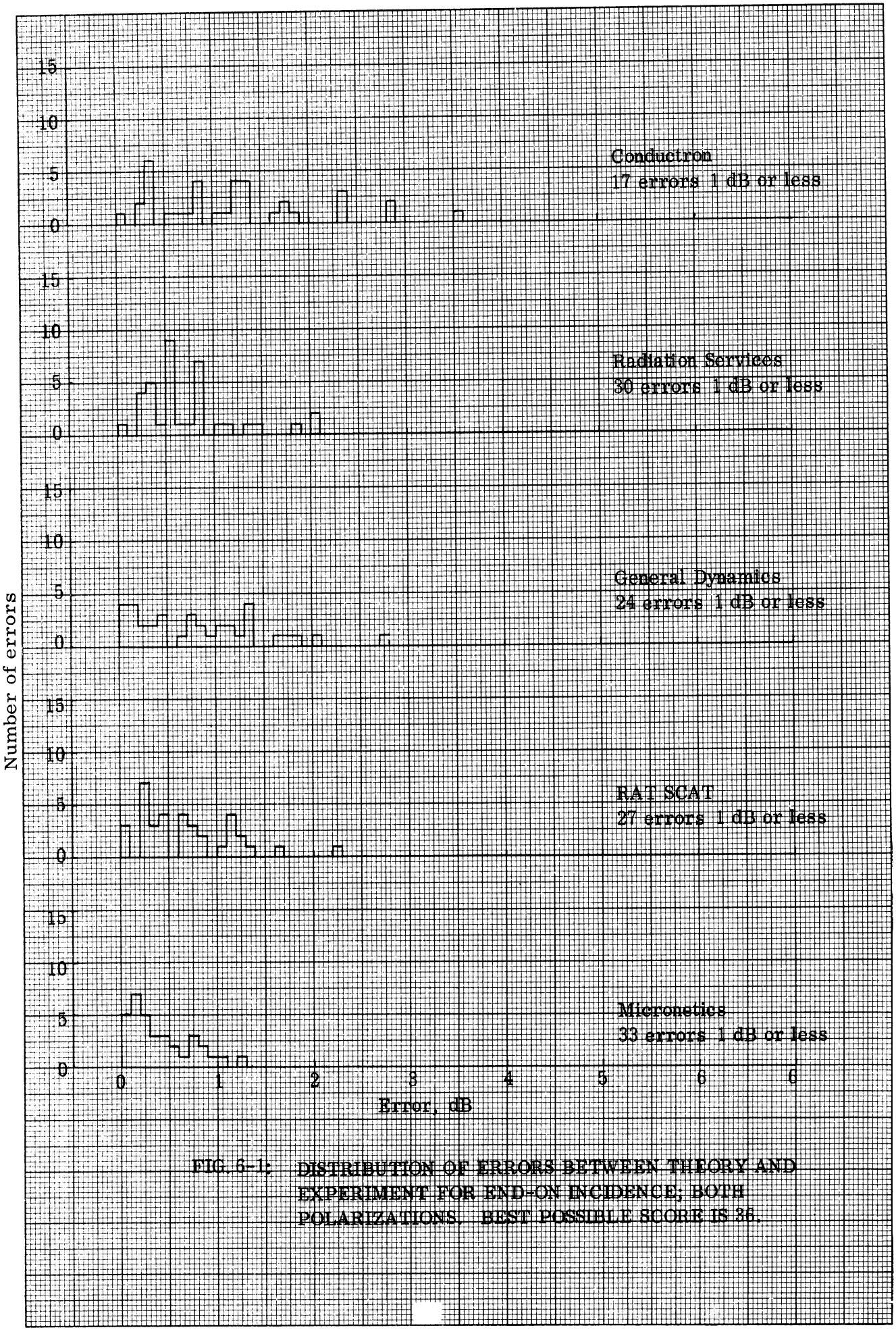

FIG. 6-1: DISTRIBUTION OF ERRORS BETWEEN THEORY AND EXPERIMENT FOR END-ON INCIDENCE; BOTH POLARIZATIONS. BEST POSSIBLE SCORE IS 36.

four errors less than 1 dB of a total of 8 measurements, it receives an E.

TABLE VI-1: ERRORS BETWEEN THEORY AND EXPERIMENT FOR END-ON INCIDENCE (see Fig. 6-1).

Range	Errors 1 dB and Less		Grade
	No.	Percent	
CC	17	47	E
RSC	30	83	B
GD/FW	24	67	D
RSS	27	75	C
MC	33	92	A
AL	4*	50	E

*of a possible 8 .

The poor results in Table VI-1 cases some suspicion on the reliability of the theory, but we pointed out in Chapter III that the end-on theoretical model was not expected to be as accurate as the broadside model. In the mathematical formulation for end-on incidence, we assumed the cylinder to be an isolated disc rather than one attached to a cylinder of finite length with another disc at the opposite end. For smaller ka, effects from the far end of the cylinder occur in the form of reflected traveling waves that weaken the end-on theory. This is, in fact, seen in the measurements of Fig. 5-2 in which the theory and experiment match better for increasing ka. In most instances of disagreement between theory and experiment in Fig. 5-2 a shift of one dB or less in the theory would align it with the average of the experimental data.

More disturbing than the lack of agreement between theory and measurement are the variations between the measurements themselves. If the measurements were more consistent among themselves it would be easy to conclude that the theory was in error by a given amount, but in many cases in Fig. 5-2 it is difficult to assign a "correct" radar cross section value.

In summary, for the end-on comparison with theory, Micronetics did very well, perhaps because its crew used an auxiliary flat plate calibration in addition to a sphere. Both Conductron and the Avionics Laboratory did poorly; General Dynamics performed only somewhat better. Radiation Service and RAT SCAT take second and third place honors, respectively, behind Micronetics.

6.2 Broadside Data

As in the end-on tests, we computed the differences between theory and experiment for broadside incidence. Since the broadside return depends upon polarization, the computations were performed for the VV and HH polarizations separately, but the errors are presented as a single group. The errors can be ascertained from the graphical displays of Figs. 6-2 and 6-3 or they can be computed by taking differences between the theoretical values of Table III-1 and the experimental values reported in Tables V-2 through V-7.

The asterisks in Figures 6-2 and 6-3 indicate that severe near field pattern distortions were observed in the experimental results. These distortions were so great that the data belonging with a particular theoretical value in some cases fell on that associated with an entirely different target. The inclusion of the distorted values in Figs. 6-2 and 6-3 would have caused much confusion, hence we omitted plotting them and merely indicated the presence of these large errors by the asterisks. The missing values are available, of course, in the tables of Chapter V.

We find better overall agreement between theory and experiment in Figs. 6-2 and 6-3 than we did in Fig. 5-2 (the end-on results) Most of the discrepancies in the broadside data are due to near field distortions which we know exist. One noticeable exception is the General Dynamics measurements of the 2-foot (1/16 scale) cylinder at 1360 MHz in Fig. 6-2. This result is almost 3 dB below the theory and measurements of the other ranges. Equally poor measurements for this case were found in Fig. 5-2, but in Fig. 6-3 (HH polarization, broadside) good agreement is found for this case both with theory and the other measurements. The errors in the GD/FW data and the other errors not attributable to near field effects, are thought to be due to one or more effects, e. g. lack of field uniformity, secondary reflections or lack of sufficient care in normal calibration procedures.

The distributions of the errors in the broadside measurements are shown

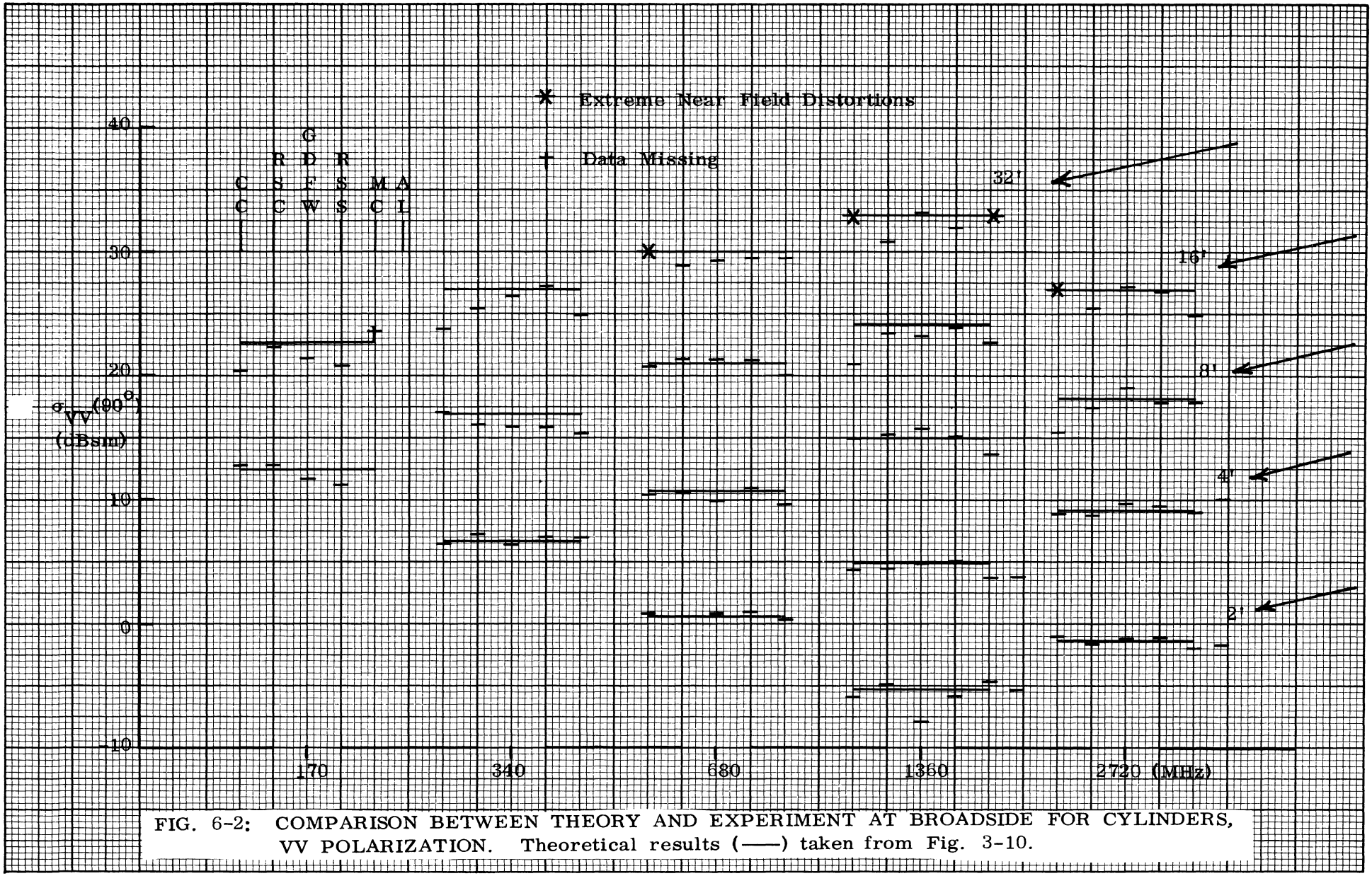

FIG. 6-2: COMPARISON BETWEEN THEORY AND EXPERIMENT AT BROADSIDE FOR CYLINDERS, VV POLARIZATION. Theoretical results (——) taken from Fig. 3-10.

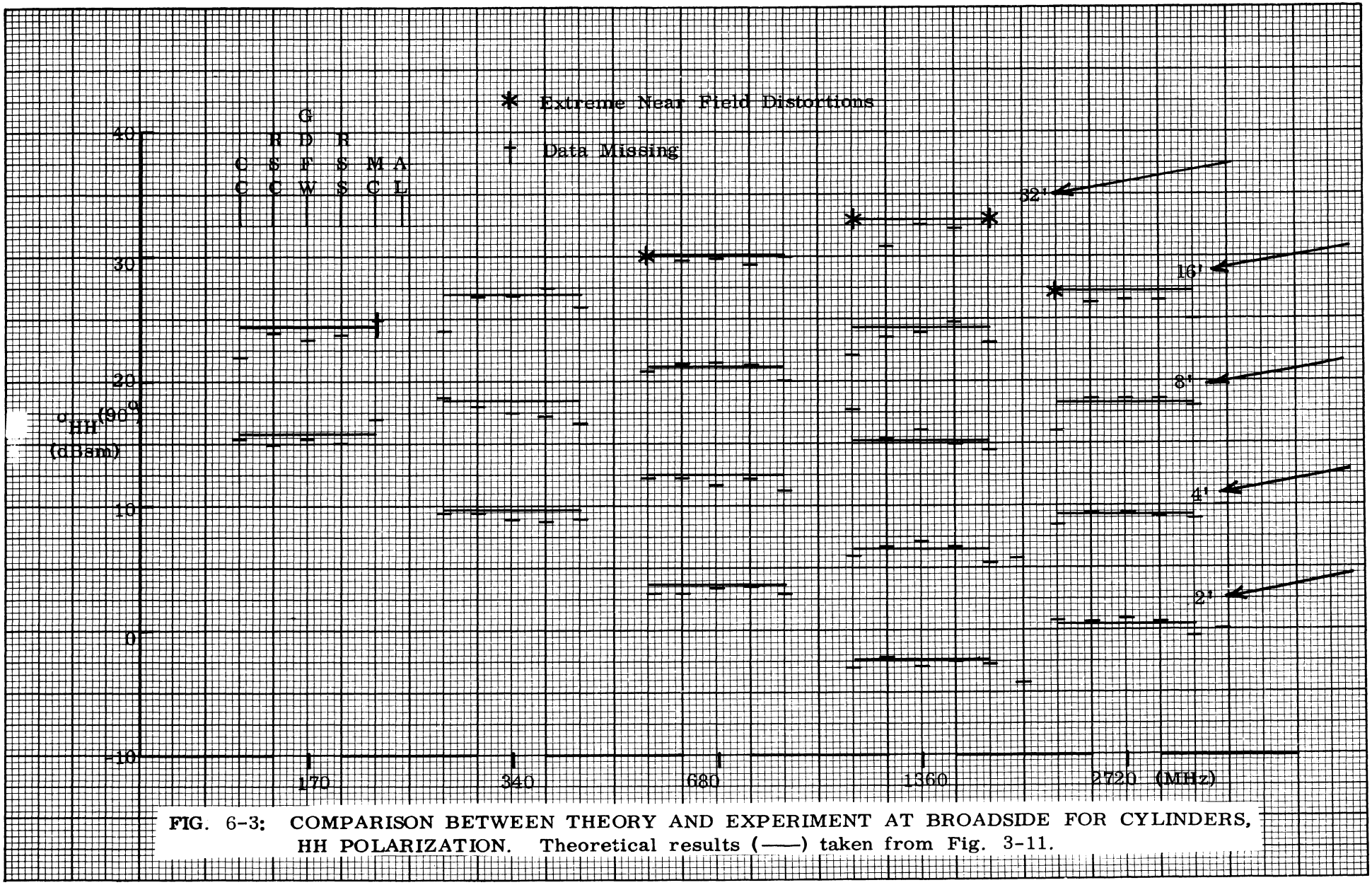

FIG. 6-3: COMPARISON BETWEEN THEORY AND EXPERIMENT AT BROADSIDE FOR CYLINDERS, HH POLARIZATION. Theoretical results (——) taken from Fig. 3-11.

in Fig. 6-4 and are summarized in Table VI-2. Note that because many of Micronetics' errors are greater than 1 dB, this range turned in the worst performance. General Dynamics shows the best performance of the outdoor ranges, but as indicated in the summary of Table VI-2, Avionics Laboratory outperformed them all.

TABLE VI-2: ERRORS BETWEEN THEORY AND EXPERIMENT AT BROADSIDE FOR BOTH POLARIZATIONS

Range	Errors 1 dB and Less		Grade
	No.	Percent	
CC	21	58	E
RSC	30	83	B
GD/FW	34	94	A
RSS	33	92	A
MC	15	42	E
AL	8*	100	A

*of a possible 8.

6.3 Sidelobe Symmetry

Measurements and theory for the sidelobes immediately to the left and right of the broadside specular return are shown in Fig. 6-5 for VV and Fig. 6-6 for HH polarization. These displays should not be confused with those in Fig. 5-2, in which differences in polarization are given. In this case the two short lines are the measured levels of the right and left sidelobes. The sidelobe data are being examined in ascertain the degree of pattern symmetry. Ideally the two short horizontal lines connected by the vertical line should be equal. Any differences, and these are indicated by the length of the vertical line, are indicative of pattern "sloppiness" or near field problems. One of the first signs of near field distortion is the disappearance of the first sidelobes, indicated by the asterisks, thus more field field problems are seen in these figures than in the broadside data.

For $ka \geq 2.72$ the theoretical sidelobe level is found by subtracting 13 dB from the broadside return since the pattern response for this aspect region is

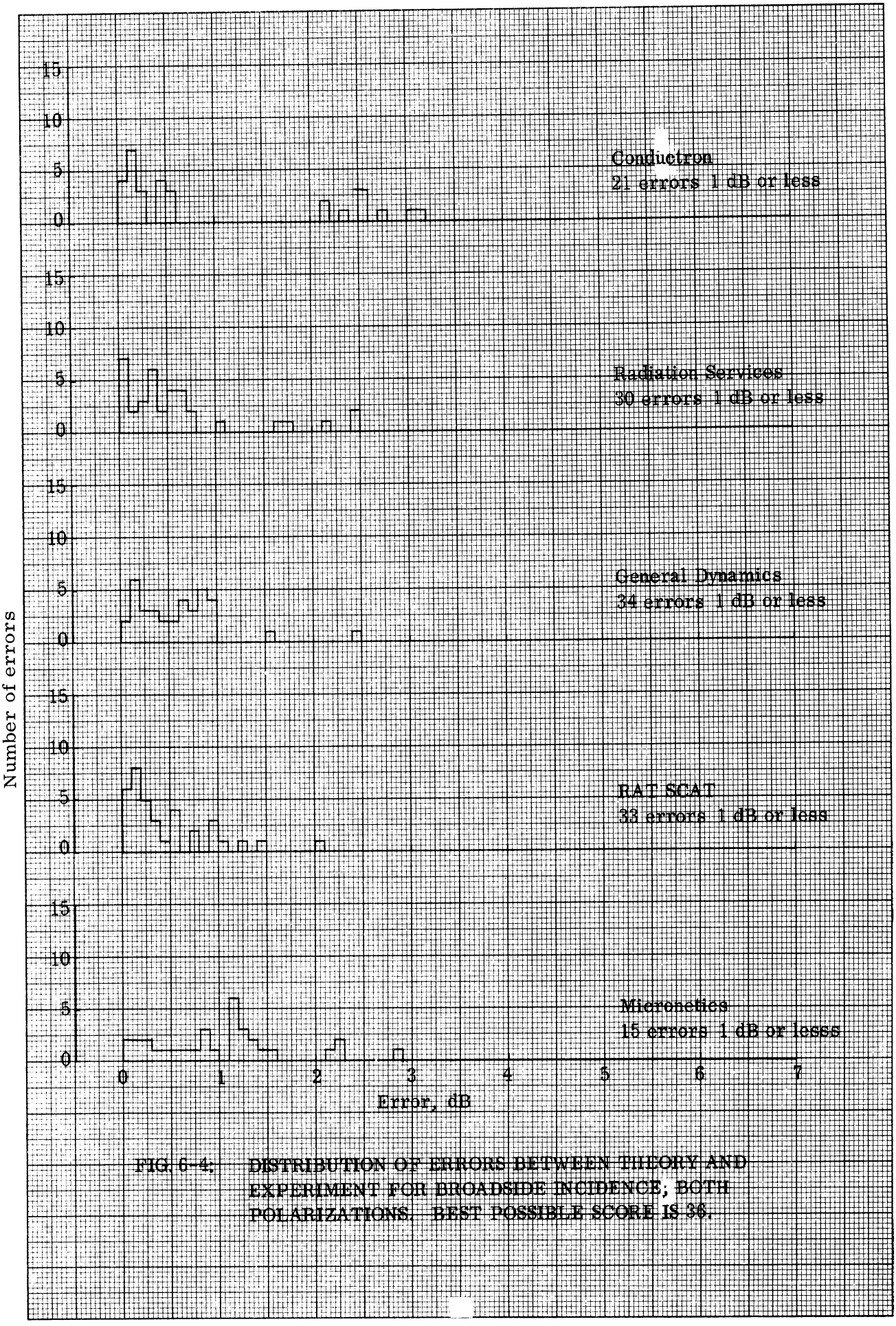

FIG. 6-4: DISTRIBUTION OF ERRORS BETWEEN THEORY AND EXPERIMENT FOR BROADSIDE INCIDENCE; BOTH POLARIZATIONS. BEST POSSIBLE SCORE IS 36.

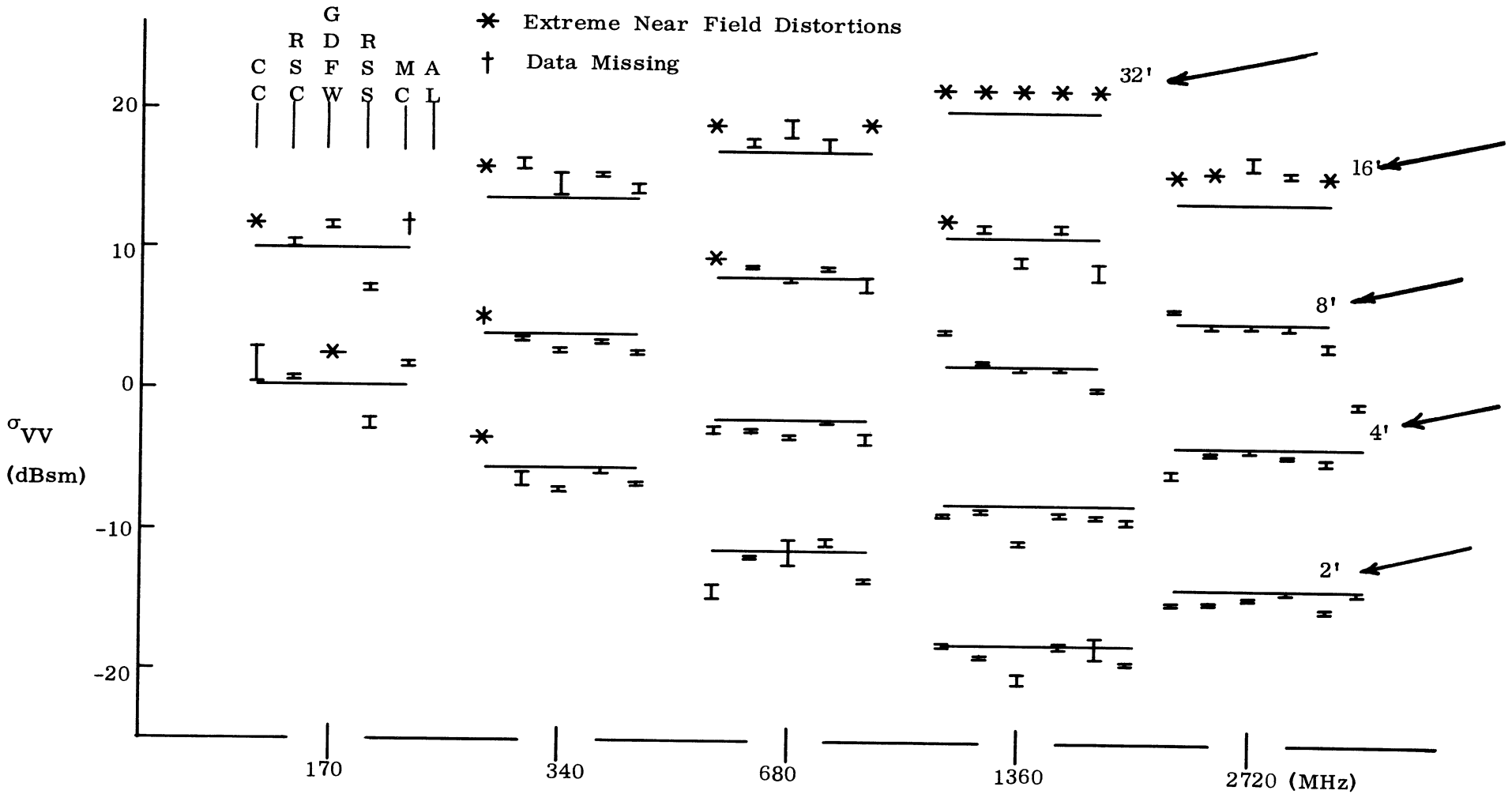

FIG. 6-5: COMPARISON BETWEEN THEORY AND EXPERIMENT AT FIRST SIDELOBES NEXT TO BROADSIDE (I) FOR CYLINDER, VV POLARIZATION.

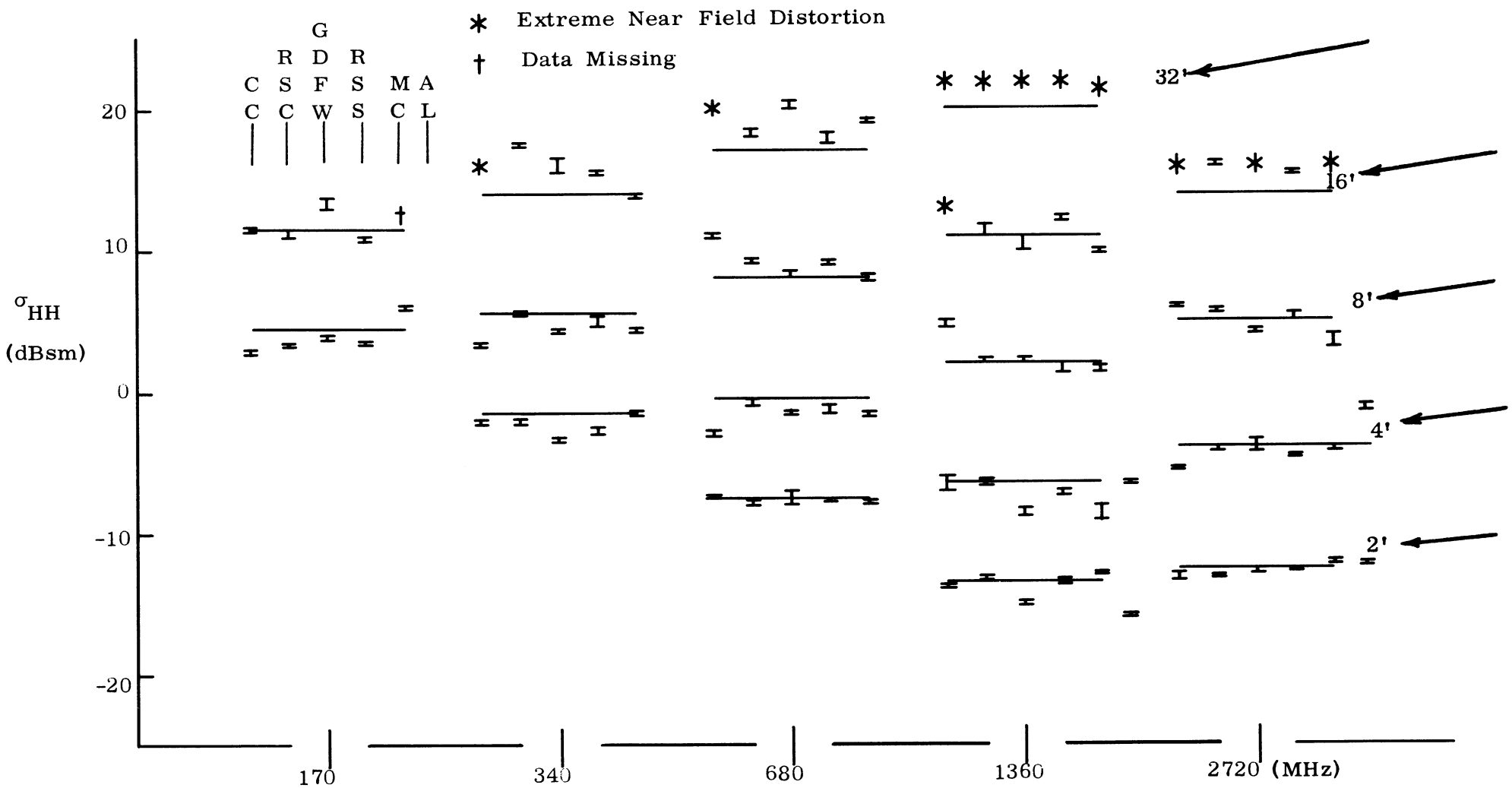

FIG. 6-6: COMPARISON BETWEEN THEORY AND EXPERIMENT AT FIRST SIDELOBES NEXT TO BROADSIDE (I) FOR CYLINDER , HH POLARIZATION.

governed by a $\sin x/x$ behavior (see Eq. 3.13),. For the case of ka=1.36 the sidelobe level is read directly from Fig. 3-2 in $dB\lambda^2$ and converged to dBm^2 for each model size.

No grades have been assigned to these measurements because they do not reveal any new sources of errors. Most of the troubles shown in Figs. 6-5 and 6-6 can be seen in the broadside and end-on comparisons. These results have been included to give additional examples showing how the data can be reduced as well as to emphasize that a primary cause of error in the test program is due to near field distortions. Another area where errors were noticeable is the ka=1.36 region and some of the evaluation tests suggest this target size is a troublesome one independently of near field effects. See the discussion on secondary reflections in Section 4.1.2.5 of Volume I.

6.4 Special Evaluation for ka=1.36

Of all the measurements submitted to us by the ranges, the ka=1.36 patterns showed the widest unexplained spread in values. To demonstrate the divergence of the data, we present the four patterns in Figs. 6-7 through 6-10, all for ka=1.36. The first two (6-7 and 6-8) summarize the measurements of the 1/2 scale cylinder at 170 MHz and the last two (6-9 and 6-10) summarize the measurements of the 1/8 scale cylinder at 680 MHz. The ranges performed somewhat better at the higher frequency than the lower.

To arrive at an evaluation of this special case, we sampled the individual range patterns at all integral values of 5^o of aspect lying between (and including) end-on and broadside. This produced 19 radar cross section values for each range and polarization for 170 and 680 MHz. In addition, we treated the theory as given by the Norair SDT (Figs. 4-17 and 4-18) as though it represented data from a sixth range. Having effectively six sets of range data (five actually from the ranges and one from the theory) we computed the mean radar cross section at each of the aspect angles shown in the figures and used these values as "standards". The departure of individual range returns from these mean values constituted "errors", which we listed and tabulated. Each range (including the theory) pattern thus bears 19 values of error for each of the four patterns, leaving us with 76 numbers to evaluate per range.

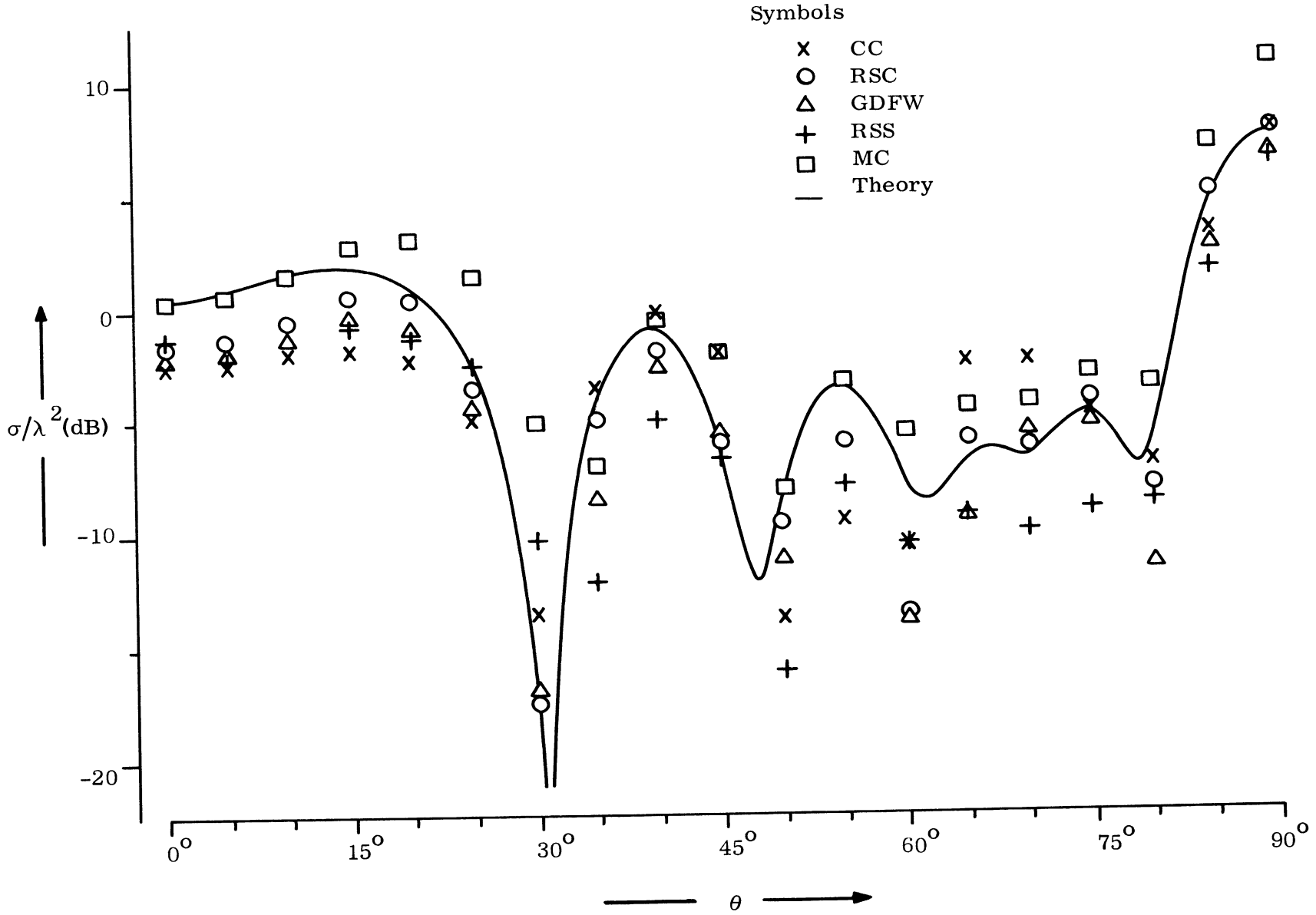

FIG. 6-7: COMPARISON BETWEEN THEORY AND EXPERIMENT FOR THE 16 FOOT CYLINDER FOR VV POLARIZATION AT 170 MHz.

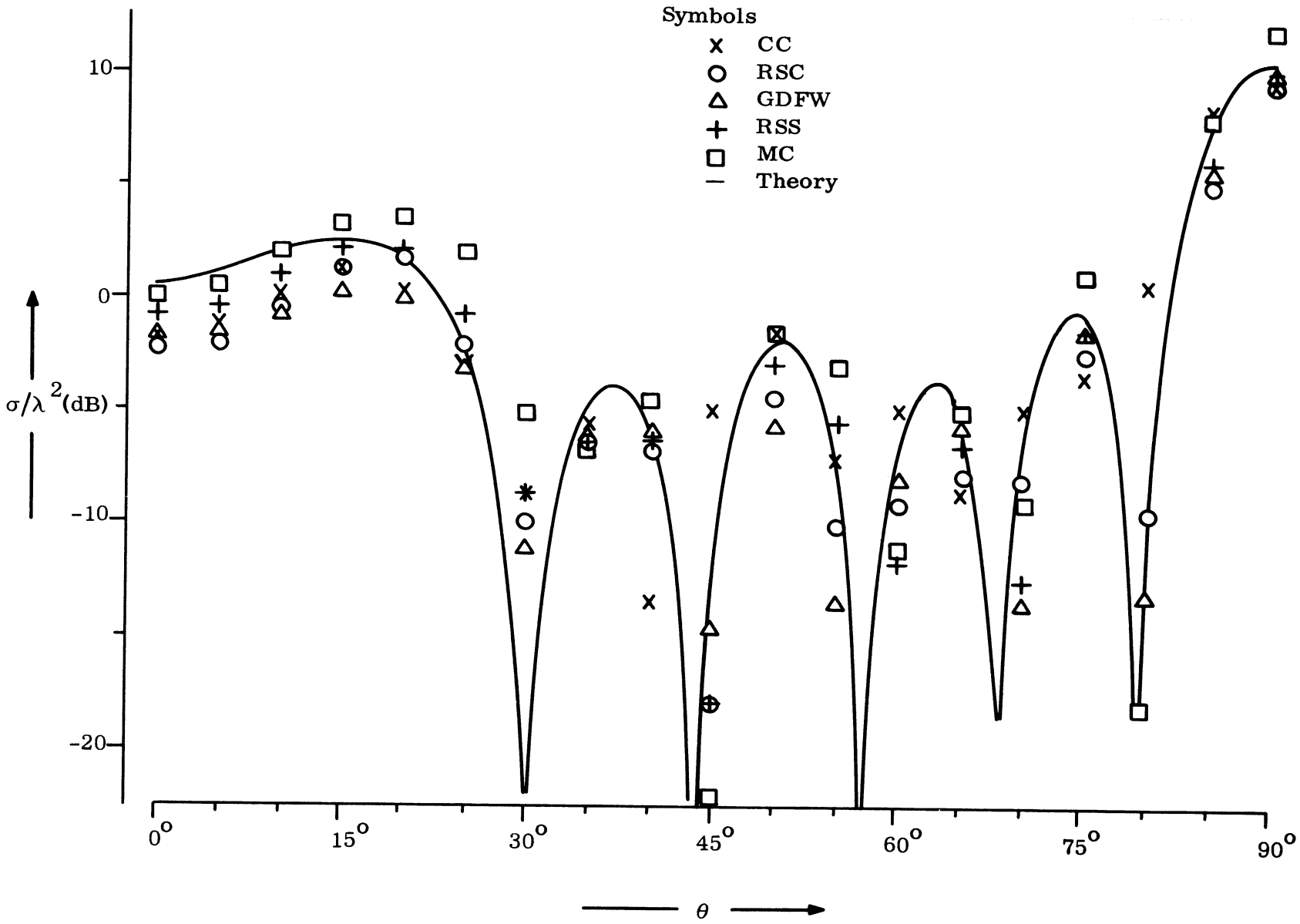

FIG. 6-8: COMPARISON BETWEEN THEORY AND EXPERIMENT FOR THE 16 FOOT CYLINDER FOR HH POLARIZATION AT 170 MHz.

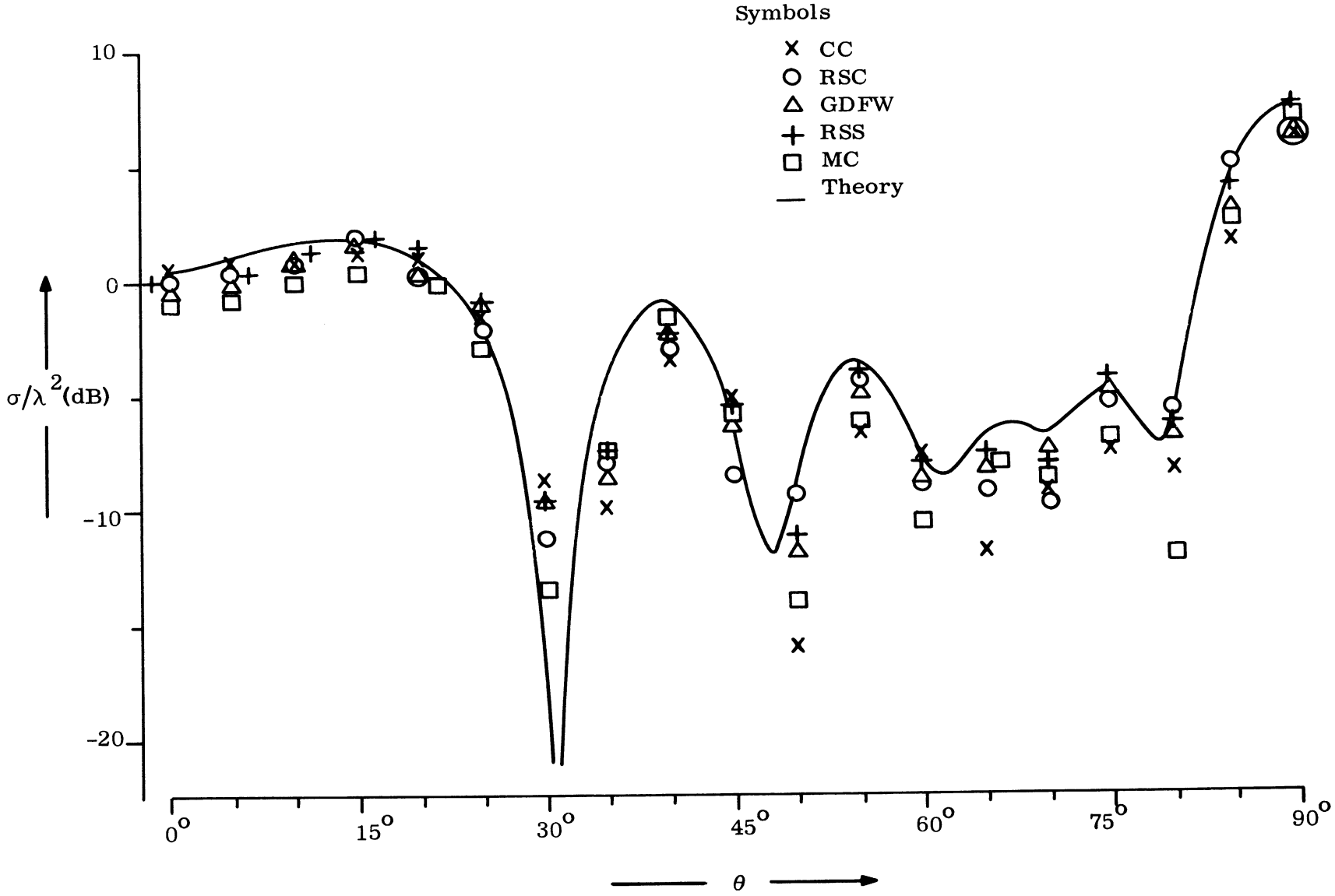

FIG. 6-9: COMPARISON BETWEEN THEORY AND EXPERIMENT FOR THE 4 FOOT CYLINDER FOR VV POLARIZATION AT 680 MHz.

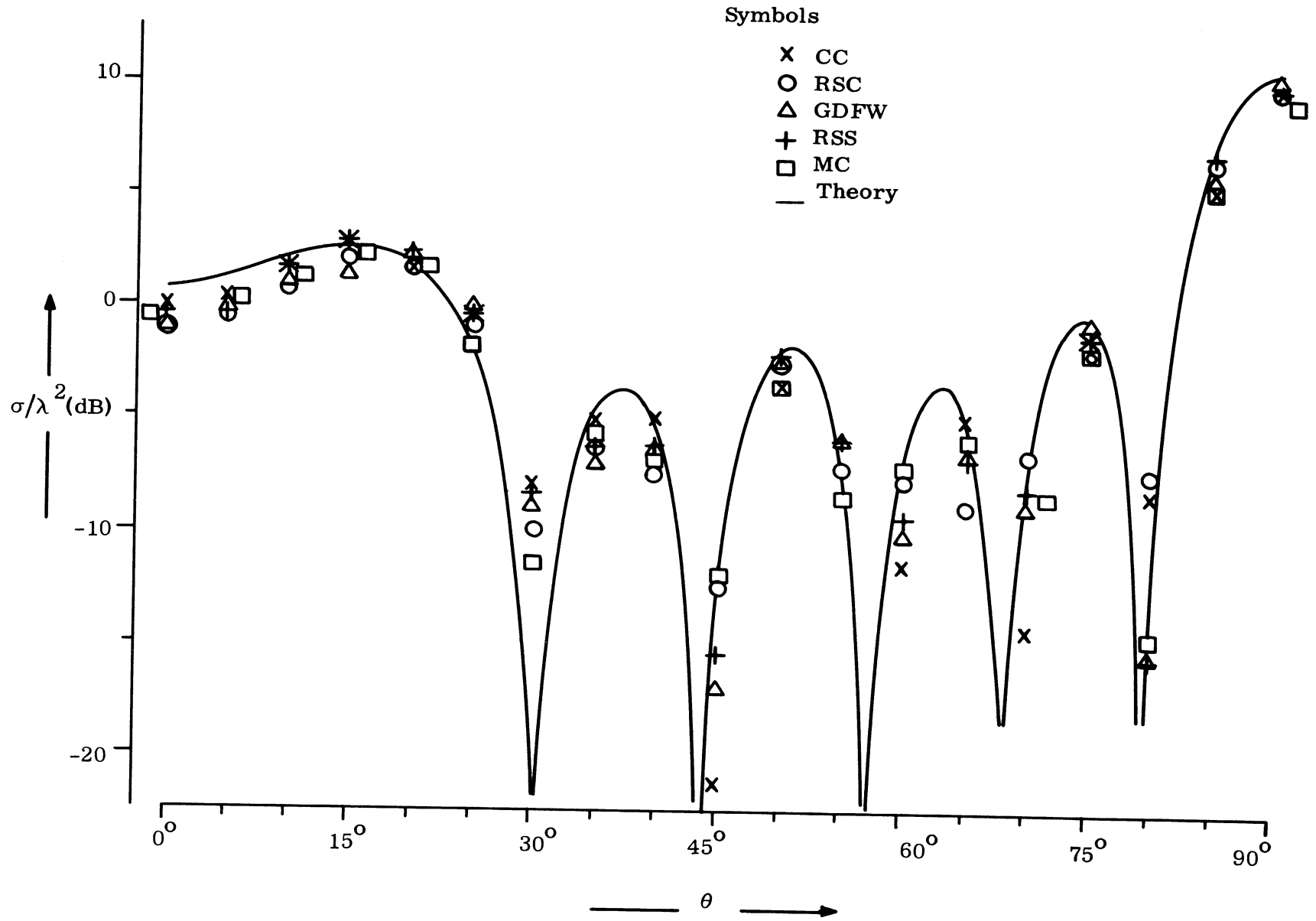

FIG. 6-10: COMPARISON BETWEEN THEORY AND EXPERIMENT FOR THE 4 FOOT CYLINDER FOR HH POLARIZATION AT 680 MHz.

The theoretical cross sections were not considered in two instances because of the deep nulls it predicts at the 30° aspect angle. We therefore excluded the two largest errors of each range from the analysis, leaving each of the six (five ranges and the theory) with 74 error values. The error distribution generated by the above analysis is shown in Fig. 6-11 and the reader will surmise from the plots that this was a severe test for all the ranges because there are substantial numbers of large errors.

The range performance for this special low ka test are summarized in Table VI-3. Note that, although we did not present the error distribution for the theory, its performance is carried in Table VI-3 like those of the five ranges. Observe that the theory "flunked" along with two other ranges, but remember that the errors summarized in Table VI-3 were generated by a comparison against mean performances, and not against theory. No range did better than "C" for this test and Micronetics, Conductron, and the theory all received an "E" grade. We want to emphasize that the poor performance of the theory in this test should not reflect on the theory used in comparisons at end-on and broadside, which is more dependable than that over the entire aspect range.

TABLE VI-3: RANGE RATINGS FOR SPECIAL PATTERN TEST (ka=1.36).

Range	Number of Errors 1 dB or less	Percentage of Errors 1 dB or less	Grade
Theory	40	54	E
CC	36	49	E
RSC	53	72	C
GD/FW	52	70	C
RSS	46	62	D
MC	30	41	E

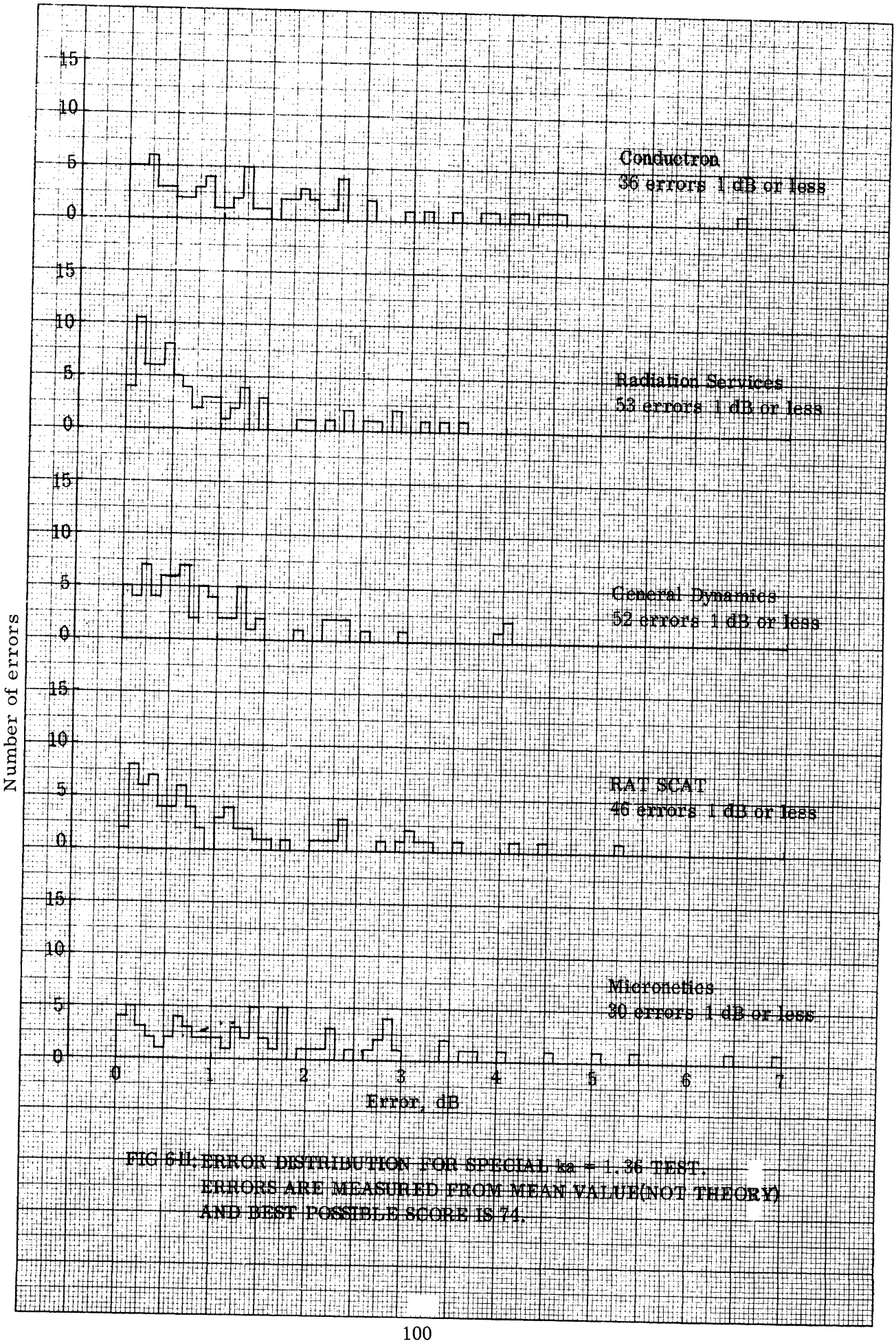

FIG 6-11: ERROR DISTRIBUTION FOR SPECIAL ka = 1.36 TEST.
ERRORS ARE MEASURED FROM MEAN VALUE(NOT THEORY)
AND BEST POSSIBLE SCORE IS 74.

6.5 Summary of Co-Polarized Measurements

In Chapters V and VI we presented an error distribution plot and a table summarizing range performance for each of five evaluation tests. The distribution of all the errors of these tests is collected and shown in Fig. 6-12, and Table VI-4 summarizes the overall range performances. Note that Avionics Laboratory was not evaluated in the special low ka test. Figure 6-12 shows that each range had a few large errors, some as large as 7 dB, but that Radiation Service is the best overall performer. Had we decided to rate the ranges on errors 0.1 dB or less, Conductron would have been the best performer.

Table VI-4 clearly shows that the poor performance with which we credit Conductron and Micronetics has been built up from a cumulation of relatively poor performances throughout the five tests . Radiation Service comes out number 1 in three tests and number 2 in two tests and number 3 in one test. The result is that this range is at the head of the list in the total accuracy evaluation of the co-polarized tests. Note that only five percentage points separate the top three positions in the outdoor ranges; it was a close race.

Two problem areas were found in the evaluation of the co-polarized data; a) in the measurement of the larger models at the higher frequencies, and b) for model-frequency combinations when ka=1.36. The cause of problem (a) was insufficient distance between target and the radar or near field distortion. Conductron had the most difficulty with this problem because their maximum range was limited to 200 feet. Micronetics also had near field distortion. For the other three ranges, these effects were just becoming visible, particularly in the sidelobe data in the last section.

The second problem (b) with the ka=1.36 data seemed to bother all the ranges especially for the 16-foot (1/2 scale) model at 170 MHz. Lack of agreement

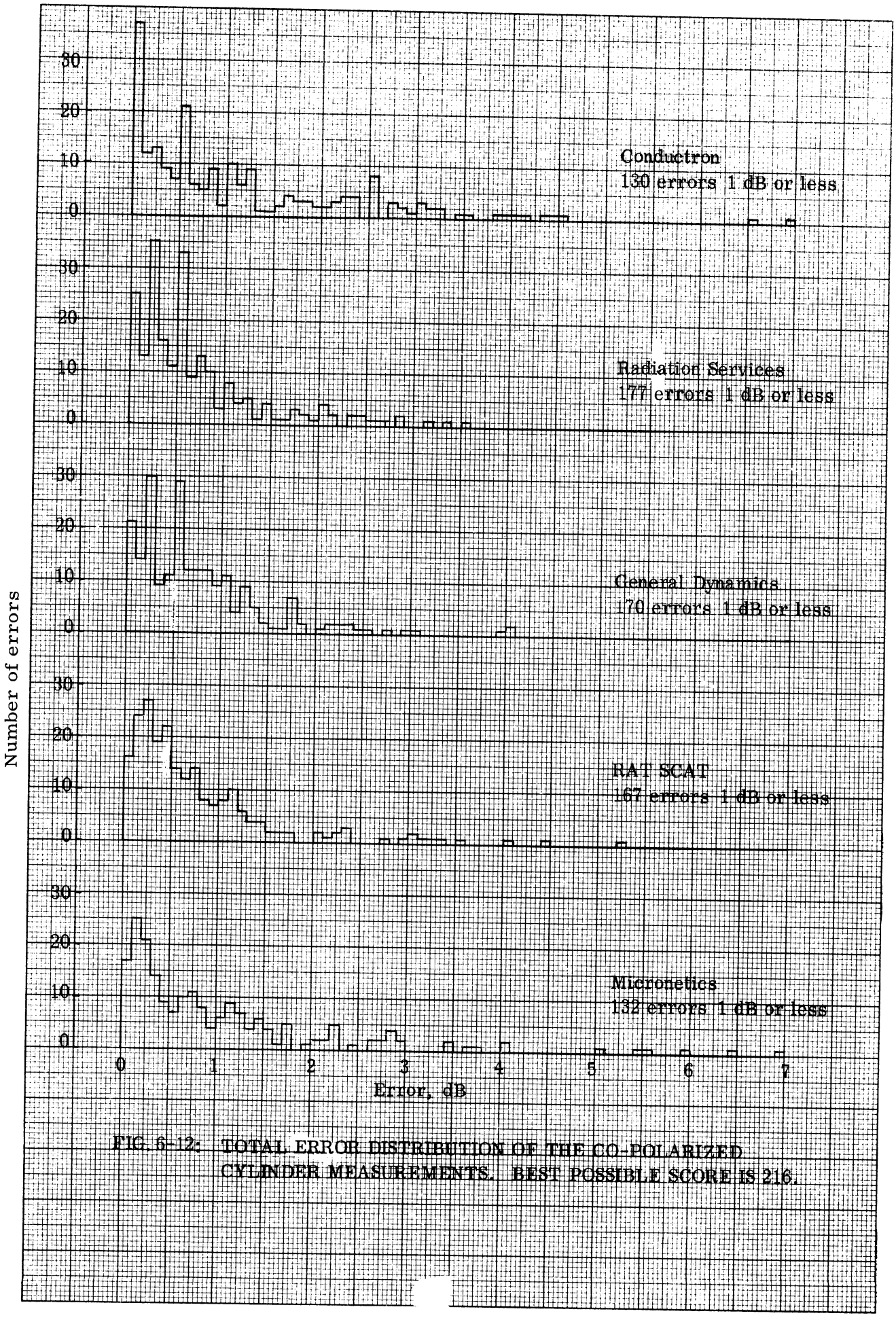

FIG. 6-12: TOTAL ERROR DISTRIBUTION OF THE CO-POLARIZED CYLINDER MEASUREMENTS. BEST POSSIBLE SCORE IS 216.

TABLE VI-4: SUMMARY OF RANGE TESTS FOR FIVE POINTS OF EVALUATION. Numbers indicate errors 1 dB or less for the range listed.

Test \ Range	CC	RSC	GD	RSS	MC	AL
Constant ka (52 possible)	40	46	43	45	41	4 (of possible 4)
End-on Polarization (18 possible)	17	18	18	16	17	4 (of possible 4)
End-on Theory (36 possible)	17	30	24	27	33	4 (of possible 8)
Broadside Theory (36 possible)	21	30	34	33	15	8 (of possible 8)
Special Low ka Test (74 possible)	36	53	52	46	30	not evaluated
Total Number of Errors (216 possible)	131	177	171	167	136	20 (of possible 24)
Percent	60	82	79	77	63	83
Grade	D	B	C	C	D	B

of the measurements with themselves and with theory was more noticeable in the end-on and sidelobe data than in the broadside data. The errors with the ka=1.36 date were not nearly as large in amplitude as the near field errors.

It is not obvious what the cause or causes for the difficulties with the measurements are when ka=1.36, particularly since there is a randomness about the types of troubles encountered. One explanation which could account for the randomness of the errors is the following. For ka=1.36, the lobe structure of the backscatter patterns is the broadest, therefore, more energy is scattered in all directions than for the larger ka cases. This is shown in the theoretical and experimental patterns in Chapters III and IV where, as ka decreases, it is seen that the backscattered power becomes more evenly distributed over this entire aspect region. Similar behavior will also occur in bistatic directions so that the power directed towards the ground and to the sides of the target increases with smaller values of ka. In other words, for smaller ka values the scattering tends to be more omnidirectional. The broader beam structure would enhance the scattering from spurious objects such as the pit, the supporting columns and other objects in the vicinity of the target, thus tending to introduce random type errors. This is a problem which all range operators are aware of and it is discussed under the heading of Secondary Reflections in Volume I. In some cases such as the General Dynamics measurements on the 2' (1/16-scale) model at 1360 MHz, it appears as though carelessness in this regard might have caused these errors.

In Volume I additional possible causes for the random errors in the ka=1.36 data are mentioned. A possible serious problem discussed there is the lack of uniformity of the incident field in the target area, particularly the fields along the radial direction between the target and radar. This is a direction which is usually not checked as carefully as that normal to this line at the pit. Since at end-on incidence the target extends the furthest into this region, it may well be causing problems in the ka=1.36 tests. Most likely there is more than a single cause for these random errors and different combinations of them exist

at each range.

In the interest of making this report as readable as possible, all the test patterns are not shown. It should be noted that measurements for the same model-frequency tests from the different ranges did agree well insofar as pattern shape is concerned. The evaluation procedures in this chapter and in Chapter V concentrated on pattern amplitudes relative to one another, and to theory,which is a more sensitive test than analyzing pattern shapes.

VII

CROSS POLARIZATION THEORY AND EXPERIMENT

Theoretical, experimental and evaluation aspects of the VH and HV cross polarization tests are discussed in this chapter. Simple theoretical arguments based on image theory are used to show why the cross polarized returns, VH and HV, should be zero when a perfectly conducting target is measured in a plane of symmetry. When experimental patterns are examined it is found that measured VH and HV returns in many cases resemble the co-polarized cross section patterns with the power level reduced by 20 to 30 dB. The level of the measured cross polarized return is too high and is generally due to coupling between the transmitting and receiving antennas; this is obvious if the cross polarized pattern is similar to the co-polarized pattern.

Our evaluation tests consists of comparing isolation levels between the cross polarized and co-polarized returns. Comparisons are made in the broadside aspect region where the largest returns are usually found for both the direct and orthogonal patterns.

7.1 Cross Polarized Theory

Combinations of image theory, the equivalence principle, and the reciprocity theorem can be invoked to prove that there is no cross polarized return from the cylinder models when measured as in this program. All of these concepts are adequately introduced and explained by Harrington (1961). When the plane in which the target is rotated is also a plane of symmetry of the target, the plane of symmetry can be replaced with a perfect conductor, S, and the lower portion of the model can be removed as in Fig. 7-1. If the conducting plane is sufficiently polished we observe the optical image of the upper portion of the model reflected from the surface as though it were the lower portion, thus making it appear as if the complete cylinder were still present. An additional condition which the target model satisfies is that it must be a good conductor like the image

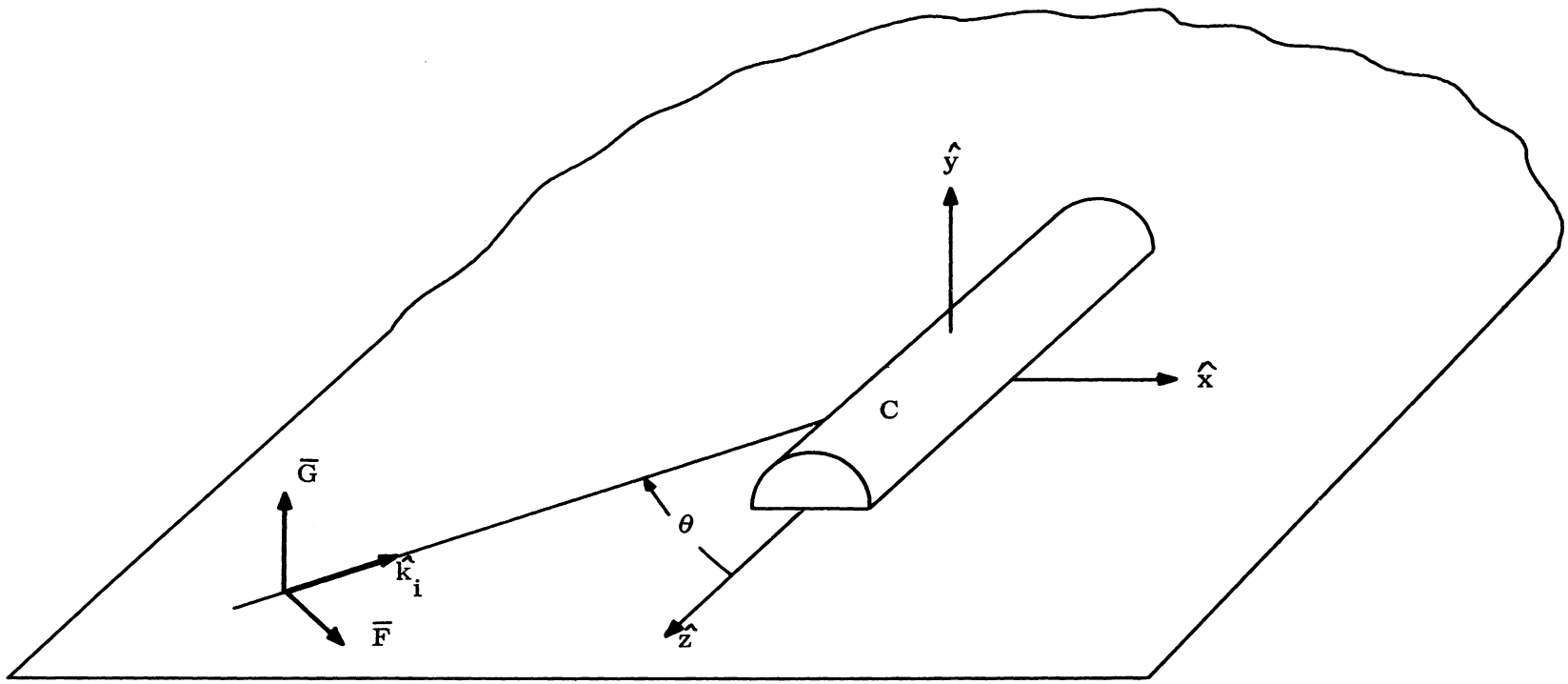

FIG. 7-1: IMAGE PLANE GEOMETRY FOR THE CYLINDER MODEL.

plane S. If the model retained all the necessary symmetry but was coated with a dielectric or plasma layer, image theory would no longer hold and, in general, cross polarized returns would be present for aspect angles different from 0^o and 90^o.

The polarization of the incident electric field $\bar{E}$ is divided into the usual vertical (V) and horizontal (H) components and analyzed separately. Assume the incident field is directed along the $\hat{k}_i$ vector at an aspect angle θ as shown in Fig. 7-1. For the first case allow the vector $\bar{G}$ which is normal to S to be the $\bar{E}$ field and the vector $\bar{F}$, which is tangent to S, to be the magnetic field $\bar{H}$; this then is the V polarization. If it is further stipulated that S is a perfect <u>electric</u> conductor then $\hat{y} \times \bar{E} = 0$ which means that all electric fields in the plane S are zero by definition. Thus no component of the backscattered $\bar{E}$ field can exist in the x-y plane, indicating that the VH return must be zero. This conclusion is valid so long as the radar lies in a plane of incidence which is also a plane of symmetry for a conducting target.

The line of reasoning for the cross polarized arguments may take at least two paths. One argument calls upon the reciprocity theorem, stating that the response of a system is unchanged if the transmitter and receiver are interchanged. All the fields and target satisfy the usual linear, bilateral conditions necessary for reciprocity. From this theory it follows that the HV return is zero if the VH return is zero.

A somewhat more physical, but less familiar , argument for the HV case is found in the equivalence principle stating that one need not know the actual sources to determine the fields in a given region; any accurate equivalent source or group of sources will suffice. This principle permits us to allow S to be a perfect <u>magnetic</u> conductor which in turn implies that $\hat{y} \times \bar{H} = 0$ or $\bar{H}$ is zero on the surface S. We now return to Fig. 7-1 and interchange $\bar{G}$ and $\bar{F}$ so that $\bar{G} = \bar{H}$ and $\bar{F} = -\bar{E}$ in order to have the appropriate propagation in the $\hat{k}_i$ direction. The target may be represented by a perfect magnetic conductor even though it is physically an electric conductor. The boundary conditions on C are such that

the incident field will be scattered back to the receiver in the correct manner. Because $\hat{y} \times \bar{H} = 0$ there can be no HV return for the horizontally polarized case either.

7.2 Cross Polarized Measurements

Unfortunately in the real world accurate cross polarized measurements are difficult to make, particularly when the VH and HV returns should be zero. In performing these measurements one invariably discovers a small but finite return when there should be none at all. Some of the causes for the erroneous returns are

a) antenna alignment and isolation
b) target alignment,
c) depolarized returns from alien scatterers.

For the test made during this program, it appears that antenna isolation problems were the main cause of spurious (finite) VH and HV returns. This conclusion follows from the fact that most of cross polarized patterns definitely resembled the VV and HH patterns as shown in Fig. 7-2. The pattern on the left in this figure is a portion of the HH pattern in Fig. 4-12 for the 32-foot cylinder at 340 MHz. On the right in Fig. 7-2 is the VH return for the same target which appears similar to the co-polarized return, but is 20 dB lower in power level.

For the VH pattern in Fig. 7-2 the peak return is located at 90°. As a rule the peak return for all the VH and HV patterns are located near, but not always exactly on, broadside. Cross polarized (VH and HV) data for peak returns near broadside in dBsm are summarized in Tables VII-1 and VII-2 for all the ranges. In these displays the values in each box are arranged according to the measuring facility as indicated in the sample box in the upper right part of the table. The frequency axis and the model size axis are the same as those used in other displays.

There are many measurements missing in these tables. The symbol (*) indicates near field distortions and (-) indicates that no data were submitted for these cases. It is not meaningful to compare cases having near field errors,

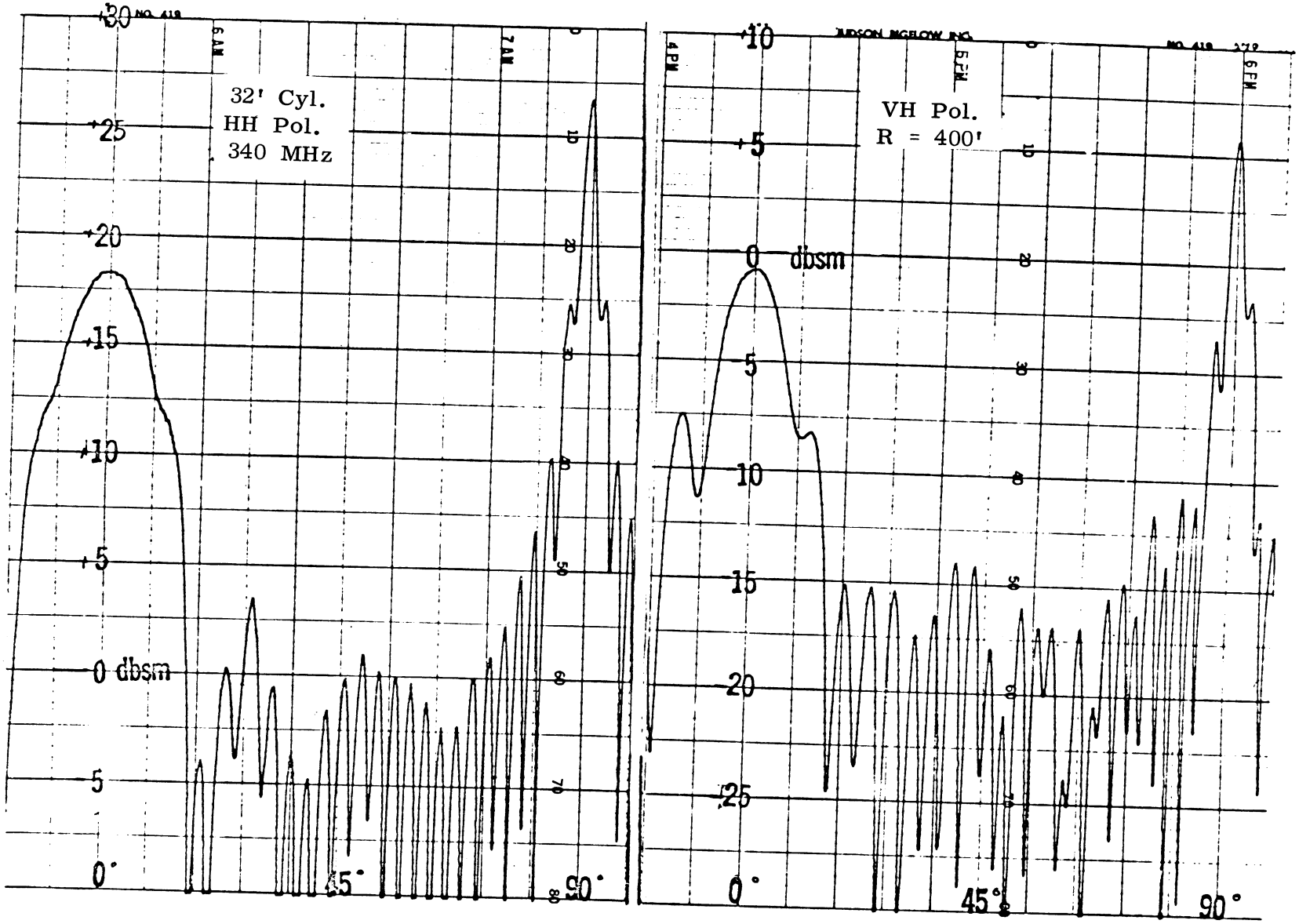

FIG. 7-2: COMPARISON BETWEEN HH AND VH POLARIZATIONS, ka = 5.44, 32 FOOT CYLINDER, 340 MHz.

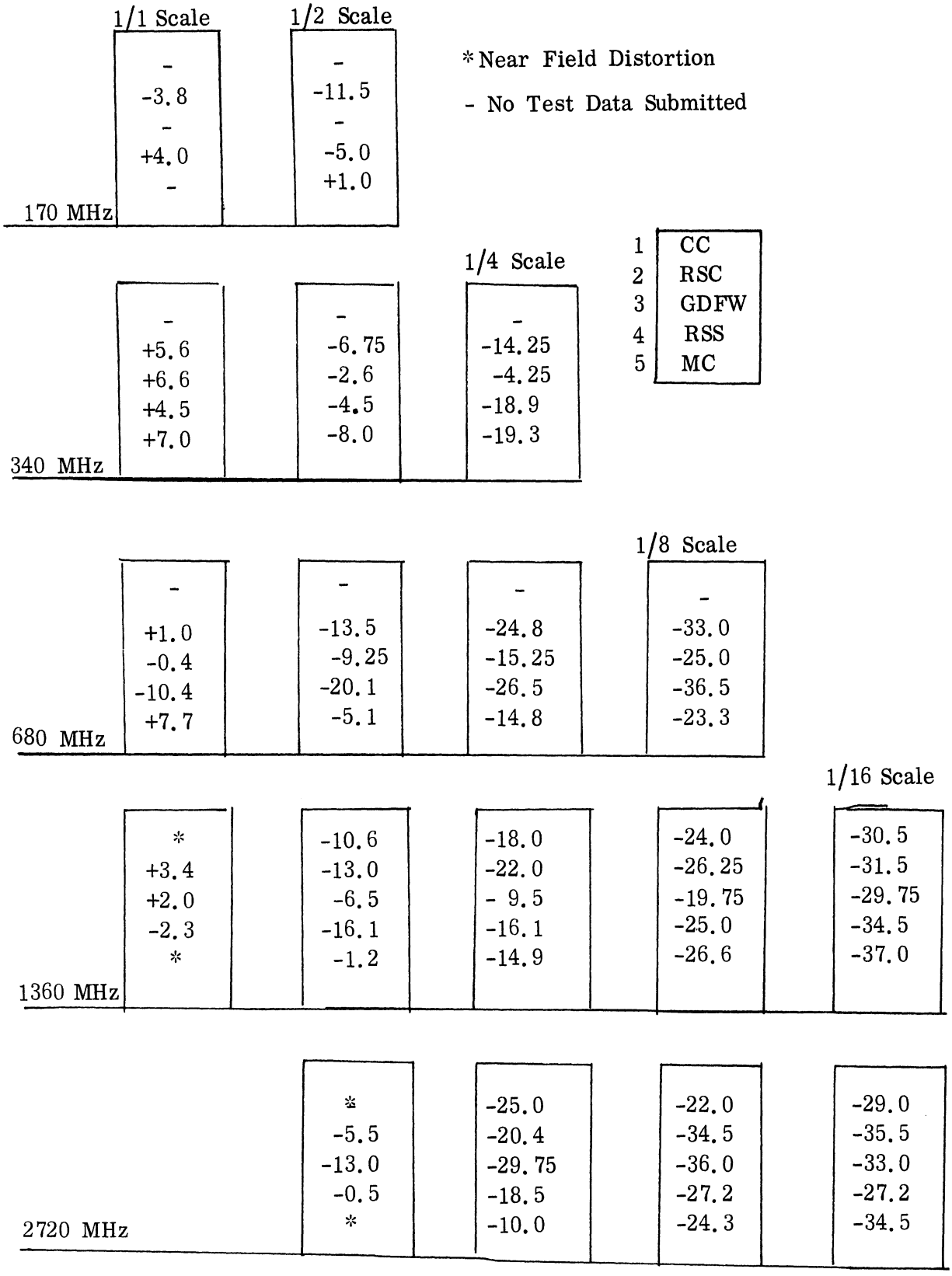

TABLE VII-1: SUMMARY OF VH CROSS POLARIZED DATA (in dBsm) FOR PEAK RETURNS NEAR BROADSIDE.

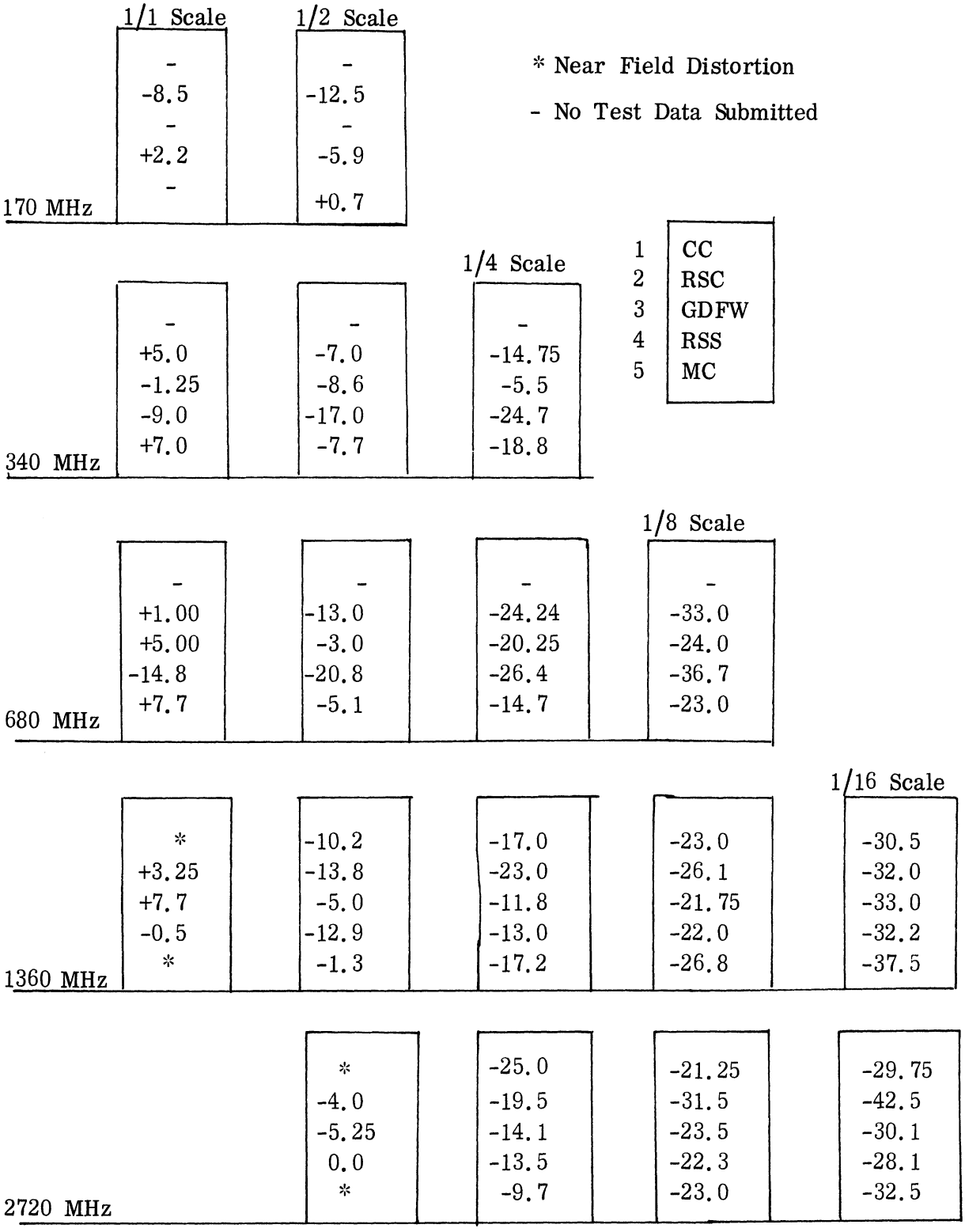

TABLE VII-2: SUMMARY OF HV CROSS POLARIZED DATA (in dBsm) FOR PEAK RETURNS NEAR BROADSIDE.

since we know they are distorted. General Dynamics made no cross polarized tests at 170 MHz and Conductron made cross polarized tests only at 1360 and 2720 MHz. Below these frequencies Conductron used the same antenna for transmitting and receiving and felt that its isolation was insufficient to record accurate data.

7.3 Evaluation of Cross Polarized Data

Many times throughout this report it has been mentioned that there are numerous ways to evaluate the results for the different tests. For the cross polarized measurements we decided to compare isolation levels between the direct and cross polarized returns. The isolation comparisons were further limited to the broadside aspect region, because these returns are the largest and easiest to recognize.

The VH and HV values in Tables VII-1 and VII-2 were subtracted from the corresponding HH and VV broadside values in Tables V-2 through V-6 according to the expressions

$$\sigma_{HH}(90^{o}) - \sigma_{VH}(\approx 90^{o})$$

and

$$\sigma_{VV}(90^{o}) - \sigma_{HV}(\approx 90^{o}) \quad .$$

The isolation differences for these comparisons are given in Tables VII-3 and VII-4.

A comparison of the numbers in any of the four tables in this chapter within a range or between the ranges shows only random behavior. This is to be expected since all the VH and HV returns are a form of noise in that the returns should be zero. For the same reason the VH and HV returns for the same frequency-model tests should not look alike. Generally one would expect the VH and HV cross sections to be equal from reciprocity considerations, but when the return looks like random noise this is not the case.

The average isolation levels for the cross polarization comparisons for each of the ranges are listed in Table VII-5 with the number of tests which the

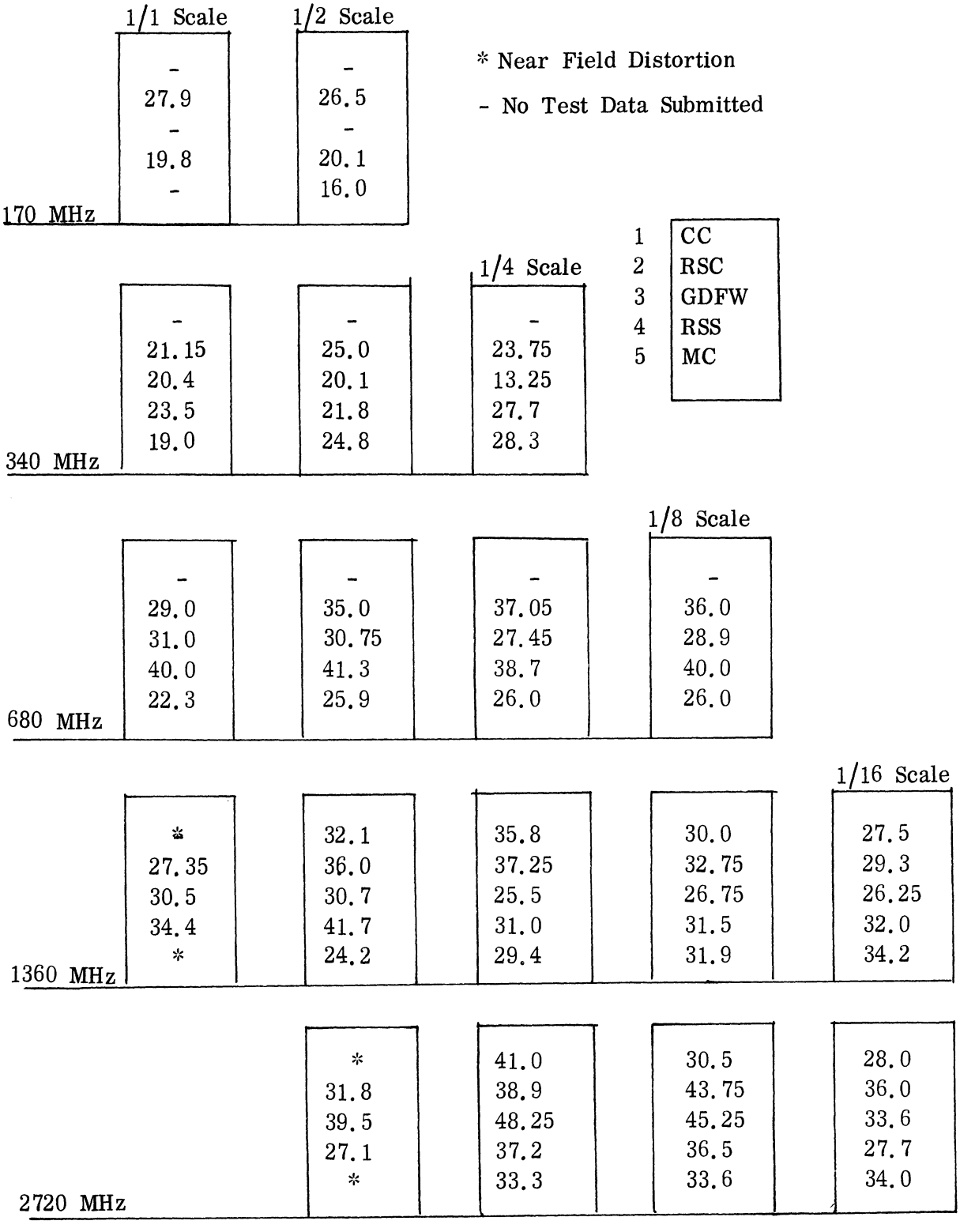

TABLE VII-3: ISOLATION COMPARISONS FOR $\sigma_{HH}(90^{o}) - \sigma_{VH}(\approx 90^{o})$.

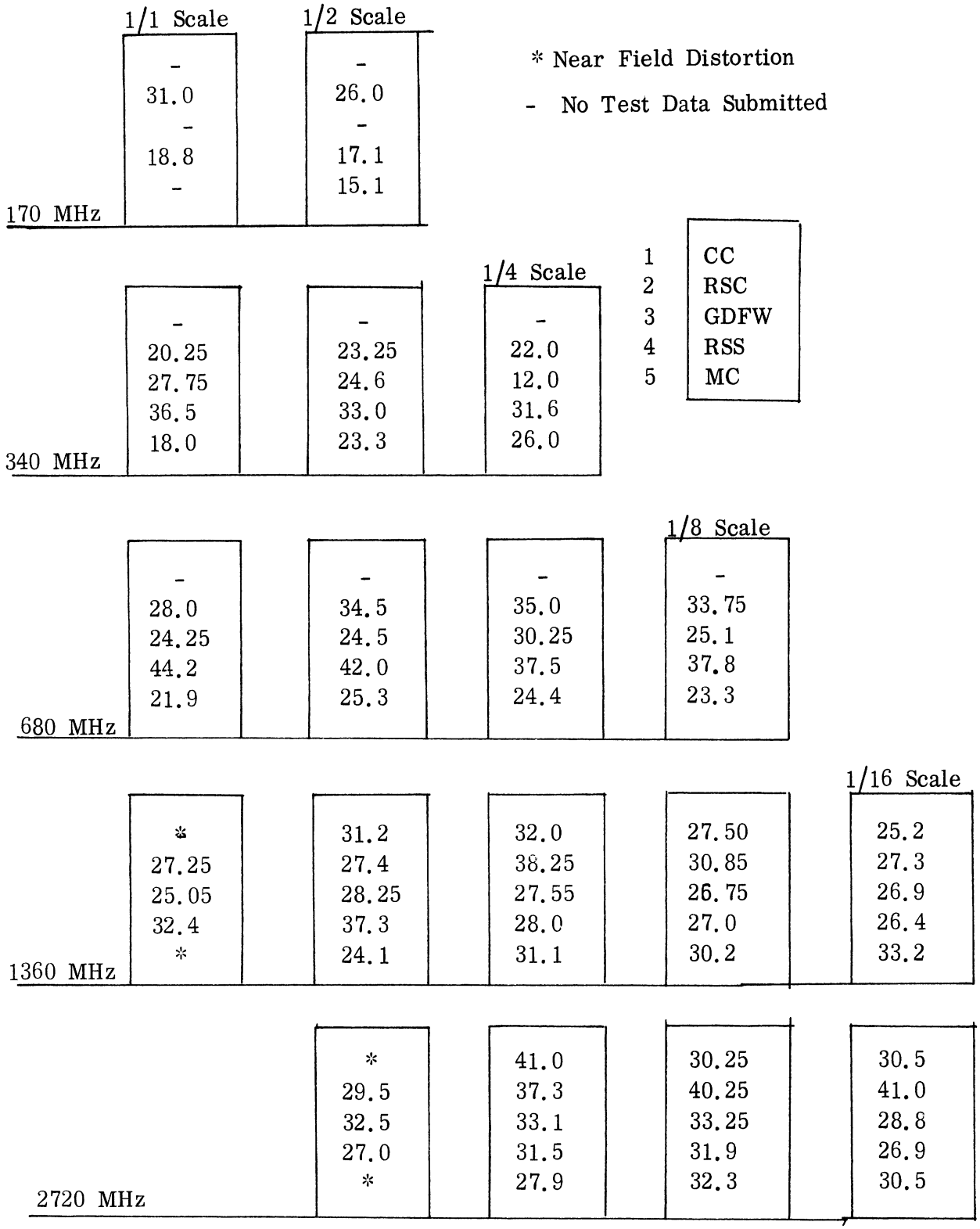

TABLE VII-4: ISOLATION COMPARISONS FOR $\sigma_{VV}(90^{o}) - \sigma_{HV}(\approx 90^{o})$.

ranges successfuly complete. A maximum of 36 VH and HV tests were considered in the isolation evaluations. RAT SCAT and Radiation Service completed all the tests and had the best overall performance with 31.5 and 30.7 dB isolation levels. Conductron had the highest level but successfully completed less than half the tests. Micronetics has a slightly lower average for this comparison because it uses the same antenna for transmitting and receiving for most of its tests, creating isolation difficulties.

TABLE VII-5: ISOLATION AVERAGES

Range	No. Tests Completed	Grade	Average Isolation for These Tests	Grade
CC	14	E	32.2 dB	C
RSC	36	A	30.7 dB	C
GD/FW	32	B	27.2 dB	D
RSS	36	A	31.5 dB	C
MC	30	B	27.5 dB	D

The required isolation needed to perform satisfactory cross polarized measurements is subject to question. Based on target identification studies we are conducting at The University of Michigan, we feel that a 30 dB isolation level is the minimum acceptable value and for some applications this may be insufficient. Additional comparisons of the cross polarized data are possible and if this is an area of interest to the reader he might wish , for example, to make evaluation tests similar to those in Chapters V and VI. Recommendations for improving cross polarized measurements are given in Volume I. Improvements in antenna design alone would produce better isolation levels.

As we demonstrated earlier in this chapter, the cross polarized echo from any conducting body of roll symmetry is theoretically zero along the principal planes. Measurement of the cross polarized return of such a target, then, represents an extremely difficult task whose only utility is to assess the isolation of the two channels and to perhaps judge the general condition of the range. A much more meaningful cross polarized measurement would have been along the

planes of maximum return. These planes lie 45° from the principal planes, as shown in Fig. 7-3, and theoretically the cross polarized echoes can be computed from the phase and amplitude of the VV and HH returns. Depending on the complexity of the antenna feeds, this technique can range from extremely simple to unduly complex, and some radar cross section ranges may be quite incapable of performing such a measurement.

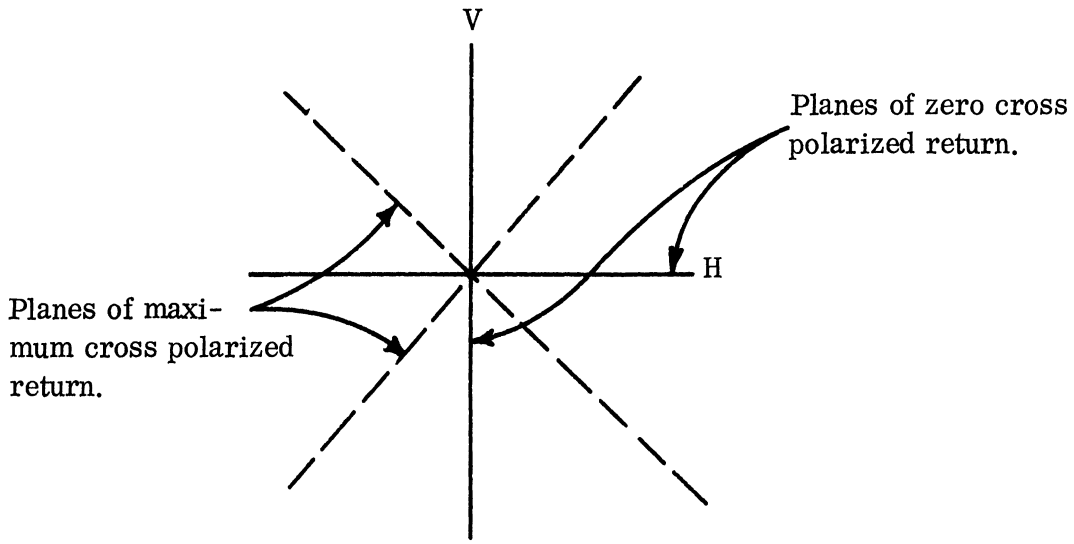

FIG. 7-3: CROSS POLARIZED MEASUREMENTS ARE BEST PERFORMED IN CUTS ANGLED 45° TO THE PRINCIPAL PLANES. The boresight axis is normal to the plane of the diagram.

VIII

CONCLUSION

Much of Volume I could be considered as a conclusion to Volume IIa, but for the sake of completeness some topics are discussed here which also are found in the first volume. Topics such as recommendations for the improvement of deficiencies and guides to optimum utilization of facilities are not restated here. We limit our concluding remarks in this chapter to the material specifically covered in Volume IIa.

Two topics mentioned at the beginning of this report are phase measurements and digital data. Only two of the ranges had the capability to measure phase. General Dynamics is equipped to measure phase over all the frequency bands in this test program (170 to 2720 MHz) but RAT SCAT can measure phase only at L band (1000 MHz to 2000 MHz). Unfortunately there were not enough accurate phase data to make meaningful comparisons. General Dynamics submitted phase patterns for all frequency-model combinations but from what we have learned, these patterns would be difficult to use because of the way they were calibrated. In order to speed up our seriously lagging time schedule at RAT SCAT, we waived the need for phase measurements there, except for the 32' and 16' cylinders at 1360 MHz. A theoretical phase pattern is presented in Fig. 3-7 to show typical phase behavior. The importance of improving phase measuring capabilities for all the ranges is discussed in Volume I.

All the ranges recorded digital data as well as the analog patterns and the various forms of digital equipment used at the ranges are shown in Table II-2. Of all the digital recording equipment, the magnetic tape system at Micronetics seemed to be the most desirable. At the beginning of the contract Rome Air Development Center was processing all digital data to verify their correspon-

dence with the analog recordings. Rome discovered several problems in converting the various formats of the individual ranges to its computer program for analysis. Digital data from RAT SCAT and Micronetics were not available until the end of the pgogram and because of these difficulties, no overall evaluation was made of the digital data. In Volume I we discuss the need for equipment that would permit the range operators to make an immediate check of the correctness of the digital data.

The remainder of our remarks below are directed towards the theoretical models in Chapter III, the co-polarized tests in Chapters V and VI, and the cross polarized tests in Chapter VII. Finally, we offer some subjective views about the outcome of these tests.

8.1 Remarks on the Theoretical Models

One of the objectives of this program was to compute expected radar cross sections for each of the cylinders under the experimental frequency and polarization conditions specified. This was done in Chapter III for the co-polarized (HH and VV) tests and in Section 7.1 for the cross polarized (VH and HV) tests. The spirit of this task was to determine the cross section with existing methods rather than to develop new theoretical approaches for calculating cross sections of finite cylinders. We believe that this portion of the contract was amply discharged and that a sound theoretical base was established for amking comparisons with experimental measurements.

Theoretical calculations were made for two reasons: first, continuous patterns as a function of aspect angle can be obtained and second, accurate cross sections at end-on and broadside aspect positions are available. The continuous theoretical patterns were used to check the gross pattern structure shown by the experimental data. Accurate cross section calculations at end-on and broadside aspect angles were compared directly with measured data in the main evaluation program. Theoretical arguments based on image theory were developed to show

that no cross polarized return should be expected for the tests made on the cylinders.

A weak point in our theoretical models for the co-polarizations at end-on incidence for the smaller ka values may be noted. We expected this to be troublesome because the mathematical formulation was based on the assumption that the cylinder at end-on would behave like a disc alone, but nevertheless, this model still appeared to be accurate to within $\pm$ 1 dB. The disagreement in the measurements from the separate ranges for this aspect region emphasized this weak spot in theory.

Considering that there is no exact solution for the fields scattered by a finite cylinder, the mathematical models employed here yielded good results. In the near future there will be improved numerical computer techniques for obtaining even more accurate cross section calculation over larger values of ka. During the course of this contract (1965-1968) developments in computer techniques have come a long way (see the references mentioned in the beginning of Chapter III) and it is reasonable to expect they will continue.

8.2 Remarks on the Co-Polarized Data

The intra-range and inter-range tests required data reduction and evaluation procedures for the co-polarized data and grades reflecting relative performance were assigned to these tests for each of the ranges. Other display and reduction techniques were included, such as the comparison of experimental data with continuous theoretical patterns over five-degree intervals and the examination of the amplitudes of the sidelobes adjacent to broadside. We felt the sidelobe tests added no significant information above that obtained in the intra-range and inter-range tests and we therefore assigned no grades to them.

A summary of the intra-and inter-range evaluations and grades has been presented at the end of Chapter VI. The grades for each test and the overall average grade for each range, assuming the five tests are of equal weight,

are shown in Table VIII-1 which is a condensed form of Tables V-8 and V-9 of Chapter V and VI-1, VI-2 and VI-4 of Chapter VI. General Dynamics and RAT SCAT both achieved overall grades of C while Radiation Services did slightly better with a grade of B. For all practical purposes these three ranges performed their tests well and had no consistent sources of error. Yet we must stress that on occasions these ranges did have noticeable errors, particularly for the lower ka cases.

TABLE VIII-1: SUMMARY OF GRADES FOR ALL EVALUATION TESTS AND AVERAGE GRADES

Range	Constant ka	End-on Polarization Comparison	End-on Theory Comparison	Broadside Theory Comparison	Special Low ka Test	Overall Performance
CC	C	A	E	E	E	D
RSC	B	A	B	B	C	B
GDFW	B	A	D	A	C	C
RSS	B	B	C	A	D	C
MC	C	A	A	E	E	D
AL	A	A	E	A	--	B

Our grading criterion was such that errors 1 dB or smaller were considered acceptable. Micronetics had many errors between 1 and 1.5 dB and this accounts for its lower grade. Micronetics also had near field distortions in a few of its patterns, but this was a minor problem compared to Conductron's difficulties in this area. Due to an accident in which the 32 foot cylinder was dropped, Micronetics was unable to make any tests on this target at 170 MHz. In our

evaluation the missing data were treated as if they had an error greater than 1 dB. Only two models were measured at two frequencies on the Avionics Laboratory range. Grades were assigned to most of its results, but since there were so few tests, one cannot attach high signficiance to these grades.

Near field distortions in the broadside aspect region were the reasons for errors in several of Conductron's patterns. The maximum antenna-to-target distance used at this facility was 200 feet, and this fell far short of the commonly accepted $2L^2/\lambda$ range criterion for many of the tests (see Table IV-1). Conductron mathematically transformed near field data to far field predictions to correct the distorted broadside pattern structure, but when the distortion is severe it extends to other lobes in the broadside region. Because of this the "corrected" values were not included in our evaluation; instead, the raw data from the patterns was used for the evaluation tests.

Secondary causes of errors in the co-polarized data are less easy to identify. We refer to the errors in the low ka value tests which were mostly random yet present in all the range data. These errors may have been due to lack of a uniform incident field, secondary reflections, or insufficient observance of other proven measurement procedures. These and other problem areas are discussed in detail in Chapter IV of Volume I.

8.3 Remarks on the Cross Polarized Data

The ranges were graded both on their capabilities to perform cross polarized measurements and on their results. It turns out that, since there is theoretically no cross polarized return from the cylinder targets, this represented a rather difficult and relatively uninformative test. The grades we assign should not be as heavily weighted as those given in the co-polarized evaluation.

There were 36 VH and HV tests to be made at each range but only Radiation Services and RAT SCAT were able to do them all. Both of these

ranges had better than 30 dB average isolation between the cross and co-polarized measurements. General Dynamics was unable to measure cross-polarization at 170 MHz; for other tests, they had a 27.2 dB isolation level.

Conductron made cross polarized measurements only at S and L bands (1000 MHz - 3000 MHz) because at lower frequencies it uses the same antenna for transmitting and receiving and in this mode of operation it felt there was insufficient isolation to obtain accurate measurements. It is interesting to note that Micronetics used one antenna for transmitting and receiving for most of its tests, yet it chose to make cross polarized measurements at all frequencies. Micronetics' average isolation was 25.7 dB, just a little poorer than General Dynamics' isolation level.

From our own experiences at the Radiation Laboratory, we feel that a minimum average isolation of 30 dB should exist between the cross and co-polarized levels when no cross polarization should be present. It would be desirable to strive for a 40 dB isolation level for these cases. By improving antenna design for better isolation, much of the additional 10 dB should be attainable. A more significant test of cross polarized measurements for a cylinder is one in which a 45^{o} polarization is transmitted and a 135^{o} polarization received.

8.4 Final Remarks

We found that accurately scaled cylindrical targets represent good targets with which to evaluate radar cross section ranges. The cylinder is a simple enough shape for which the end-on and broadside returns can be predicted with an accuracy of one dB or better, yet its scattering behavior is sufficiently complex to test range performance. The cylinder is also a practical shape because it is often a component of many aerospace vehicles and boosters.

Our analysis of the range data acquired for the cylindrical targets shows that some ranges have difficulty in measuring large objects at some of the higher frequencies and that all ranges have difficulty if the accuracy requirements are unduly stringent. In this program we arbitrarily refer to errors less than or equal to one dB, and this error level is reflected in the results of Table VIII-1. If we had set our sights a little higher, say at 0.5 dB, no range would have been acceptable; had we specified 2 dB, on the other hand, all would have turned in very good performances. Thus we emphasize that, depending on the rating system adopted, range performances can run the gamut of totally unacceptable to totally acceptable.

The evaluations presented in this Volume IIa of the Final Report are summarized in less detail in Volume I, but form a part of a more general comparison of range capabilities. The reader will find in Volume I a critique of the shortcomings of radar cross section ranges and a list of possible improvements that can be made. Among these improvements is the recommendation that the range customer establish a close liaison with range personnel, who, in turn, must be unusually diligent in performing their tasks. The acquisition of highly accurate and reliable data is accomplished only through the expenditure of hard work and honest endeavor.

REFERENCES

Air Force Missile Development Center (1965), "RAT SCAT Radar Target Scatter Site Brochure."

Bachman, C.G., H.E. King and R.C. Hansen (1963), "Techniques for Measurement of Reduced Radar Cross Sections," Microwave J., 6, Pt. 1, pp. 61-67 (February), Pt. 2, pp. 95-101 (March), Pt. 3, pp. 80-86 (April).

Bahret, W.F. (1964), "Avionics Laboratory Radar Cross Section Measurements Facility," Radar Reflectivity Measurements Symposium, II, AD go1365, pp. 201-202.

Blacksmith, P., R.E. Hiatt and R.B. Mack (1965), "Introduction to Radar Cross Section Measurements," Proc. IEEE, 53, pp. 901-920.

DiFrancia, G.T. (1953), Electromagnetic Waves, Interscience Publishers, New York, p. 37.

General Dynamics (1964), "Radar Cross Section Measurement Capabilities," General Dynamics/Fort Worth Brochure FZE-366.

Fisher, F.E. (1967), "Theoretical Approximation to Resonant Cylinder Scattering," Company Publication, Radiation Service Co., Radiation Inc., Melbourne, Florida, August 1967.

Harrington, R.F. (1961), Time-Harmonic Electromagnetic Fields, Chapter 3, McGraw-Hill, New York, New York.

Honer, R.E. and W.D. Fortner (1964), "Outdoor Pulsed Radar Reflectivity Range," Radar Reflectivity Measurements Symposium, II, AD 601365, pp. 274-285.

Kouyoumjian, R.G. and L. Peters (1965), "Range Requirements in Radar Cross Section Measurements," Proc. IEEE, 35, No. 8, pp. 920-929.

Landfried, J.E. and W.L. Williamson (1964), "Static Radar Reflectivity Measurement Facilities at Radiation Incorporated," Radar Reflectivity Measurements Symposium, II, AD 601365, pp. 299-302.

Marlow, H.C., D.C. Watson, C.H. VanHoover and C.C. Freeny (1965), "The RAT SCAT Cross Section Facility," Proc. IEEE, 53, pp. 946-953.

Mentzer, J.R. (1955), Scattering and Diffraction of Radio Waves, Pergamon Press, p. 34 and p. 64.

Oshiro, F.K. and C.W. Su (1965), "A Source Distribution Technique for the Solution of General Electromagnetic Scattering Problems," Northrop-Norair Report No. NOR-65-271.

Oshiro, F.K. et al (1967), "Calculation of Radar Cross Sections," Northrop-Norair Second Quarterly Report No. NOR-67-31 (January).

Schmitt, H.J. (1959), "Back Scattering Measurements with a Space-Separation Method," IRE Trans. Ant. and Prop., AP-7, No. 1, January, pp. 15-22.

Also, see King, R.W.P. and T.T. Wu (1959), Scattering and Diffraction of Waves, Harvard University Press, p. 129.

Wren, A.W. (1964), "Conductron Corporation's Cross Section Range," Radar Reflectivity Measurements Symposium, II, AD 601365, pp. 359-362.

APPENDIX A

PHYSICAL OPTICS MODEL FOR SCATTERING BY A FINITE CYLINDER

In this appendix expressions are derived for the amplitude and phase of the scattered fields from a finite cylinder. Knowing the scattered fields, one can estimate the radar cross section of the cylinder. The physical optics procedure, which is used to evaluate the fields, is an approximate technique whose accuracy increases for growing values of ka.

The monostatic (or back) scattering cross section of an object is defined as (Blacksmith, 1965)

$$\sigma = 4\pi R^2 \left| \frac{\bar{H}^s}{\bar{H}^i} \right|^2 \tag{A.1}$$

where $\bar{H}^i$ and $\bar{H}^s$ are the magnetic field intensities of the incident and backscattered fields respectively and R is the distance from the scattering target to the transmitter-receiver location in the far field. For the monostatic case the transmitter and receiver are located at the same position P(R). When the transmitter is placed in the far field, the incident field $\bar{H}^i$ may be treated as a plane wave.

In this analysis the scattering object is a finite cylinder of length ℓ and radius a as shown in Fig. A-1. Since there is no exact solution for the scattered fields from a finite cylinder, an approximate model is introduced to obtain an expression for the fields. In the approximate model the fields scattering from a cylinder $\bar{H}_c^s$ and a circular flat plate $\bar{H}_p^s$ are summed as phasors to obtain an expression for the total backscattered field $\bar{H}^s$.

$$\bar{H}^s = \bar{H}_c^s + \bar{H}_p^s$$

$$\bar{H}^s = \bar{H}_c e^{j\psi_c} + \bar{H}_p e^{j\psi_p} \tag{A.2}$$

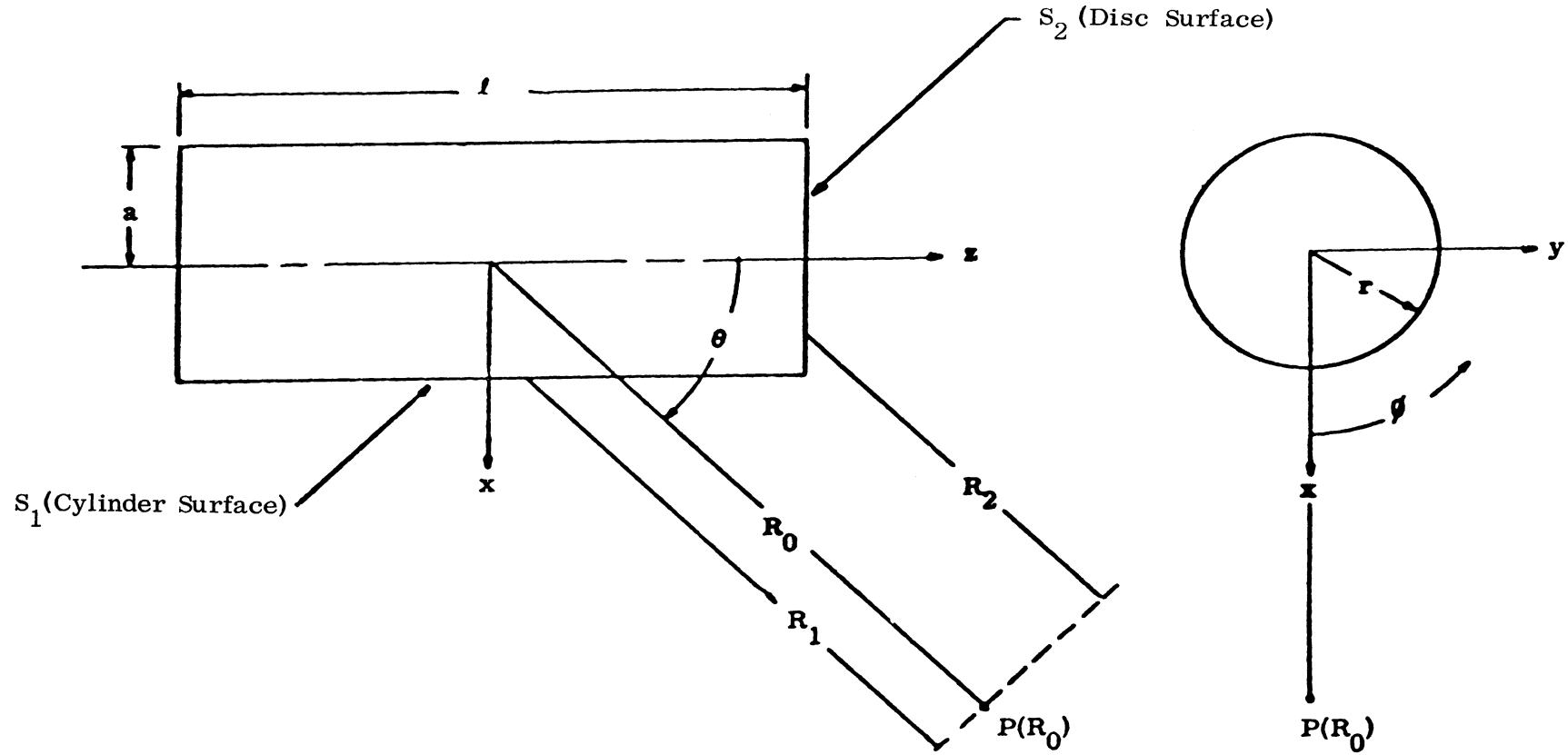

FIG. A-1: FINITE CYLINDER GEOMETRY.

where $\bar{H}_c$ and $\bar{H}_p$ are the amplitude and ψ_c and ψ_p are the phase components of the scattered field from the cylinder and the plate. No attempt is made to consider the scattering contribution from the edge where the cylinder and plate are joined. This omission of the edge effect produces noticeable but small errors in the aspect region near and about 45^o. If more accurate behavior of the edge effects are desired, the reader is referred to method (b).

If the backscattered fields of (A.2) are substituted into (A.1), then

$$\sigma = 4\pi R_o^2 \left[\frac{\left|\bar{H}_c\right|^2 + \left|\bar{H}_p\right|^2 + 2\left|\bar{H}_c\right| \left|\bar{H}_p\right| \cos(\psi_c - \psi_p)}{\left|\bar{H}^i\right|^2} \right] \qquad \text{(A. 3)}$$

The amplitudes $\bar{H}_c$ and $\bar{H}_p$ are well known and are found in cross section tables (e.g. Oshiro and Su, 1965), but the phase components ψ_c and ψ_p are not easily found. In order to determine the precise value of ψ_c and ψ_p, $\bar{H}_c^s$ and $\bar{H}_p^s$ are evaluated by the physical optics procedure. Even though the physical optics model becomes effective only when ka is greater than 5.44, this procedure does offer a physical insight into the scattering behavior irrespective of the ka value.

Assume a plane parallel-polarized field is obliquely incident upon a perfectly conducting cylinder of finite length at an aspect angle θ as shown in Fig. A-1. The field $\bar{H}^i$ originates at $P(R_o)$ in the far field and in the vicinity of the cylinder is represented as

$$\bar{H}^i = \hat{y} H_o e^{jk(z\cos\theta + x\sin\theta)} , \qquad \text{(A. 4)}$$

where k is the wave number, H_o the harmonic amplitude of the magnetic field intensity, and $\hat{y}$ is a unit vector. Harmonic time dependence has been assumed to be $e^{j\omega t}$. A formulation of this problem in terms of the incident electric field

will lead to the same expressions as the magnetic field formulation which demonstrates that the physical optics approximation is polarization independent (i.e. VV and HH patterns are the same).

The surface current density $\bar{J}_s$ generated on the scattering surface by the incident field is $\bar{J}_s = 2(\hat{n} \times \bar{H}^i)$ for the physical optics model, where $\hat{n}$ is the outward normal to the scattering surface. This representation of the current is valid for surfaces which are large and flat compared to a wavelength. As curvature is introduced in the scattering surface, the model becomes less valid. When the radius of the cylinder is on the order of or smaller than a wavelength ($ka \leq 6$) the model no longer applies and the polarization effects are noticeable.

Following the procedures outlined by Mentzer (1955), the physical optics expression for the scattered field $\bar{H}^s(R_o)$ is

$$\bar{H}^s(R_o) = \frac{-1}{4\pi} \iint_S 2(\hat{n} \times \bar{H}^i) \times \nabla\psi \, dS \qquad \text{(A.5)}$$

where S is the portion of the scattering surface illuminated by $\bar{H}^i$ and ψ is the spherical Green's function. Equation (A.5) has been derived from Maxwell's equations. When kR is large, $\nabla\psi$ is approximately

$$\nabla\psi \cong -j \frac{\hat{R} k e^{-jkR}}{R} \qquad \text{(A.6)}$$

where $\hat{R} = \hat{x} \sin\theta + \hat{z} \cos\theta$ is the unit vector which is always in the plane of incidence (x - z plane).

For the finite cylinder the illuminated surface is broken into two parts, the cylinder S_1 and the flat circular plate S_2. All fields in the shadow region are assumed to be zero. Due to the symmetry of the cylinder, $\bar{H}^s$ has to be determined only for θ between 0^o and 90^o. When $\theta = 0^o$, $P(R_o)$ is located at the end-on

position and when $\theta = 90^{o}$, at the broadside position. If S_1 is divided into S_1 and S_2, Eqs. (A.5) and (A.6) lead to

$$\bar{H}^{s}(R_o) = \frac{jk}{2\pi R_o}\left[\int\int_{S_1} (\hat{n}_1 \times \bar{H}^{i}) \times \hat{R}\, e^{-jkR_1}\, dS_1 + \int\int_{S_2} (\hat{n}_2 \times \bar{H}^{i}) \times \hat{R}\, e^{-jkR_2}\, dS_2\right] . \qquad (A.7)$$

In the denominator of (A.7) the far field approximation allows $R_1 = R_2 = R_o$. With the aid of Fig. A-1, the parameters related to S_1 are

$$\hat{n}_1 = \hat{x}\cos\phi + \hat{y}\sin\phi$$

$$dS_1 = a\, d\phi\, dz\,, \quad -\pi/2 \leq \phi \leq \pi/2 \quad \text{and} \quad -\ell/2 \leq z \leq \ell/2$$

$$R_1 = R_o - a\cos\phi\sin\theta - z\cos\theta$$

and those related to S_2 are

$$\hat{n}_2 = \hat{z}$$

$$dS_2 = r\, dr\, d\phi. \quad 0 \leq r \leq a \quad \text{and} \quad 0 \leq \phi \leq 2\pi$$

$$R_2 = R_o - r\cos\phi\sin\theta - \ell/2\cos\theta \quad .$$

The above parameters are substituted into (A.7) and four integrations are performed. Only one of the integrations is difficult and it is accomplished by taking

advantage of the physical optics approximation that $2ka \sin\theta$ is large in the integral over S_1. The troublesome integral has the form

$$\int_{-\pi/2}^{\pi/2} e^{j\beta \cos\phi} \cos\phi \, d\phi \tag{A.8}$$

where $\beta = 2ka \sin\theta$. When β is large, (A.8) yields to the method of stationary phase (De Francia, 1953) and

$$\int_{-\pi/2}^{\pi/2} e^{j\beta \cos\phi} \cos\phi \, d\phi \longrightarrow \left(\frac{2\pi}{j\beta}\right)^{1/2} e^{j\beta} \quad . \tag{A.9}$$

The solutions for the two double integrals in (A.7) are

$$\overline{H}_c^s = \hat{y} \frac{H_o \sqrt{ka\,\ell^2 \sin\theta}}{2R_o \sqrt{\pi}} \left[\frac{\sin(k\ell \cos\theta)}{k\ell \cos\theta}\right] e^{-jkR_o} e^{j\left[\frac{\pi}{4} + 2ka \sin\theta\right]} \tag{A.10}$$

and

$$\overline{H}_p^s = \hat{y} \frac{H_o ka^2}{2R_o} \left[\frac{J_1(2ka \sin\theta)}{ka \tan\theta}\right] e^{-jkR_o} e^{j\left[\frac{\pi}{2} + k\ell \cos\theta\right]} \tag{A.11}$$

where $J_1(2ka \sin\theta)$ is the Bessel function of order unity. The phase difference $\psi_c - \psi_p$, which is being sought for (A.3), can be determined from the exponential terms in (A.10) and (A.11) and is

$$\psi_c - \psi_p = 2ka \sin\theta - k\ell \cos\theta - \frac{\pi}{4} \quad . \tag{A.12}$$

With the proper substitution of (A.10), (A.11) and (A.12) into (A.9) the total backscattering cross section is

$$\sigma = \sigma_c + \sigma_p + 2\sqrt{\sigma_c \sigma_p} \cos\left[2ka \sin\theta - k\ell \cos\theta - \frac{\pi}{4}\right] \qquad \text{(A.13)}$$

where

$$\sigma_c = ka\,\ell^2 \sin\theta \left[\frac{\sin(k\ell \cos\theta)}{k\ell \cos\theta}\right]^2$$

and

$$\sigma_p = \pi(ka^2)\,2\left[\frac{J_1(2ka \sin\theta)}{ka \tan\theta}\right]^2 .$$

The expressions in (A.13) can be normalized relative to a square wavelength (λ^2) in which case they become

$$\frac{\sigma}{\lambda^2} = \frac{\sigma_c}{\lambda^2} + \frac{\sigma_p}{\lambda^2} + \frac{2}{\lambda^2}\sqrt{\sigma_c \sigma_p} \cos\left[2ka \sin\theta - k\ell \cos\theta - \frac{\pi}{4}\right] \qquad \text{(A.14)}$$

and

$$\frac{\sigma_c}{\lambda^2} = ka\left(\frac{k\ell}{2\pi}\right)^2 \sin\theta \left[\frac{\sin(k\ell \cos\theta)}{k\ell \cos\theta}\right]^2$$

$$\frac{\sigma_p}{\lambda^2} = \frac{(ka)^4}{\pi}\left[\frac{J_1(2ka \sin\theta)}{2ka \tan\theta}\right]^2 .$$

As ka and $k\ell$ increase in value beyond six, (A.13) and (A.14) become better representations for the backscattering cross section of finite circular cylinders and VV and HH patterns tend to become indistinguishable.

It is possible to derive theoretical expressions from the physical optics model which indicate roughly how the measured phase data should appear. By substituting the scattering expressions of (A.10) and (A.11) into (A.2), the total scattered field $\bar{H}^s$ may be factored into the form

$$\bar{H}^s = \hat{y}\left[H_c \cos\psi_c + H_p \cos\psi_p\right]\left[1 + j\tan\delta\right] \qquad (A.15)$$

where δ is the phase angle for the scattered field measured relative to the center of the cylinder ($R_o = 0$ in Fig. A-1). The other parameters in (A.15) are

$$H_c = \frac{H_o}{2R_o}\sqrt{\frac{ka\,\ell\,\sin\theta}{\pi}}\left[\frac{\sin(k\ell\cos\theta)}{k\ell\cos\theta}\right]$$

$$H_p = \frac{H_o ka^2}{2R_o}\left[\frac{J_1(2ka\sin\theta)}{ka\sin\theta}\right]$$

$$\psi_c = \frac{\pi}{4} + 2ka\sin\theta \qquad \psi_p = \frac{\pi}{2} + k\ell\cos\theta$$

The phase angle δ is defined as

$$\delta = \tan^{-1}\left[\frac{H_c \sin\psi_c + H_p \sin\psi_p}{H_c \cos\psi_c + H_p \cos\psi_p}\right] \qquad (A.16)$$

Like the cross section expressions in (A.13) and (A.14), the physical optics approximation for phase becomes meaningful only for larger values of ka.

UNCLASSIFIED
Security Classification

DOCUMENT CONTROL DATA - R & D

(Security classification of title, body of abstract and indexing annotation must be entered when the overall report is classified)

1. ORIGINATING ACTIVITY *(Corporate author)*
The University of Michigan Radiation Laboratory, Dept. of Electrical Engineering, 201 Catherine St., Ann Arbor, MI 48108

2a. REPORT SECURITY CLASSIFICATION
UNCLASSIFIED

2b. GROUP
n/a

3. REPORT TITLE
Evaluation of Selected Radar Cross Section Measurement Ranges
Vol IIa. Cylinder Tests & Range Evaluation Procedures

4. DESCRIPTIVE NOTES *(Type of report and inclusive dates)*
Final Report, Vol. IIa, July 1965 thru April 1968

5. AUTHOR(S) *(First name, middle initial, last name)*
Smith, Thomas M
Knott, Eugene F.
Hiatt, Ralph E.

6. REPORT DATE	7a. TOTAL NO. OF PAGES	7b. NO. OF REFS
March 1969	148	17

8a. CONTRACT OR GRANT NO.	9a. ORIGINATOR'S REPORT NUMBER(S)
AF30(602)-3872	
b. PROJECT NO. 6512	7462 - 1 - F
c. Task No. 651207	9b. OTHER REPORT NO(S) *(Any other numbers that may be assigned this report)*
d.	RADC-TR-68-238, Volume IIa

10. DISTRIBUTION STATEMENT
This document is subject to special export controls and each transmittal to foreign governments, foreign nationals or representatives thereto may be made only with prior approval of RADC (EMASP), GAFB, NY 13440.

11. SUPPLEMENTARY NOTES	12. SPONSORING MILITARY ACTIVITY
	Rome Air Development Center, EMASP Griffiss AFB, NY 13440

13. ABSTRACT

This is the second part of a three part final report on the evaluation of radar cross section measuring facilities. In Vol. IIa, the results from measurements on five right circular cylinders, which are scale models of one another, are discussed in detail. Evaluation procedures are set forth in order to determine how well each of the ranges performed their tasks. These procedures involve the comparison of measurements on cylinders which should give the same results, or results which should differ by known scale factors, and secondly the comparison of theoretical and experimental results for end-on and broadside aspect angles. Five outdoor radar ranges took part in this evaluation program. Limited tests were made on two of the smaller cylinder models at a sixth facility, an indoor range.

DD FORM 1 NOV 65 1473

UNCLASSIFIED
Security Classification

14. KEY WORDS	LINK A		LINK B		LINK C	
	ROLE	WT	ROLE	WT	ROLE	WT
Radar Reflectivity						
Static Radar Cross Section						
Amplitude						
Phase						
Range Evaluation						
Inter-range comparison						
Intra-range comparison						
Scattering Theory						
Models - Cylinders & Satellites						

AFLC—Griffiss AFB NY 28 Apr 69-87